THE ANALYSIS AND PERFORMANCE OF A TUNABLE STATE VARIABLE FILTER EMPLOYING SWITCHED RESISTOR ELEMENTS

BY

Paul Michael Embree

B. S., Lehigh University, 1981

THESIS

Submitted in partial fulfillment of the requirements
for the degree of Master of Science in Electrical Engineering
in the Graduate College of the
University of Illinois at Urbana-Champaign, 1982

Urbana, Illinois

ACKNOWLEDGEMENT

I wish to extend special thanks to my thesis advisor, Professor William Kenneth Jenkins, for his much appreciated guidance and encouragement. I also wish to thank Bell Telephone Laboratories for support of this thesis as well as my education. Finally, I wish to extend warm appreciation to Sandra Lee Malek for her long hours of proofreading and continued interest.

TABLE OF CONTENTS

CHAPTER PAGE

LIST OF FIGURES

FIGURE PAGE

Chapter 1 - BACKGROUND

1.1 Introduction

In order to properly design modern communication systems a variety of precision high quality filters are required. Often the characteristics of key filtering elements (bandwidth for example) determines the performance of a communication channel. System engineers often do not know exactly what filter specifications will meet the channel requirements and still make the system cost effective. For this reason the search for a versatile, integratable, high quality filter building block has developed.

In some applications, such as speech synthesis or adaptive equalization, the characteristics of a filter must be continuously tunable by digital means. Clearly, such a digitally tunable building block would make a very versatile filter. Filters could be made with programmable read only memory (PROM) to give the filter designer complete freedom during development of a system. The same filter could also be equipped with random access memory (RAM) for time varying filter applications, such as speech or music synthesis.

The class of state variable filters which can realize a

general biquadratic transfer function have long been used as the basic filter building block. These second order sections are relatively compact and simpler to analyze than other filter topologies (transversal filters, for example). In addition, active filters designed by using LC simulation techniques tend to use a relatively large number of amplifiers and would result in very complicated tuning systems.

State variable filters can be digitally tuned in several ways. Some authors have suggested the use of multiplying digital-to-analog converters (MDACs) for tuning [1-2]. Although the method has the advantage of digital control of the filter characteristics, it is expensive and requires a great deal of integrated circuit area. For this reason, several authors have suggested periodically switching resistors as a simple and inexpensive means of tunning RC active filters [3-5]. Switched resistor filters can be tuned by changing the duty cycle of the switching signal. Simple digital circuits can be used to create a signal with a duty cycle programmed by a suitable binary digital word (a counter could be used, for example). Thus, switched resistor filters can be tuned in a relatively simple digital fashion.

Switched resistor filters may also offer better noise

performance than other switched element filtering systems. This can be seen by recognizing that all switches sample uncorrelated thermal noise present in each signal in the filter. Thus, the noise generated by the large number of switches in a switched capacitor system may be much greater than the noise generated in an equivalent switched resistor system. In addition, the high frequency distortion components added to the output of a filter by switched resistor elements may be less than the output distortion added by the equivalent switched capacitor elements.

The purpose of this thesis, therefore, is to analyze the effects of tuning a second order state variable switched resistor section and to investigate the performance of a typical prototype. The circuit topology presented here uses two switching signals to tune both the center frequency and bandwidth of the filter.

1.2 Switched Capacitor Filters

Switched capacitor recursive filters have seen a great deal of popularity recently, as is apparent by the large volume of literature [6-9]. The first switched capacitor filters were designed by replacing resistors in analog circuits with switched capacitor equivalents [10]. (R=T/C

where C is the value of the capacitor and T is the sampling period.) This equivalent resistance concept is accurate only when the sampling frequency is very high compared to the frequency content of the signal.

More recently, switched capacitor filters have been designed by sampled data techniques [11-12]. These discrete time techniques use the Z-transform to obtain the exact transfer function of the switched capacitor filter. These techniques are much more accurate and allow complicated structures to be analyzed by computer simulation [13].

Switched capacitor filters can be tuned. Since the equivalent integration constant of a switched capacitor integrator is proportional to the sampling period, switched capacitor filters can be tuned by changing the sampling frequency [14]. Normally every switch in a filter section is operated at the same rate, so independent control of the filter charateristics is difficult. The resulting filter has a tunable center frequency and a constant Q. Furthermore, the constraints on the sampling frequency can be rather severe. The Nyquist rate determines the minimun sampling frequency; technology limitaions determine the maximum. This results in a relatively narrow range of tuning capability. Also, a digitally programmable sampling rate is rather difficult to generate.

Independent control of switched capacitor filter coefficients could be obtained by using structures similar to those used in MDACs. This was suggested and fabricated by Allstot et al. in 1979 [15]. Their circuit had only a 3-bit control for center frequency and 6-bit control for quality factor. Although this may be sufficient for speech synthesis, it does not meet the general filter specifications stated herein. Based on their prototype's die size (6 mm^2) a reasonably large high accuracy filter system (say 10th order) would not be practical. Others have used complicated time shared switched capacitor elements to make practical 10th order vocal tract vocoders [16]. However, the number of bits of quantiztion of the controllable filter parameters is not sufficent for general filter applications.

1.3 MOS Technology Considerations

The main reason that switched capacitor filters are popular is that they are very well suited for integration using metal oxide semiconductor (MOS) technologies. Although MOS analog circuit design techniques are by no means mature, MOS offers many advantages to the filter designer.

The biggest problem with the existing monolithic integrated circuit technology is the wide variation of the relative resistor values in a single integrated circuit. Variations in processing parameters (temperature, impurity dose, time) can cause the resistivity of diffused resistors to vary more than 1% on the same chip. Furthermore, this variation is uncorrelated to the variation of capacitance per unit area. Together these two effects cause RC products to vary by a factor of two using the best processing currently available.

The growth of silicon dioxide on silicon is subject to similar processing variations (temperature and time) but in this case impurities are not added. For this reason the thickness of thermally grown oxide layers on a wafer does not change very much across the wafer surface. In fact capacitors in MOS technology can be matched within 0.1% [7]. Thus any filter topology with a transfer function dependent on the ratio of capacitors is ideal for unipolar (MOS) integration.

Recently, researchers have introduced techniques which eliminate resistors by replacing them with field effect transistors (MOSFETs) biased in the linear (ohmic) region of operation [17]. The technique switches the MOSFETs in and out of the circuit by using CMOS switches. When the MOSFETs

are switched out of the cicuit they are placed in an RC oscillator circuit which effectively measures the MOSFET's resistance, since the frequency of oscillation is dependent on the RC product. In order to maintain circuit integrity, an identical MOSFET, biased at the same point, replaces the one being measured by the oscillator circuit. The switching rate is very slow (5 Hz) to allow the oscillator to stabilize. Unfortunatly, the low frequency switching introduces transients in the filter circuit and causes many side frequencies to appear at the filter output. These created frequencies near the input frequencies could be disasterous in some applications.

1.4 Switched Resistor Filters

With the development of similar techniques which eliminate diffused resistors from filter circuits the possibility exists that periodically switched resistor filters may offer a simple and inexpensive means of digitally tuning state variable filters. Although the integration of a large filtering system is required in order to make it cost effective for production applications, discrete switched resistor filters may be attractive in other applications. At switching speeds greater than 1 MHz MOS switched capacitor filter performance begins to degrade.

This makes the use of switched capacitor filters impractical above about 20 kHz. Also, the noise associated with all MOS switches and MOS amplifiers makes the dynamic range too small for demanding high fidelity audio applications. Another dynamic range limitation is the fundamental low breakdown voltage of MOS transistors. Current technologies do not allow signals above approximately 8V peak to peak. For these reasons, switched resistor filters may become practical in certain future applications.

Chapter 2 - SECOND ORDER STATE VARIABLE FILTERS

2.1 State Variable Biquadratic Sections

Biquads based on state variable filter design techniques realize a second order transfer function with integrators and summers. This approach was originally used in analog computers and is, therefore, quite well developed. The basic signal flow graph diagram and transfer function of a two-integrator biquad is shown in Figure 1. The first circuit realization, developed by Kerwin, Huelsman and Newcomb, is known as the KHN biquad [18]. Further refinements by Thomas [19] allowed bandpass and lowpass transfer functions to be provided with only three operational amplifiers. This type of circuit is shown in Figure 2. Many other biquad circuits have been developed using as few as one operational amplifier; but these biquads do not have low passive component sensitivity or do not have independent control of the Q factor and center frequency. Other circuits based on the ladder simulation approach require as many as four elements to be changed simultaneously to change the center frequency [20]. Also, these circuits do not provide bandpass and lowpass outputs at the same time. It appears that the state variable biquad is the best choice for a biquad building block.

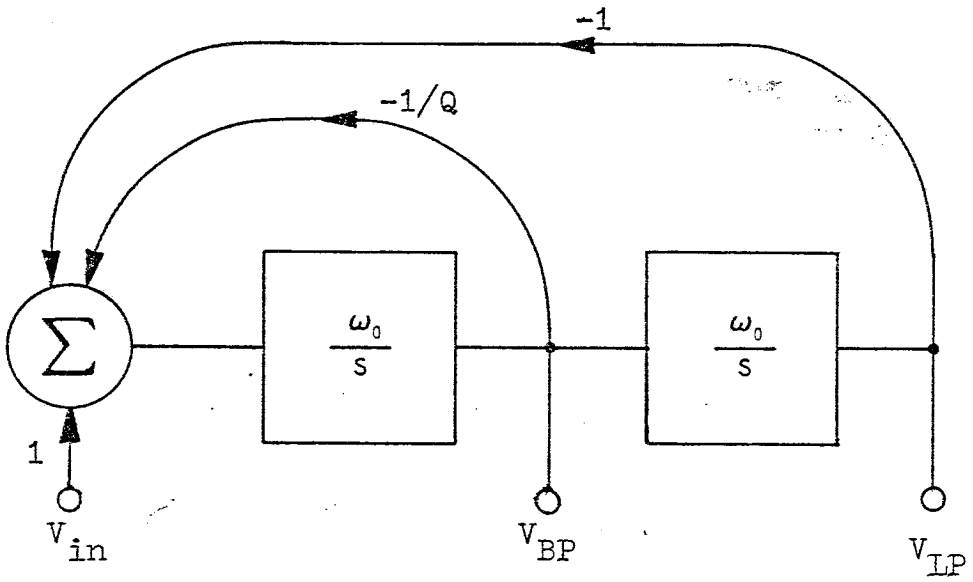

$$\frac{V_{BP}}{V_{in}} = \frac{s\,\omega_o}{s^2 + s\,(\omega_o/Q) + \omega_o^2}$$

$$\frac{V_{LP}}{V_{in}} = \frac{\omega_o^2}{s^2 + s\,(\omega_o/Q) + \omega_o^2}$$

Figure 1 - Two-integrator state variable biquad signal flow graph and transfer functions.

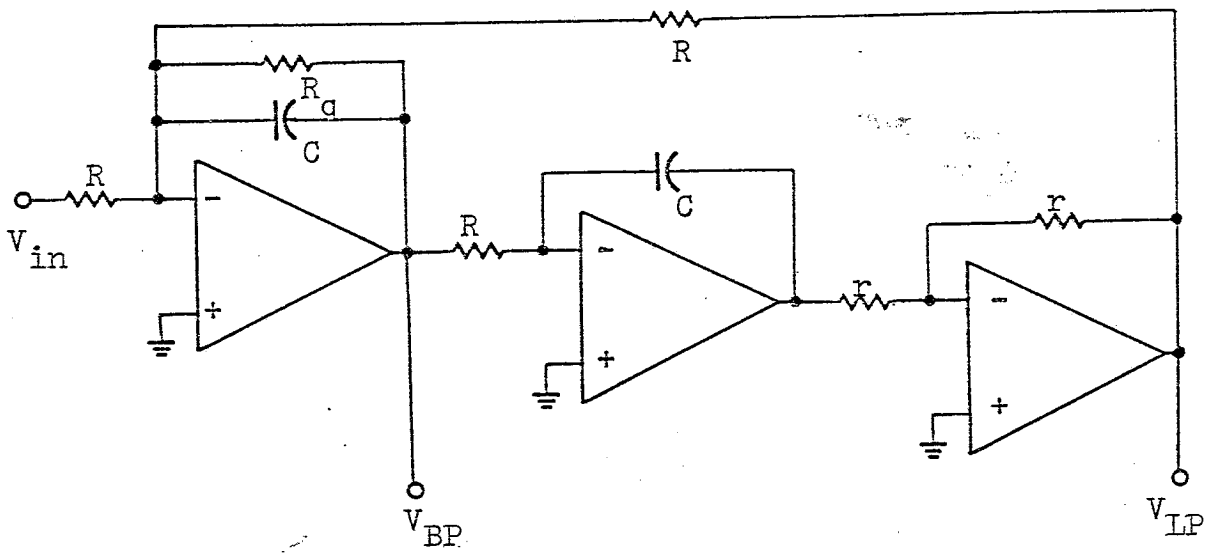

$$\omega_o = \frac{1}{C\,R} \qquad Q = \frac{R_q}{R}$$

Figure 2 - Thomas state variable biquad.

The sensitivity of the three-amplifier biquad to passive component variation is quite low, suggesting it is a preferred structure in many applications. However, the sensitivity to operational amplifier high frequency limitations can be quite severe. Several texts have analyzed this effect, commonly called Q enhancement [21-22]. As the desired Q-center-frequency-product is increased, the actual Q obtained is increased and the resulting center frequency is slightly lower than desired. Thus, the pole locations move closer to the imaginary axis and at some point cause the system to become unstable. The approximate increase in the Q factor for the three-amplifier biquad is given by [21] as:

$$Q = \frac{Q_d}{1 - 4 Q_d \left(\frac{\omega_o}{\omega_t}\right)} \qquad (2.1)$$

where:

Q_d = desired quality factor.

ω_o = center frequency (rad/sec).

ω_t = gain-bandwidth product of amplifiers (rad/sec).

Compensation for the relatively severe Q enhancement effects has been suggested by several authors [23-25]. Some techniques use passive compensation [19,23] and others use additional amplifiers for active compensation [24-25]. The active techniques seem more practical because of the

temperature drift of amplifier characteristics. A more detailed discussion of this topic will be presented in Chapter 4 where actual circuit performance is evaluated.

2.2 Switched Resistor Integrators

As was indicated in Figure 2, the integrator normally used is the inverting (Miller) integrator. By replacing the resistance by a series resistor-switch combination the circuit shown in Figure 3(a) is obtained. If the switch is operated in a periodic fashion, the input-output relationship is,

$$V_{out}(t) = V_{out}(0) - \frac{1}{C}\int_0^t I_{in}\ dt \qquad (2.2)$$

where:

$I_{in} = \frac{V_{in}}{R_1}$ when the switch is closed.

and

$I_{in} = 0$ when the switch is open.

Thus, the output voltage does not change when the switch is open. By replacing the switch by a multiplying element, an analysis of the integrator transfer function can be obtained. This replacement is shown in Figure 3(b). One input to the current multiplier is the input signal (I_{in}) and the other input is the periodic switching signal, s(t), remaining at 1 for a time τ_f and at 0 for the remainder of the period ($T - \tau_f$).

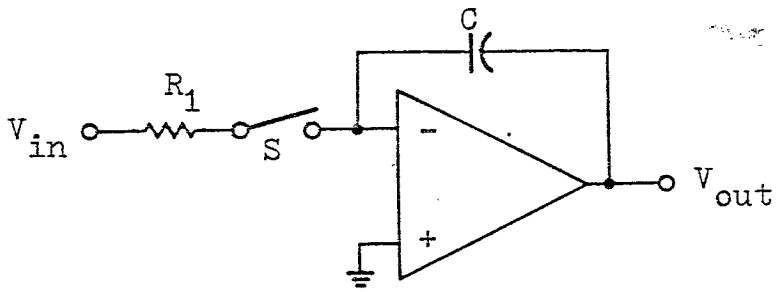

(a)

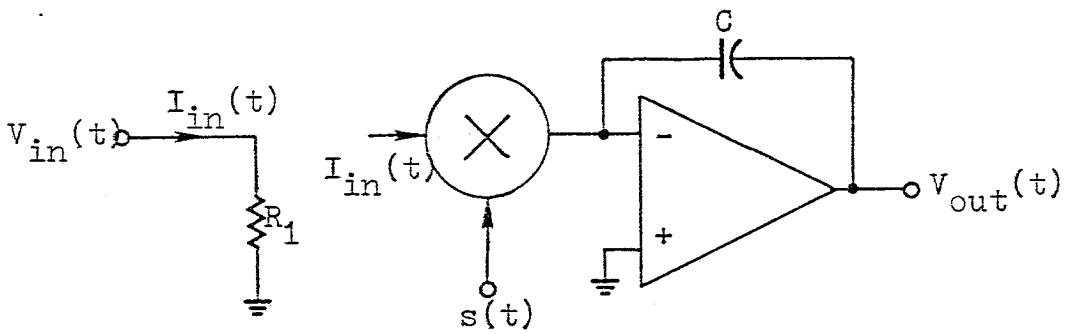

(b)

Figure 3 - (a) Switched resistor Miller integrator.
(b) Switchless equivalent used in analysis.

The resulting frequency spectrum of the current input to the amplifier is given by the following convolution:

$$I_{in}(f) = \frac{1}{R_1} [S(f) * V_{in}(f)]$$

thus,

$$V_{out}(f) = \frac{-1}{2 \pi f j R_1 C} [S(f) * V_{in}(f)] \qquad (2.3)$$

where:

f = real frequency variable (Hz).

$S(f)$ = frequency spectrum of switching signal, $s(t)$.

$V_{in}(f)$ = frequency spectrum of input signal, $V_{in}(t)$.

$I_{in}(f)$ = frequency spectrum of current input to amplifier, $I_{in}(t)$.

The switching spectrum [S(f)] is a Fourier series given by:

$$S(f) = \sum_{n=-\infty}^{\infty} \frac{\text{SIN} (n \pi \tau_f / T)}{n} \delta (f - n/T) \qquad (2.4)$$

By assuming that the input signal (V_{in}) is bandlimited and the sampling frequency (1/T) is greater than the Nyquist rate (twice the maximum input frequency), equation (2.3) can be evaluated. After some manipulation, the output spectrum is given by:

$$V_{out}(f) = \frac{-1}{2\pi f j R_1 C} [\frac{\tau_f}{T} V_{in}(f) + \sum_{\substack{n=-\infty \\ n \neq 0}}^{\infty} \frac{\text{SIN}(n\pi\tau_f/T)}{n} V_{in}(f - n/T)] \qquad (2.5)$$

The second term of equation (2.5) represents frequencies near multiples of the sampling frequency as would be expected in any sampled data system. Thus, if these higher frequencies are filtered out of the output, the integrator becomes tunable with a transfer function which can be written as follows:

$$\frac{V_{out}(s)}{V_{in}(s)} = \left.\frac{-\tau_f}{s R_1 C T}\right| \text{frequencies low compared to } 1/2T. \qquad (2.6)$$

Thus the equivalent resistor, R, has a value inversely proprotional to the duty cycle, or

$$R = T R_1 / \tau_f \ . \qquad (2.7)$$

This analysis shows that if an integrator of this type is used in a state variable biquad, the integration constant, and therefore the center frequency of the filter, can be adjusted by changing the duty cycle (τ_f/T) of the switching signal. The center frequency is proportional to the duty cycle of the periodic switching signal, as was assumed by Pavin and Hostetter [26].

2.3 Constant Q Switched Resistor Biquad

If the integrator shown in Figure 3(a) is used in a biquad circuit similar to the one shown in Figure 2, a tunable center frequency filter is obtained. The Q factor

is fixed by R_q, since $Q = R_q/R$. In order to make the gain of the circuit at the center frequency equal to unity, the circuit is rearranged as shown in Figure 4. The switched resistor integrators have also been added to this figure. In this circuit, the center frequency is τ_f/TRC in rad/sec and the Q factor is fixed at R_q/R. Unfortunately, many filter applications require that the bandwidth (or Q factor) and the center frequency be independently controllable.

2.4 The Totally Tunable Switched Resistor Biquad

By replacing R_q with a series switch and resistor combination, a biquad circuit is realized for which both the center frequency and bandwidth are independently tunable. The schematic of this circuit is shown in Figure 5. By assuming that the equivalent resistance of a switch and resistor combination is given by equation (2.7), the center frequency is again $\tau_f/T \cdot R \cdot C$ and the Q factor is $R_{bw}\ \tau_f\ /\ R\ \tau_b$ where τ_b is the time switch S_b is on and τ_f is the time switches S_f are on. Therefore, the bandwidth is $\tau_b/\ T\ R_{bw} \cdot C$ in rad/sec.

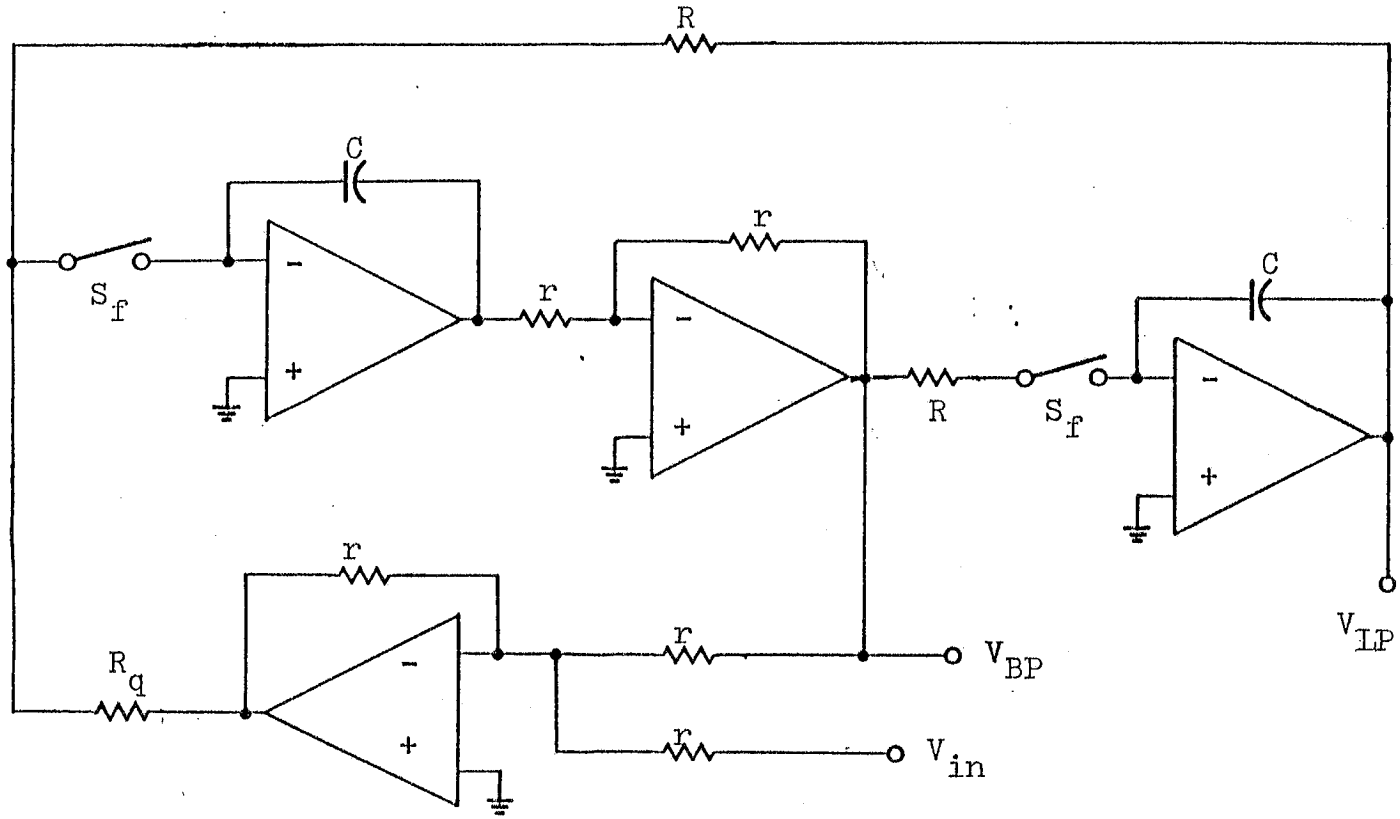

$$Q = R_q/R \qquad \omega_o = \tau_f / TRC$$

$$\frac{V_{BP}}{V_{in}} = \frac{-s\omega_o/Q}{s^2 + s(\omega_o/Q) + \omega_o^2} \qquad \frac{V_{LP}}{V_{in}} = \frac{\omega_o^2/Q}{s^2 + s(\omega_o/Q) + \omega_o^2}$$

Figure 4 - Constant Q switched resistor filter circuit and transfer functions.

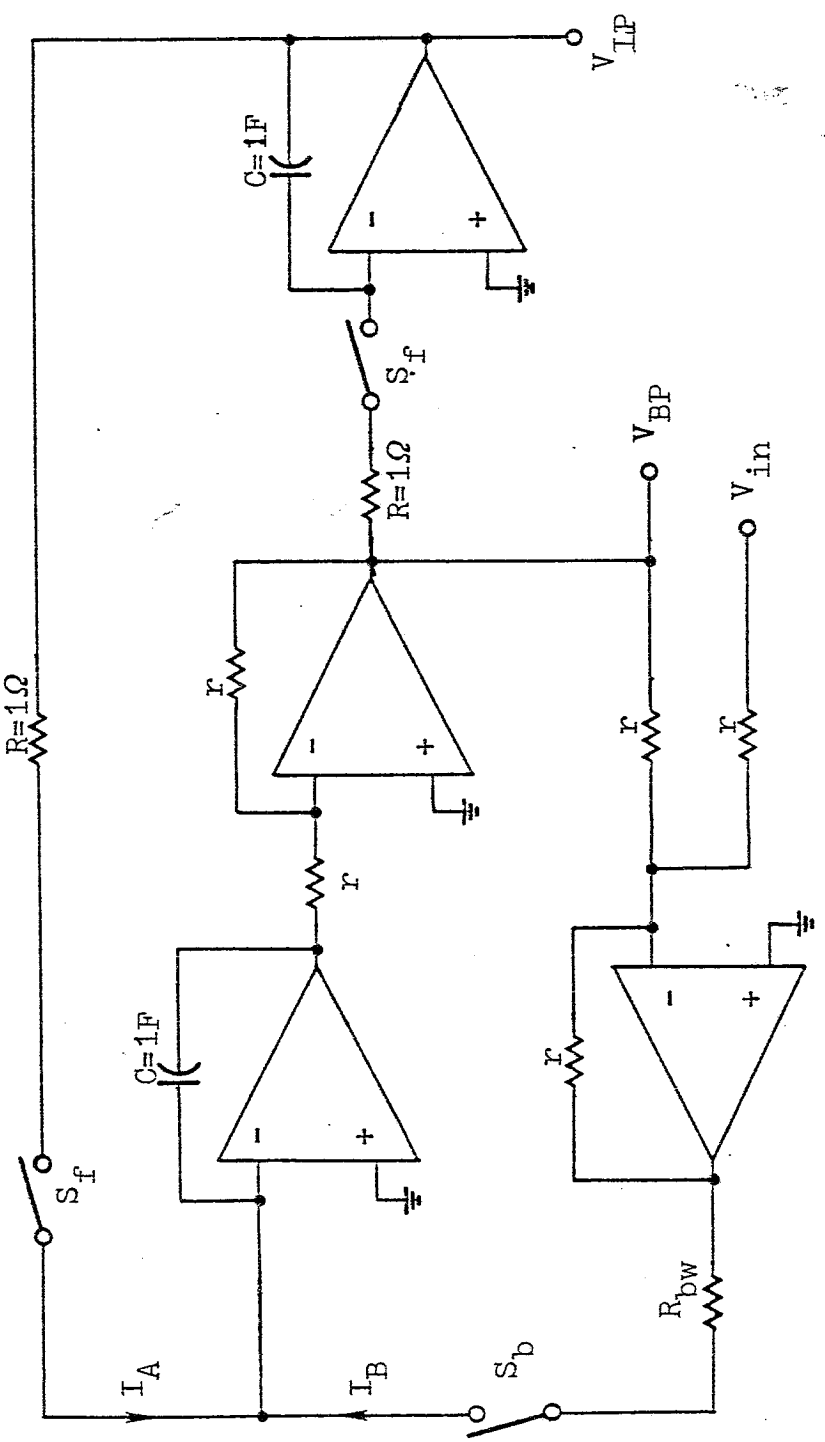

Figure 5 - Totally tunable normalized switched resistor biquad.

To simplify the subsequent discussion and analysis, the switched resistor biquad will be normalized such that when all switches are closed, the center frequency is 1 rad/sec. This is accomplished by setting R = 1 Ω and C = 1 F as shown in Figure 5. The bandwidth is then τ_b / T R_{bw} and the center frequency is τ_f /T.

The above simplified analysis would suggest a relatively simple solution to make the biquad of Figure 4 totally tunable. Unfortunately as will be shown in the next chapter, the different duty cycles of the switches cause distortion in the filter transfer function.

Chapter 3 - SWITCHED RESISTOR FILTER ANALYSIS

3.1 State Variable Analysis

In this section the derivation of the frequency response of the normalized sampled data switched resistor system shown in Figure 5 is presented. The analysis is generalized to include the constant Q case where all three switches are operated simultaneously.

The timing relationship of the three switches in the system can change the transfer function. The analysis which follows assumes that the two switches which control the center frequency are on at the same time and that the closing of the switch which controls the bandwidth (S_b) coincides with the closing of the other switches. The bandwidth switch is closed for a time period T_1. These assumptions divide the switching period, T, into three distinct regions (region I, II, and III), shown in Figure 6. This timing diagram also defines the two critical time periods (τ_1, τ_2) and the three state vectors which specify the current state of the system (x_N), the state at the end of region I ($x_{N+\gamma}$), and the state at the beginning of the next sampling period (x_{N+1}). Two different cases during region II can be identified from this figure. The first

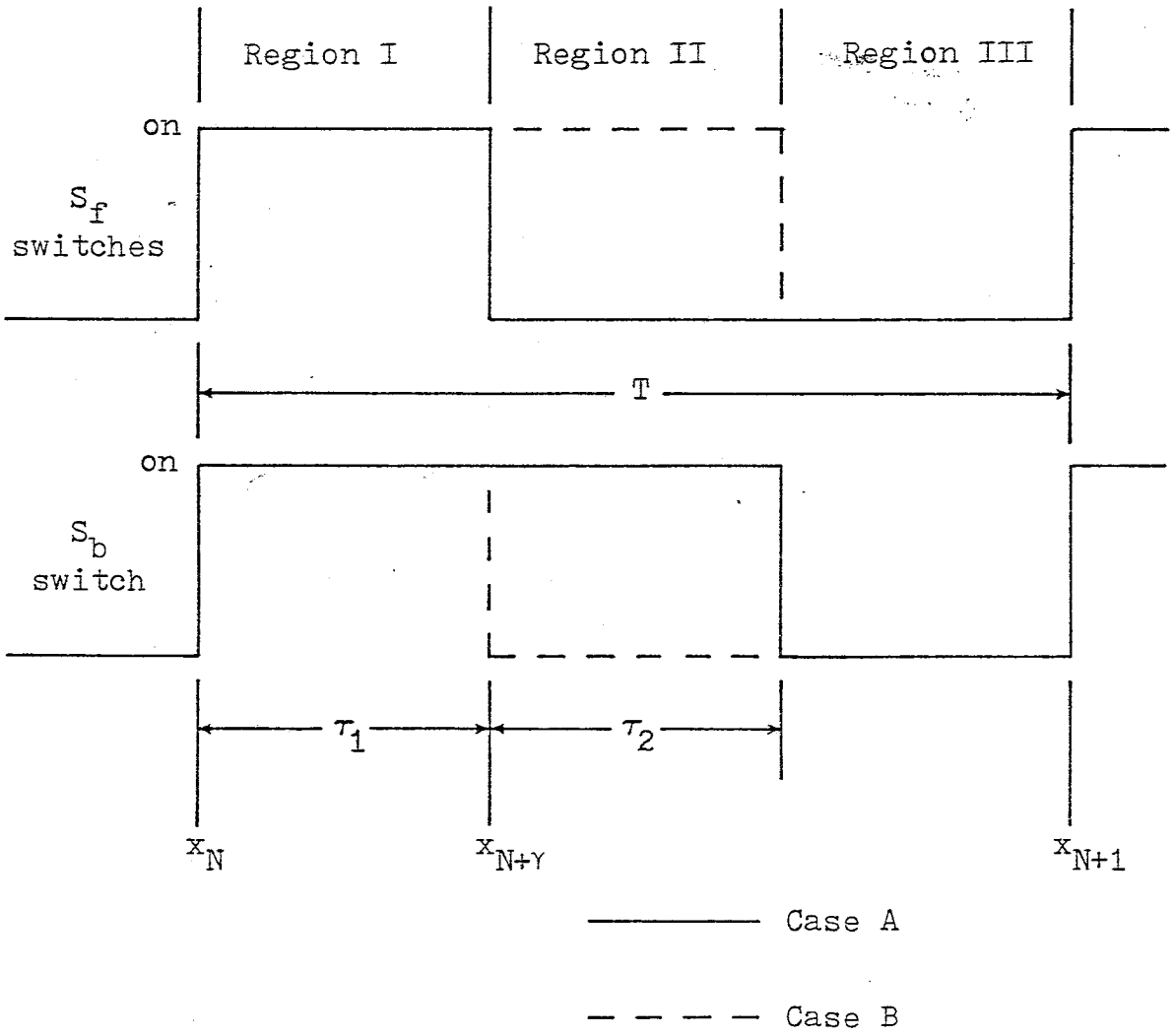

Figure 6 - Switch timing diagram.

case (case A) is when the bandwidth switch is closed and the center frequency switches are open and the other case (case B) is when the position of the switches is reversed. With these definitions, state equations can be developed as shown below.

During Region I: [S_b and S_f closed]

$$I_B = \frac{-V_{BPF} - V_{IN}}{R_{BW}}$$

$$I_A = V_{LPF}$$

$$V_{BPF} = \int (I_A + I_B)dt$$

$$V_{LPF} = - \int (V_{BPF})dt$$

$$\frac{dV_{BPF}}{dt} = V_{LPF} - \frac{V_{BPF}}{R_{BW}} - \frac{V_{IN}}{R_{BW}}$$

$$\frac{dV_{LPF}}{dt} = - V_{BPF}$$

$$\text{Let} \quad x = \begin{bmatrix} V_{LPF} \\ V_{BPF} \end{bmatrix} .$$

$$\frac{dx}{dt} = \begin{bmatrix} 0 & -1 \\ 1 & -\frac{1}{R_{BW}} \end{bmatrix} x + \begin{bmatrix} 0 \\ -\frac{1}{R_{BW}} \end{bmatrix} V_{IN}$$

$$A_I = \begin{bmatrix} 0 & -1 \\ 1 & -\frac{1}{R_{BW}} \end{bmatrix}, \quad b_I = \begin{bmatrix} 0 \\ -\frac{1}{R_{BW}} \end{bmatrix}$$

During Region II:

Case A: [S_b closed, S_f open]

$$\frac{dV_{LPF}}{dt} = 0$$

$$I_A = 0$$

$$I_B = \frac{-V_{BPF} - V_{IN}}{R_{BW}}$$

$$\frac{dV_{BPF}}{dt} = - \frac{V_{BPF}}{R_{BW}} - \frac{V_{IN}}{R_{BW}}$$

$$\frac{dx}{dt} = \begin{bmatrix} 0 & 0 \\ 0 & - \frac{1}{R_{BW}} \end{bmatrix} x + \begin{bmatrix} 0 \\ - \frac{1}{R_{BW}} \end{bmatrix} V_{IN}$$

$$A_{IIA} = \begin{bmatrix} 0 & 0 \\ 0 & - \frac{1}{R_{BW}} \end{bmatrix}, \quad b_{IIA} = \begin{bmatrix} 0 \\ - \frac{1}{R_{BW}} \end{bmatrix}$$

Case B: [S_b open, S_f closed]

$$I_A = V_{LPF}$$

$$I_B = 0$$

$$\frac{dV_{BPF}}{dt} = V_{LPF}$$

$$\frac{dV_{LPF}}{dt} = - V_{BPF}$$

During Region II, Case B (continued):

$$\frac{dx}{dt} = \begin{bmatrix} 0 & -1 \\ 1 & 0 \end{bmatrix} x$$

$$A_{IIB} = \begin{bmatrix} 0 & -1 \\ 1 & 0 \end{bmatrix}, \quad b_{IIB} = \begin{bmatrix} 0 \\ 0 \end{bmatrix}$$

During Region III:

$$\frac{dV_{BPF}}{dt} = \frac{dV_{LPF}}{dt} = 0$$

$$\frac{dx}{dt} = 0$$

SOLUTION

CASE A: $[T_1 > \tau_1]$

$$x_{N+\gamma} = e^{A_I \tau_1} x_N + \int_0^{\tau_1} e^{A_I(\tau_1 - t)} b_I V_{IN}(NT+t)\,dt$$

$$x_{N+1} = e^{A_{IIA}\tau_2} x_{N+\gamma} + \int_0^{\tau_2} e^{A_{IIA}(\tau_2 - t)} b_{IIA} V_{IN}(NT+\tau_1+t)\,dt$$

CASE B: $[\tau_1 > T_1]$

$$x_{N+\gamma} = e^{A_I \tau_1} x_N + \int_0^{\tau_1} e^{A_I(\tau_1 - t)} b_I V_{IN}(NT+t)\,dt$$

$$x_{N+1} = e^{A_{IIB}\tau_2} x_{N+\gamma} + \int_0^{\tau_2} e^{A_{IIB}(\tau_2 - t)} b_{IIB} V_{IN}(NT+\tau_1+t)\,dt$$

Thus, a relationship exists between x_{N+1} and x_N, namely:

CASE A:

$$x_{N+1} = e^{A_{IIA}\tau_2}\left[e^{A_I\tau_1}x_N + \int_0^{\tau_1} e^{A_I(\tau_1-t)}b_I V_{IN}(NT+t)dt\right] + \int_0^{\tau_2} e^{A_{IIA}(\tau_2-t)}b_{IIA}V_{IN}(NT+\tau_1+t)dt \quad . \tag{3.1}$$

CASE B:

$$x_{N+1} = e^{A_{IIB}\tau_2}\left[e^{A_I\tau_1}x_N + \int_0^{\tau_1} e^{A_I(\tau_1-t)}b_I V_{IN}(NT+t)dt\right] + \int_0^{\tau_2} e^{A_{IIB}(\tau_2-t)}b_{IIB}V_{IN}(NT+\tau_1+t)dt. \tag{3.2}$$

Equations (3.1) and (3.2) are rather complicated second order difference equations. They can be solved for the case of a complex frequency input as follows:

With $V_{IN}(t) = e^{j\omega t}$, let

$$E_1(\tau_1) = e^{A_I\tau_1},$$

$$c_1(\tau_1,t) = e^{A_I(\tau_1-t)}b_I,$$

$$E_{2A}(\tau_2) = e^{A_{IIA}\tau_2},$$

$$E_{2B}(\tau_2) = e^{A_{IIB}\tau_2},$$

$$c_{2A}(\tau_2,t) = e^{A_{IIA}(\tau_2-t)} b_{IIA} ,$$

$$c_{2B}(\tau_2,t) = e^{A_{IIB}(\tau_2-t)} b_{IIB} .$$

Then:

CASE A:

$$x_{N+1} = E_{2A}(\tau_2)E_1(\tau_1)x_N + E_{2A}(\tau_2)\int_0^{\tau_1} c_1(\tau_1,t)e^{j\omega(NT+t)}dt + \int_0^{\tau_2} c_{2A}(\tau_2,t)e^{j\omega(NT+\tau_1+t)}dt . \quad (3.3)$$

CASE B:

$$x_{N+1} = E_{2B}(\tau_2)E_1(\tau_1)x_N + E_{2B}(\tau_2)\int_0^{\tau_1} c_1(\tau_1,t)e^{j\omega(NT+t)}dt + \int_0^{\tau_2} c_{2B}(\tau_2,t)e^{j\omega(NT+\tau_1+t)}dt \quad (3.4)$$

It can be shown that if $\zeta = \frac{1}{2R_{BW}}$ and $\beta = \sqrt{1-\zeta^2}$, then

$$A_I = \begin{bmatrix} 0 & -1 \\ 1 & -2\zeta \end{bmatrix} , \qquad b_I = \begin{bmatrix} 0 \\ -2\zeta \end{bmatrix} .$$

$$E_1(\tau_1) = e^{-\zeta\tau_1}\begin{bmatrix} 1 & 0 \\ \zeta & \beta \end{bmatrix}\begin{bmatrix} \cos(\beta\tau_1) & -\sin(\beta\tau_1) \\ \sin(\beta\tau_1) & \cos(\beta\tau_1) \end{bmatrix}\begin{bmatrix} 1 & 0 \\ -\frac{\zeta}{\beta} & \frac{1}{\beta} \end{bmatrix} \quad (3.5)$$

$$A_{IIA} = \begin{bmatrix} 0 & 0 \\ 0 & -2\zeta \end{bmatrix} \qquad b_{IIA} = \begin{bmatrix} 0 \\ -2\zeta \end{bmatrix}$$

$$E_{2A}(\tau_2) = \begin{bmatrix} 1 & 0 \\ 0 & e^{-2\zeta\tau_2} \end{bmatrix} \tag{3.6}$$

$$A_{IIB} = \begin{bmatrix} 0 & -1 \\ 1 & 0 \end{bmatrix} \qquad b_{IIB} = \begin{bmatrix} 0 \\ 0 \end{bmatrix}$$

$$E_{2B}(\tau_2) = \begin{bmatrix} \cos(\tau_2) & -\sin(\tau_2) \\ \sin(\tau_2) & \cos(\tau_2) \end{bmatrix} \tag{3.7}$$

$$c_1(\tau_1,t) = \begin{bmatrix} -\frac{2\zeta}{\beta} e^{-\zeta(\tau_1-t)} \sin[\beta(\tau_1-t)] \\ \left\{-\frac{2\zeta^2}{\beta}\sin[\beta(\tau_1-t)] + 2\zeta\cos[\beta(\tau_1-t)]\right\} e^{-\zeta(\tau_1-t)} \end{bmatrix} \tag{3.8}$$

$$c_{2A}(\tau_2,t) = \begin{bmatrix} 0 \\ 2\zeta e^{-2\zeta(\tau_2-t)} \end{bmatrix} \tag{3.9}$$

$$c_{2B}(\tau_2,t) = \begin{bmatrix} 0 \\ 0 \end{bmatrix} \tag{3.10}$$

$$\int_0^{\tau_1} c_1(\tau_1,t)\, e^{j\omega(NT+t)}\,dt =$$

$$\left[\begin{array}{l} \displaystyle\int_0^{\tau_1} -\frac{2\zeta}{\beta}\, e^{-\zeta(\tau_1-t)} \sin[\beta(\tau_1-t)]\, e^{j\omega(NT+t)}\,dt \\ \\ \displaystyle\int_0^{\tau_1} -\frac{2\zeta^2}{\beta}\, e^{-\zeta(\tau_1-t)} \sin[\beta(\tau_1-t)]\, e^{j\omega(NT+t)}\,dt \\ \\ \displaystyle\quad +\int_0^{\tau_1} 2\zeta e^{-\zeta(\tau_1-t)} \cos[\beta(\tau_1-t)\, e^{j\omega(NT+t)}\,dt \end{array}\right] . \qquad (3.11)$$

$$\int_0^{\tau_2} c_{2A}(\tau_2,t)\, e^{j\omega(NT+\tau_1+t)}\,dt =$$

$$\left[\begin{array}{l} \displaystyle\int_0^{\tau_2} 2\zeta e^{-2\zeta(\tau_2-t)}\, e^{j\omega(NT+\tau_1+t)}\,dt \end{array}\right] . \qquad (3.12)$$

$$\int_0^{\tau_2} c_{2B}(\tau_2,t)\cos[\omega NT+\omega\tau_1+\omega t]\,dt = 0 \quad . \qquad (3.13)$$

It can be seen that equation (3.11) can be written in terms of two definite integrals defined by the following:

$$I_1(\tau_1) = \int_0^{\tau_1} e^{(\zeta+j\omega)t} \sin[\beta(\tau_1-t)\,dt$$

$$= \frac{e^{j\beta\tau_1}}{2j}\int_0^{\tau_1} e^{(\zeta+j\omega-j\beta)t}\,dt - \frac{e^{-j\beta\tau_1}}{2j}\int_0^{\tau_1} e^{(\zeta+j\omega+j\beta)t}\,dt$$

$$= \frac{1}{2j(\zeta+j\omega-j\beta)}\left[e^{(\zeta+j\omega)\tau_1} - e^{j\beta\tau_1}\right]$$

$$- \frac{1}{2j(\zeta+j\omega+j\beta)}\left[e^{(\zeta+j\omega)\tau_1} - e^{-j\beta\tau_1}\right] .$$

$$I_2(\tau_1) = \int_0^{\tau_1} e^{(\zeta+j\omega)t}\cos[\beta(\tau_1-t)]dt =$$

$$= \frac{1}{2(\zeta+j\omega-j\beta)}\left[e^{(\zeta+j\omega)\tau_1} - e^{j\beta\tau_1}\right]$$

$$+ \frac{1}{2(\zeta+j\omega+j\beta)}\left[e^{(\zeta+j\omega)\tau_1} - e^{j\beta\tau_1}\right] .$$

With these definitions, equation (3.11) becomes:

$$\int_0^{\tau_1} c_1(\tau_1,t)e^{j\omega(NT+t)}dt = \begin{bmatrix} -\frac{2\zeta}{\beta} e^{-\zeta\tau_1} I_1(\tau_1) \cdot e^{j\omega NT} \\ \left\{2\zeta[I_2(\tau_1) - \frac{\zeta}{\beta} I_1(\tau_1)]e^{-\zeta\tau_1}\right\} \\ \cdot e^{j\omega NT} \end{bmatrix} \tag{3.14}$$

It can be shown that after integration equation (3.12) becomes:

$$\int_0^{\tau_2} c_{2A}(\tau_2,t)e^{j\omega(NT+\tau_1+t)}dt =$$

$$\begin{bmatrix} 0 \\ \frac{2\zeta\, e^{j\omega\tau_1}}{2\zeta + j\omega}\left[e^{j\omega\tau_2} - e^{-2\zeta\tau_2}\right]e^{j\omega NT} \end{bmatrix} . \tag{3.15}$$

Thus, for case A, where the center frequency is τ_1/T and the bandwidth is $2\zeta(\tau_1+\tau_2)/T$, the state equation (equation 3.3) is determined to be as follows:

$$x_{N+1} = A_A x_N + b_A e^{j\omega NT} \tag{3.16}$$

where:

$$A_A = \begin{bmatrix} 1 & 0 \\ 0 & e^{-2\zeta\tau_2} \end{bmatrix} \begin{bmatrix} 1 & 0 \\ \zeta & \beta \end{bmatrix} \begin{bmatrix} \cos(\beta\tau_1) & -\sin(\beta\tau_1) \\ \sin(\beta\tau_1) & \cos(\beta\tau_1) \end{bmatrix} \begin{bmatrix} 1 & 0 \\ -\frac{\zeta}{\beta} & \frac{1}{\beta} \end{bmatrix} e^{-\zeta\tau_1}$$

$$b_A = \begin{bmatrix} 1 & 0 \\ 0 & e^{-2\zeta\tau_2} \end{bmatrix} \begin{bmatrix} -\frac{2\zeta}{\beta} e^{-\zeta\tau_1} I_1(\tau_1) \\ 2\zeta[I_2(\tau_1) - \frac{\zeta}{\beta} I_1(\tau_1)]e^{-\zeta\tau_1} \end{bmatrix}$$

$$+ \begin{bmatrix} 0 \\ \frac{2\zeta e^{j\omega\tau_1}}{2\zeta + j\omega}\left[e^{j\omega\tau_2} - e^{-2\zeta\tau_2}\right] \end{bmatrix}$$

The 2x2 matrix A_A and vector b_A can be expanded into very complicated expressions. In order to expedite the expansion process and reduce algebraic errors, an algebraic manipulation package, called REDUCE [27], was used to expand the above matrix expressions. Because REDUCE can not handle greek letters, the variables τ_1, τ_2, ω, ζ and β will be

replaced by t1, t2, w, L, and B respectively. Also, REDUCE produces an unambiguous FORTRAN-like output using the operators *, / and +. With this change of notation, the four elements of A_A become:

```
A_A(1,1) = (SIN(t1*B)*L + COS(t1*B)*B)/(E^(t1*L)*B)

A_A(1,2) = ( - SIN(t1*B))/(E^(t1*L)*B)

A_A(2,1) = (SIN(t1*B)*(L^2 + B^2))/(E^(2*t2*L + t1*L)*B)

A_A(2,2) = (-SIN(t1*B)*L + COS(t1*B)*B)/(E^(2*t2*L + t1*L)*B)
```

In REDUCE notation, the two elements of b_A are

```
b_A(1) = (((E^((w*j + L)*t1 + t1*j*B) - 1)*(w*j + L - j*B) -
 E^(t1*j*B)*(E^((w*j + L)*t1) - E^(t1*j*B))*(w*j+L+j*B))*L)
   / (E^(t1*L + t1*j*B)*(w*j+L+j*B)*(w*j+L-j*B)*j*B)

b_A(2) = (((-E^((w*j+L)*t1+t1*j*B)*2*w*B+E^(2*t1*j*B)*w*L*j
  + E^(2*t1*j*B)*w*B + E^(2*t1*j*B)*L^2 + E^(2*t1*j*B)*B^2
  -w*L*j-w*B-1)*(w*j+2*L) + 2*E^(t1*w*j+t1*L+t1*j*B)
  * (E^(t2*w*j+2*t2*L) -1)*(w*j+L+j*B)*(w*j+L-j*B)*j*B)*L)
/E^(2*t2*L+t1*L+t1*j*B)*(w*j+2*L)*(w*j+L+j*B)*(w*j+L-j*B)*j*B
```

For case B where the center frequency is $(\tau_1 + \tau_2)/T$ and the bandwidth is $2\zeta\tau_1/T$, the state equation (equation 3.4) is determined to be as follows:

$$x_{N+1} = A_B x_N + b_B e^{j\omega NT} \tag{3.17}$$

where:

$$A_B = \begin{bmatrix} \cos(\tau_2) & -\sin(\tau_2) \\ \sin(\tau_2) & \cos(\tau_2) \end{bmatrix} \begin{bmatrix} 1 & 0 \\ \zeta & \beta \end{bmatrix}$$

$$\cdot \begin{bmatrix} \cos(\beta\tau_1) & -\sin(\beta\tau_1) \\ \sin(\beta\tau_1) & \cos(\beta\tau_1) \end{bmatrix} \begin{bmatrix} 1 & 0 \\ -\frac{\zeta}{\beta} & \frac{1}{\beta} \end{bmatrix} e^{-\zeta\tau_1}$$

$$b_B = \begin{bmatrix} \cos(\tau_2) & -\sin(\tau_2) \\ \sin(\tau_2) & \cos(\tau_2) \end{bmatrix} \begin{bmatrix} -\frac{2\zeta}{\beta} e^{-\zeta\tau_1} I_1(\tau_1) \\ 2\zeta[I_2(\tau_1) - \frac{\zeta}{\beta} I_1(\tau_1)]e^{-\zeta\tau_1} \end{bmatrix}$$

Expanding the four elements of A_B results in the following REDUCE output:

$$A_B(1,1) = (-SIN(t1*B)*SIN(t2) + SIN(t1*B)*COS(t2)*L + COS(t1*B)*COS(t2)*B)/(E^{(t1*L)}*B)$$

$$A_B(1,2) = (SIN(t1*B)*SIN(t2)*L - SIN(t1*B)*COS(t2) - SIN(t2)*COS(t1*B)*B)/(E^{(t1*L)}*B)$$

$$A_B(2,1) = (SIN(t1*B)*SIN(t2)*L + SIN(t1*B)*COS(t2) +$$

$$SIN(t2)*COS(t1*B)*B)/(E^{(t1*L)*B})$$

$$A_B(2,2) = (- SIN(t1*B)*SIN(t2) - SIN(t1*B)*COS(t2)*L$$

$$+ COS(t1*B)*COS(t2)*B)/(E^{(t1*L)*B})$$

Similarly, b_B becomes:

$$b_B(1) = ((((E^{((w*j + L)*t1 + t1*j*B)} - 1)*(w*j+L-j*B) -$$

$$E^{(t1*j*B)}*(E^{((w*j + L)*t1)} - E^{(t1*j*B)})*(w*j+L+j*B))*COS(t2)$$

$$+2*E^{((w*j + L)*t1 + t1*j*B)}*w*B - E^{(2*t1*j*B)}*w*L*j$$

$$- E^{(2*t1*j*B)}*w*B - E^{(2*t1*j*B)}*L^2 - E^{(2*t1*j*B)}*B^2$$

$$+ w*L*j - w*B + 1)*SIN(t2))*L)$$

$$/ (E^{(t1*L + t1*j*B)}*(w*j+L+j*B)*(w*j+L-j*B)*j*B)$$

$$b_B(2) = ((((E^{((w*j + L)*t1 + t1*j*B)} - 1)*(w*j+L-j*B)$$

$$- E^{(t1*j*B)}*(E^{((w*j + L)*t1)} - E^{(t1*j*B)})*(w*j+L+j*B))*SIN(t2)+$$

$$(-2*E^{((w*j + L)*t1 + t1*j*B)}*w*B + E^{(2*t1*j*B)}*w*L*j$$

$$+ E^{(2*t1*j*B)}*w*B + E^{(2*t1*j*B)} - w*L*j + w*B - 1)*COS(t2))*L)$$

$$/(E^{(t1*L + t1*j*B)}*(w*j + L + j*B)*(w*j + L - j*B)*j*B)$$

The Z-transform of equations (3.16) and (3.17) can be used to find the steady state frequency response of the sampled data system.

Let H(z) be the transfer function vector defined as follows:

$$H(z) = \begin{bmatrix} \frac{V_{LPF}(z)}{V_{IN}(z)} \\ \\ \frac{V_{BPF}(z)}{V_{IN}(z)} \end{bmatrix}$$

Then the steady state frequency response is

$$H(z)\Big|_{z = e^{j\omega T}}$$

Solving equations (3.16) and (3.17) for H(z):

CASE A:

$$H_A(z) = [zI - A_A]^{-1} b_A \qquad (3.18)$$

CASE B:

$$H_B(z) = [zI - A_B]^{-1} b_B \qquad (3.19)$$

The steady state frequency response vectors shown above (H_A and H_B) can also be expanded. Even in REDUCE output

format, these expressions are excessively long and are, therefore, presented in the appendix. The vectors H_A and H_B give the steady state frequency response of the sampled data system for both elements of the output state vector. That is, they describe the discrete time frequency response of the system with an ideal impulse sampler and ideal lowpass filter on each output. The ideal lowpass filter that follows the impulse sampler would have a cutoff frequency of half the sampling rate. This frequency response is the frequency response to a single complex input frequency, as assumed in this analysis. This does not limit the generality of the analysis since any bandlimited input can be decomposed into a finite number of complex frequencies and any linear time-varying system obeys the superposition property as long as the input frequencies are less than half of the Nyquist rate.

Since the ideal lowpass filter is non-causal and impulse sampling is practically impossible, the frequency response generated by H_A and H_B is not realizable. A close approximation can be obtained if sample and hold circuits and rather expensive reconstruction filters are used. Furthermore, the discrete time frequency response can give some insight into the performance of the filter as well as provide the intial condition values for the actual analog output to be computed in Chapter 4.

3.2 The Sampled Data Frequency Response

The REDUCE algebraic manipulation package is capable of generating a FORTRAN executable program of the expanded equations in order to investigate numerical evaluation of the manipulated equations. Such a program was created to generate plots of the steady state sampled data frequency response. This program was used to generate frequency response curves for 15 different cases (3 constant Q cases, 6 case A's and 6 case B's). These plots were then compared to indicate general tends in the distortion of the frequency response. In each case the damping factor, ζ, was set to 0.05 giving a maximum bandwidth of 0.1 rad/sec. The sampling frequency was set to 4 rad/sec (four times the maximum center frequency) so that input frequencies of up to 2 rad/sec can be used without aliasing. Note that the sampled data frequency response above 2 rad/sec no longer indicates a true frequency response. Above 2 rad/sec the input frequency is alaised and the output appears at a frequency of the difference between the input frequency and half of the sampling rate. Thus, the input frequencies and output frequencies are different making the filter unusable at these frequencies.

It was discovered that four different cases exist. These four cases are shown in Figures 7-14 for the lowpass

and bandpass outputs. In each Figure, the magnitude and phase characteristic of the filter is shown with a solid line; the ideal continuous time response is shown with a dashed line.

Figure 7 and 8 show the bandpass and lowpass responses for the constant Q case where τ_2 is zero. At low frequencies both transfer functions agree with the continuous time response almost exactly. As the input frequency is increased toward 2 rad/sec the bandpass magnitude starts to increase above the ideal response while the lowpass magnitude actually decreases below the ideal response.

Figures 9 and 10 show a second case, where a center frequency of 0.5 rad/sec and a bandwidth of 0.1 rad/sec was selected. This is a special form of case A where the bandwidth switch is always closed. In this case the bandpass filter is close to the ideal response in phase and magnitude at high frequencies but at low frequencies the response deviates greatly. In fact, the DC response is -28 dB where it should be infinitely attenuated (no DC response). The lowpass filter appears quite close to ideal at low frequencies and at high frequencies a response above the ideal is noted. Note that this result is the oposite of the first case which was shown in Figure 8.

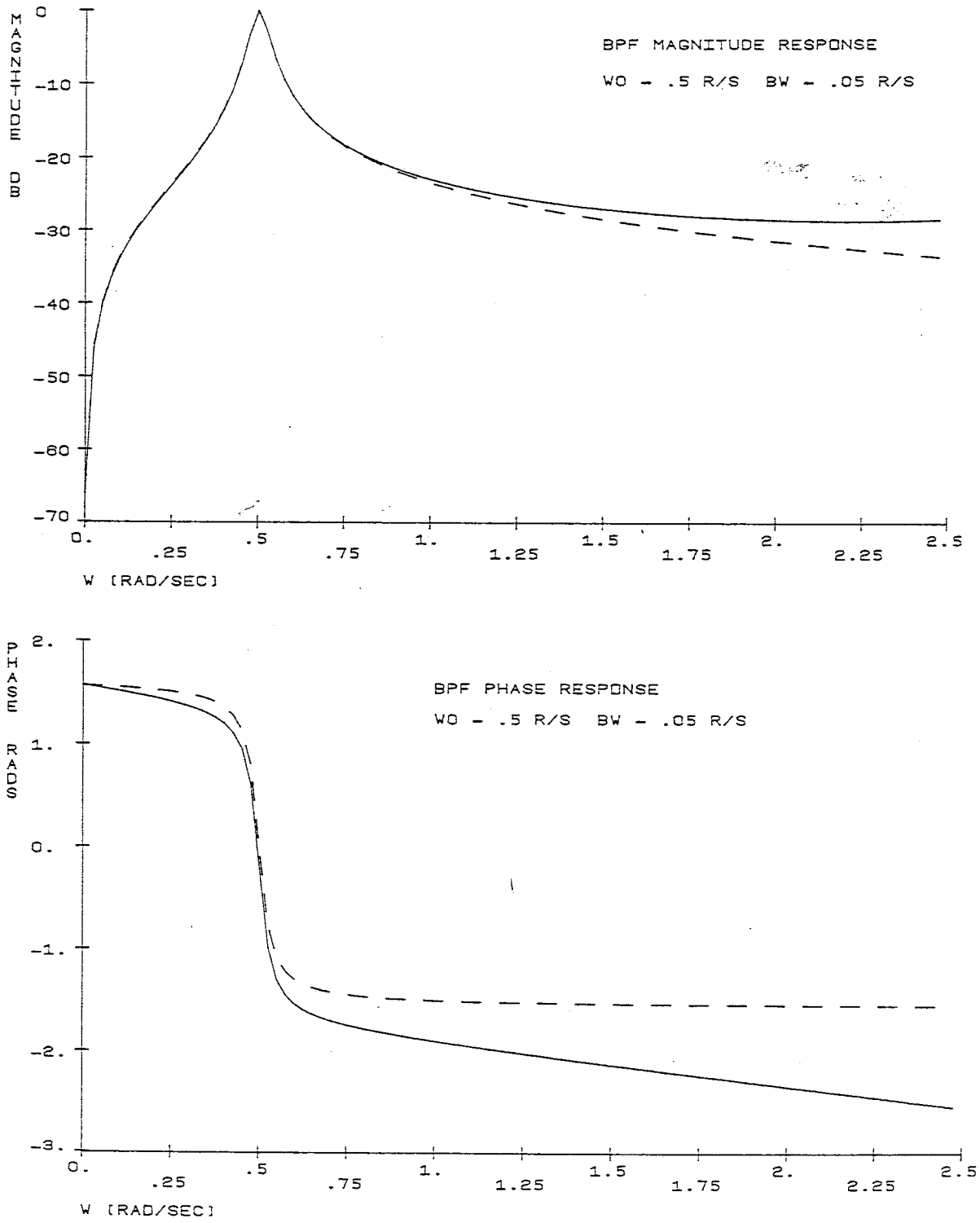

Figure 7 - Bandpass sampled data frequency response for the constant Q case.

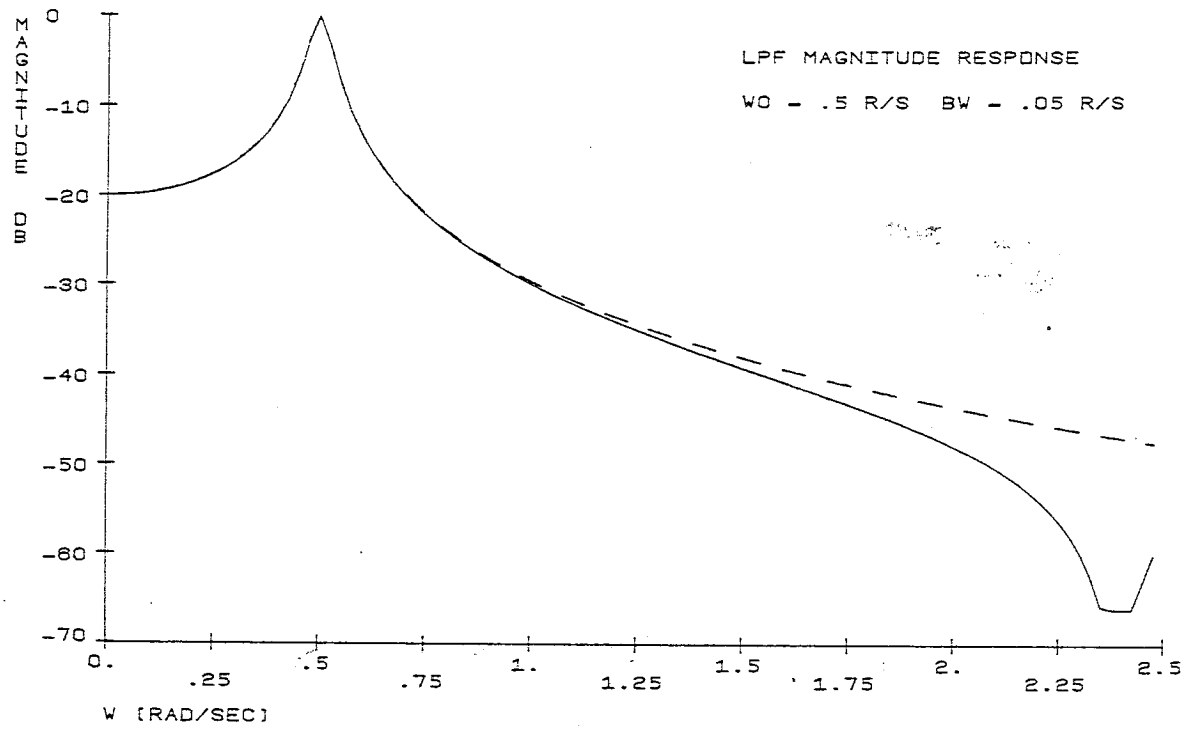

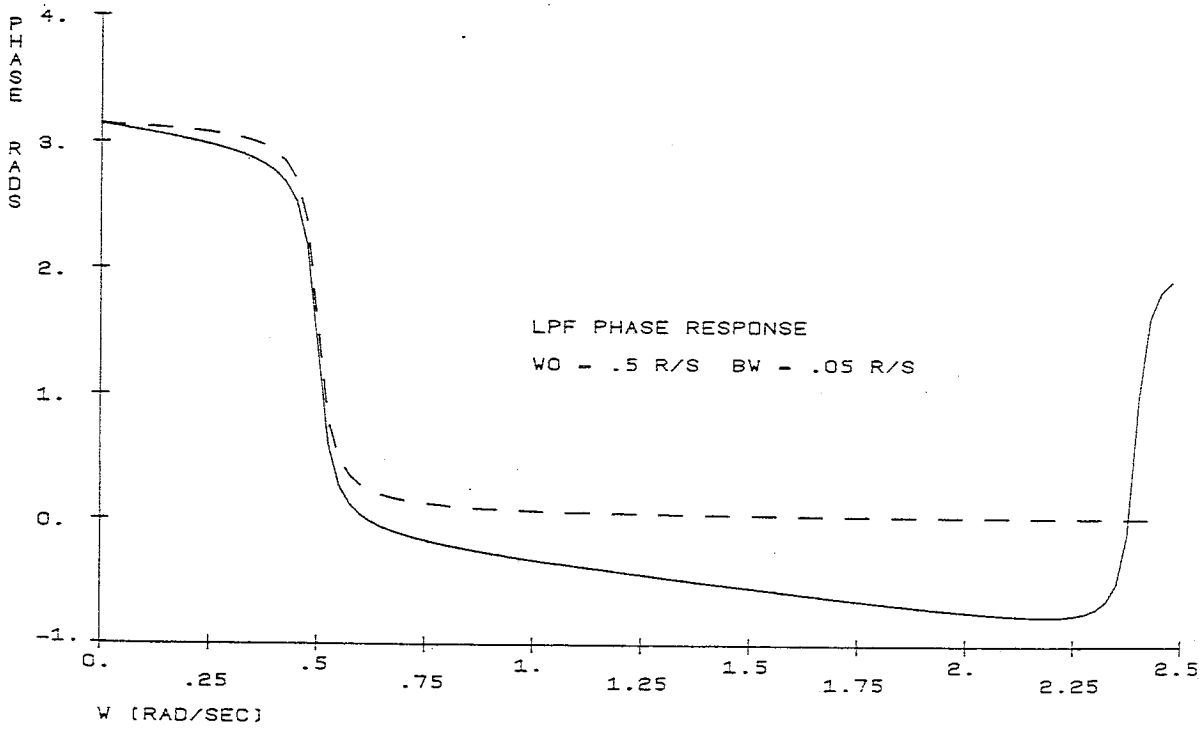

Figure 8 - Lowpass sampled data frequency response for the constant Q case.

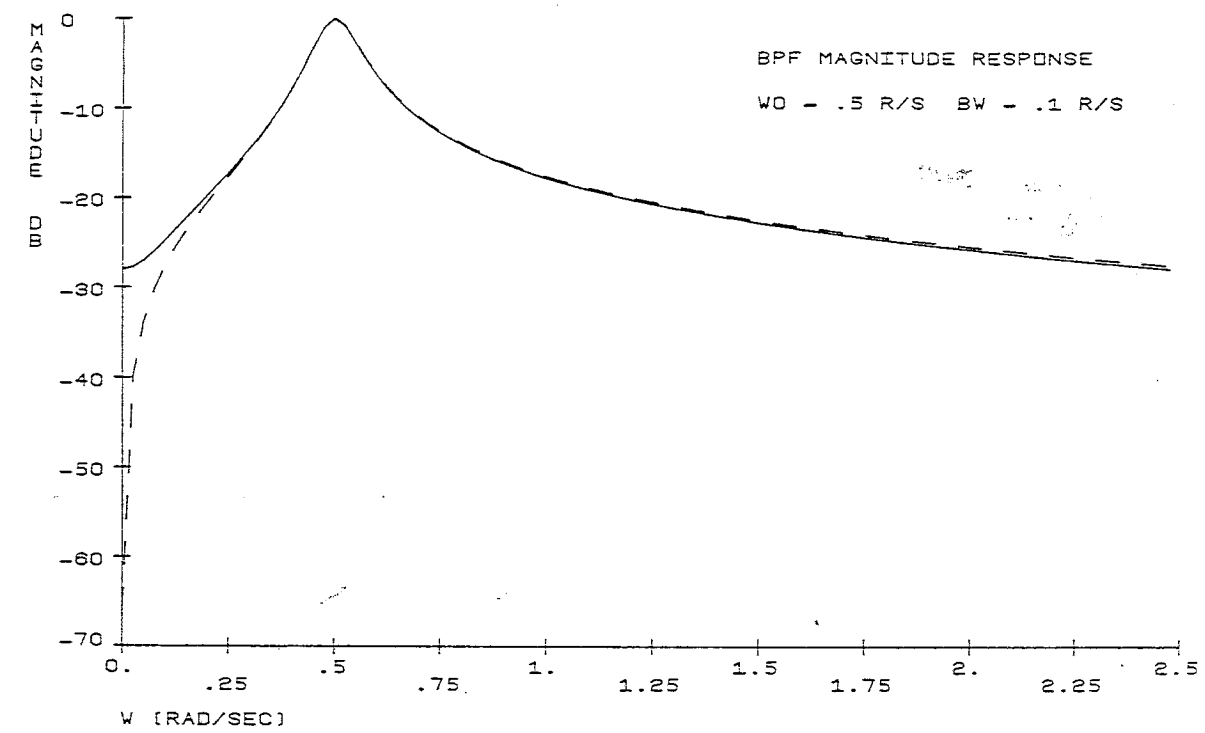

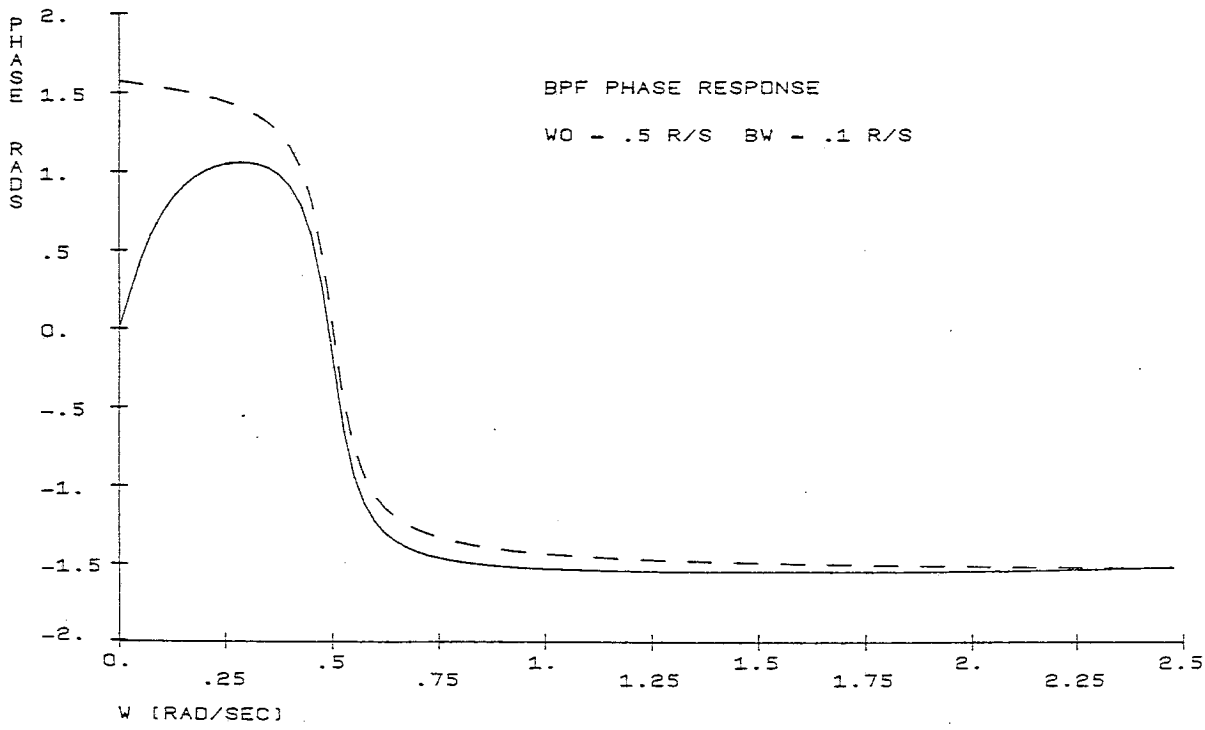

Figure 9 - Bandpass sampled data frequency response for case A.

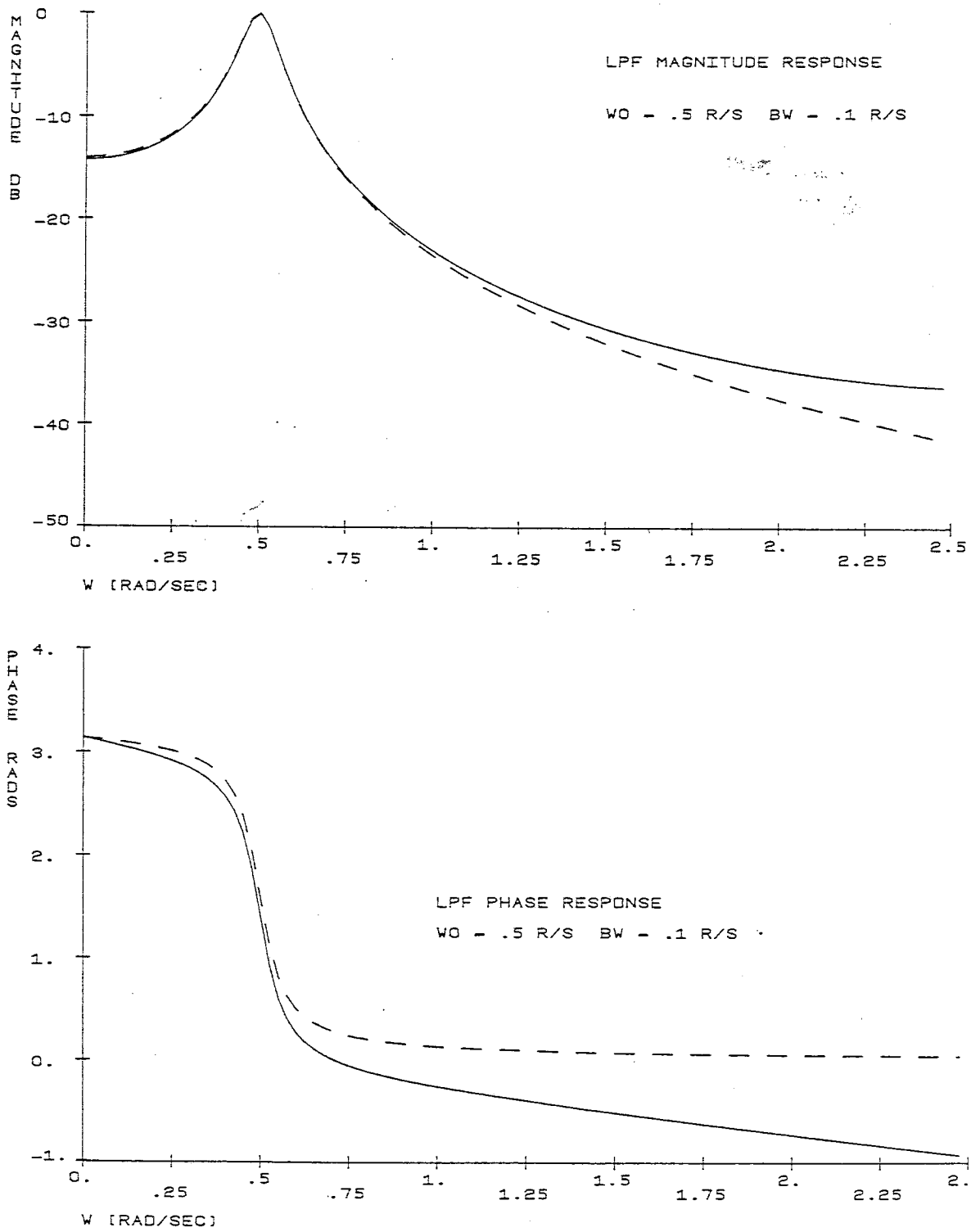

Figure 10 - Lowpass sampled data frequency response for case A.

Figures 11 and 12 show a third case where the center frequency is 1 rad/sec and the bandwidth is 0.075 rad/sec. This is an example of case B where the center frequency switches are always closed. In this case the bandpass response at both high frequencies and low frequencies is higher than the ideal response. The lowpass response is slightly higher at low frequencies and lower at high frequencies. This result is typical of all case B responses, even when the center frequency switches are not closed for the entire period.

Figures 13 and 14 show a final example where the center frequency is 0.75 rad/sec and the bandwidth is 0.025 rad/sec. It is typical of the general case A where all switches operate. In this case the overlap period is half of the switching period ($\tau_2/T = 0.5$). The bandpass response is of the same form as in the previous case but the lowpass response is higher at high frequencies instead of lower as in the previous case.

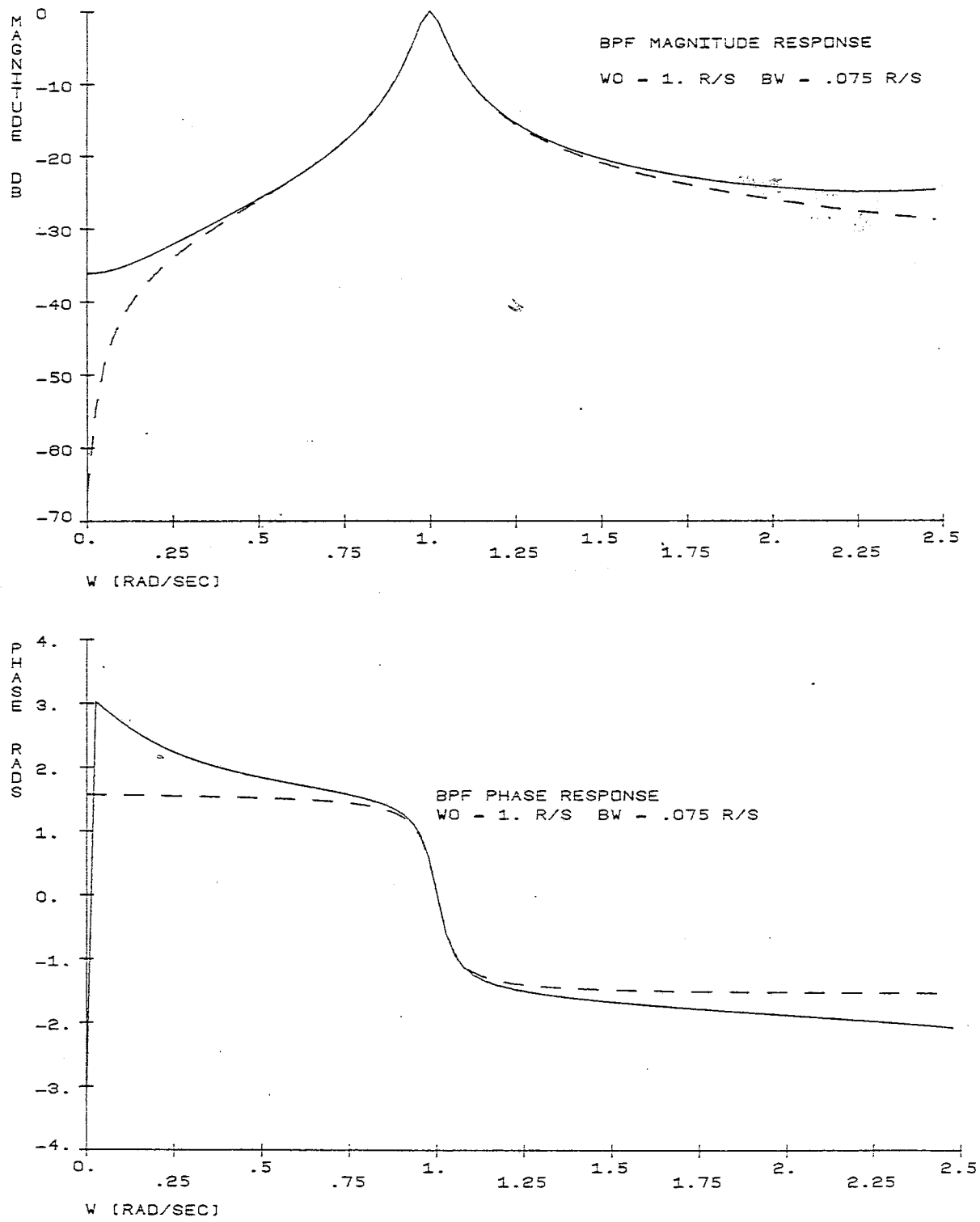

Figure 11 - Bandpass sampled data frequency response for case B.

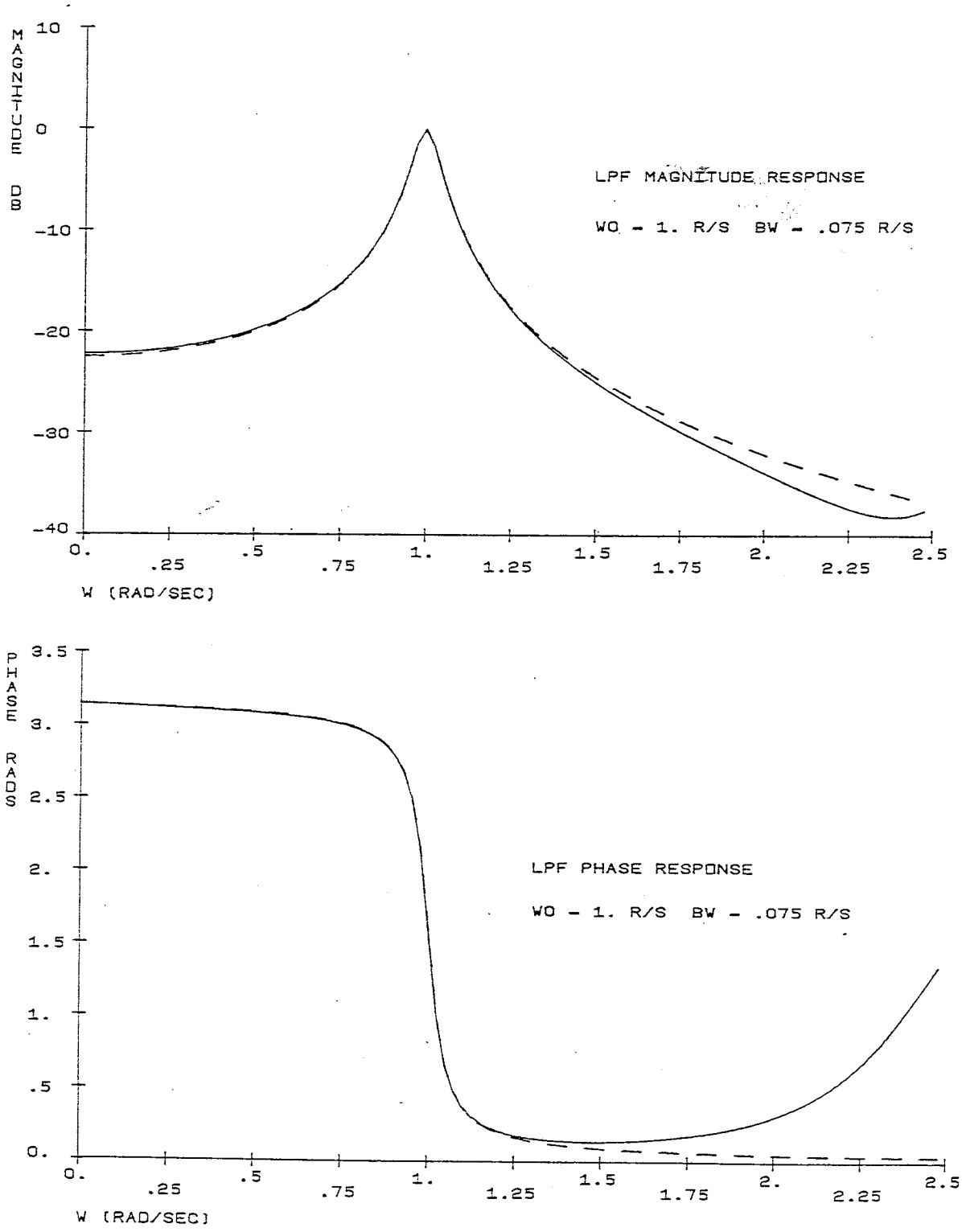

Figure 12 - Lowpass sampled data frequency response for case B.

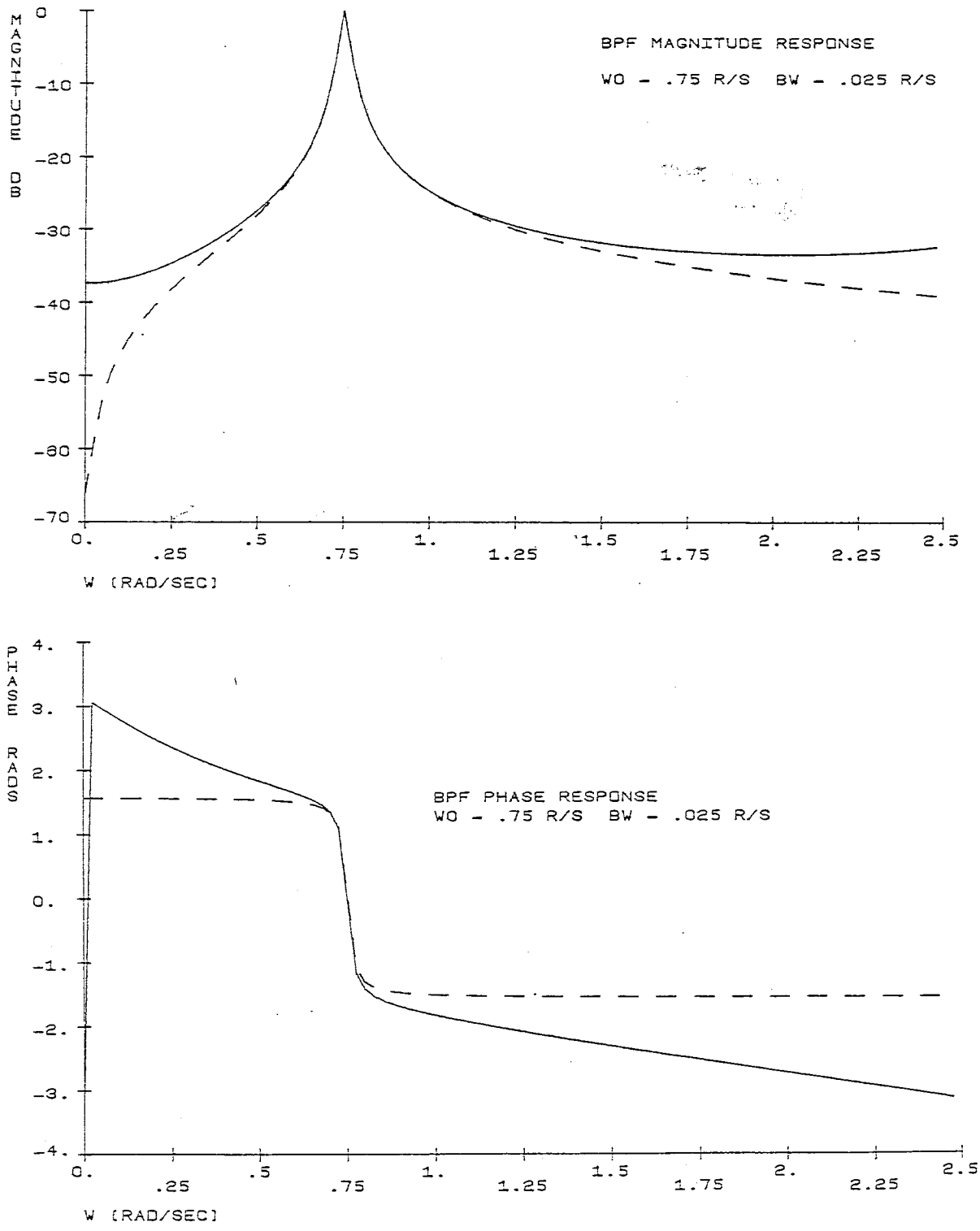

Figure 13 - Bandpass sampled data frequency response for a special case A.

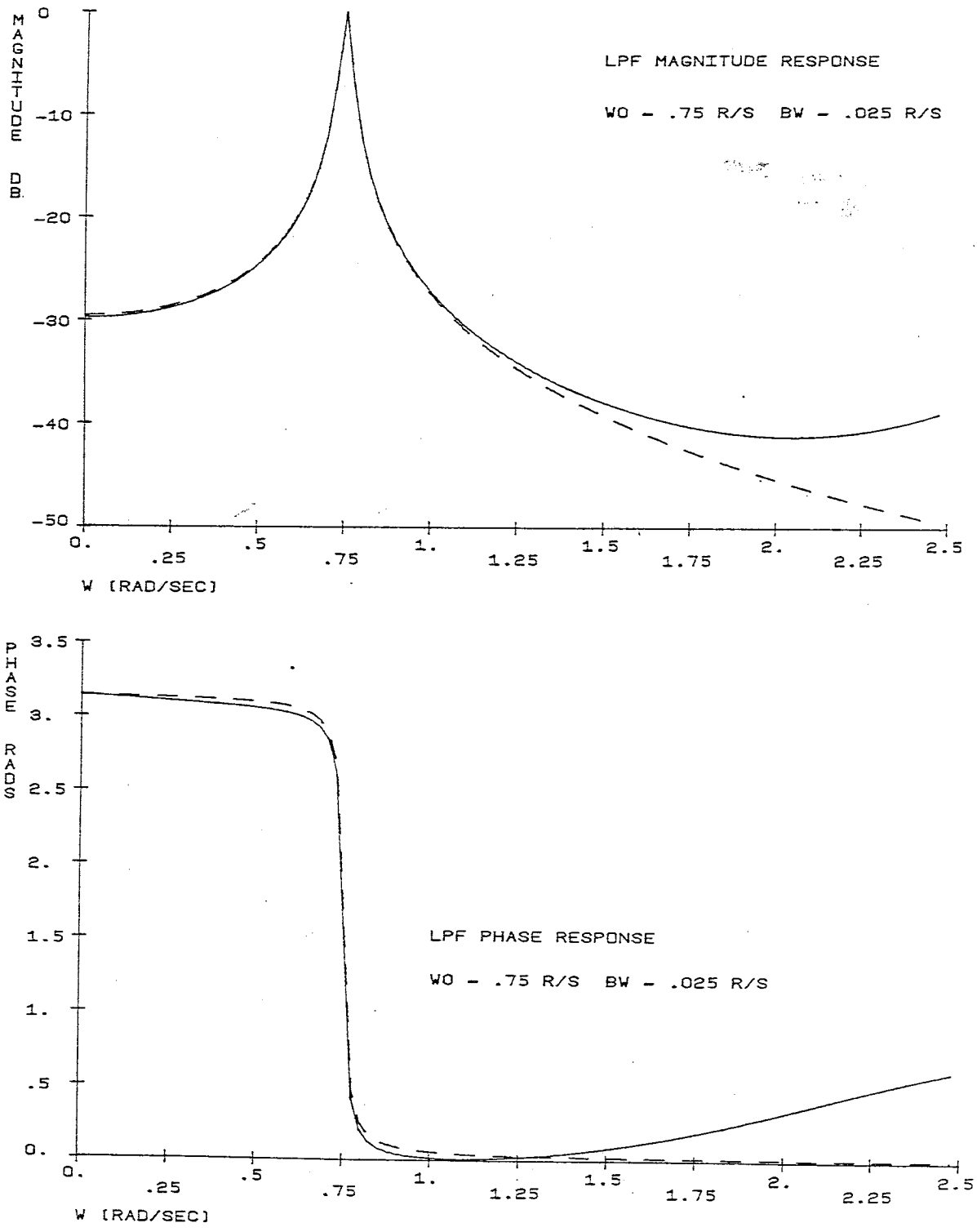

Figure 14 - Lowpass sampled data frequency response for a special case A.

The sampled data frequency response described in this section is not the most pertinent from a practical stand point. The addition of a sample and hold circuit may actually cause further distortion to the filter's transfer function and will add more high frequency components to the output. For these reasons, the actual frequency content of the output of the filter will be investigated in the next chapter.

Chapter 4 - FILTER OUTPUT FREQUENCY SPECTRUM

4.1 Frequency Spectrum of a Sampled Data System

Any analog sampled data system with a sample and hold circuit or any system with a stair-step output will cause distortion of the output signal. The distortion added by a sample and hold circuit (zero-order hold) is representive of the distortion caused by many discrete time systems. If the input, $S_{in}(f)$ of a sample and hold circuit is bandlimited to frequencies below 1/2T (1/2 of the sampling frequency) then the output spectrum, $S_{out}(f)$ is given by:

$$S_{out}(f) = \frac{\text{SIN } (f \pi T)}{f \pi T} \sum_{n=-\infty}^{\infty} S_{in}(f - n/T) \qquad (4.1)$$

where $S_{in}(f)$ is non-zero between f= -1/2T and 1/2T.

Thus, if a continuous time filter is followed by a sample and hold circuit, the transfer function is attenuated according to the above relationship (n=0). Also, high frequency distortion components are introduced near multiples of the sampling rate.

In order to quantify the distortion in a signal, the concept of total harmonic distortion (THD) has been introduced. It can be defined as follows:

$$\% \text{ THD} = \frac{100 \sqrt{\sum \left(|S(f)| \text{ above fundamental} \right)^2}}{\text{fundamental magnitude}} \qquad (4.2)$$

As shown, THD gives the percent of the RMS power in the frequencies above the fundamental compared to the fundamental. Although this does not indicate the frequency distribution of the signal, it does provide a convienent way to compare the performance of systems.

4.2 Continous Time Output of the Switched Resistor System

As indicated previously, the steady state frequency response can be used to start the system such that the response calculated by the state equation will be the continuous time output under steady state conditions. This is much easier than starting the system at an arbitrary point (say both state variables at zero) and waiting a sufficient amount of time for the zero input response to decay to zero. Not only would this require a great deal of computation but it would be difficult to judge when steady state was reached.

Using the intial conditions given by equations (3.18) and (3.19), the steady state continuous time filter output can be computed by using the state equation (3.16) for case A and (3.17) for case B. Once a state x_N is defined,

intermediate values during regions I and II can be determined by choosing suitable intermediate values of τ_1 and τ_2. Note that during region III the output state vector does not change.

A computer program was written which uses the REDUCE equivalent FORTRAN code for equations (3.16), (3.17), (3.18) and (3.19) to calculate the frequency normalized filter output every $\pi/64$ seconds. The sampling rate was again set to 4 rad/sec. The sampling period, $\pi/2$ seconds, is thus divided into 32 equal segments. A total of 1024 points are calculated which allows one cycle of a 0.125 rad/sec signal to fit in the 50.27 second time interval. A typical plot of the real part of the bandpass and lowpass filter outputs is shown in Figure 15 for an input frequency of 0.5 rad/sec. The real part shown is the filter response to a real cos(0.5t) input since the complex input frequency which was assumed can be decomposed into real (cosine) and imaginary (sine) parts. In this case B example, shown in Figure 15, $\tau_1/T = 0.25$ and $\tau_2/T = 0.5$ giving a center frequency of 0.75 rad/sec and bandwidth of 0.025 rad/sec. This output for case B can be compared to the output shown in Figure 16 for the constant Q case with $\tau_1/T = 0.5$ and input frequency of 0.25 rad/sec. It can easily seen that the constant Q outputs have less distortion than the case B outputs shown in Figure 15.

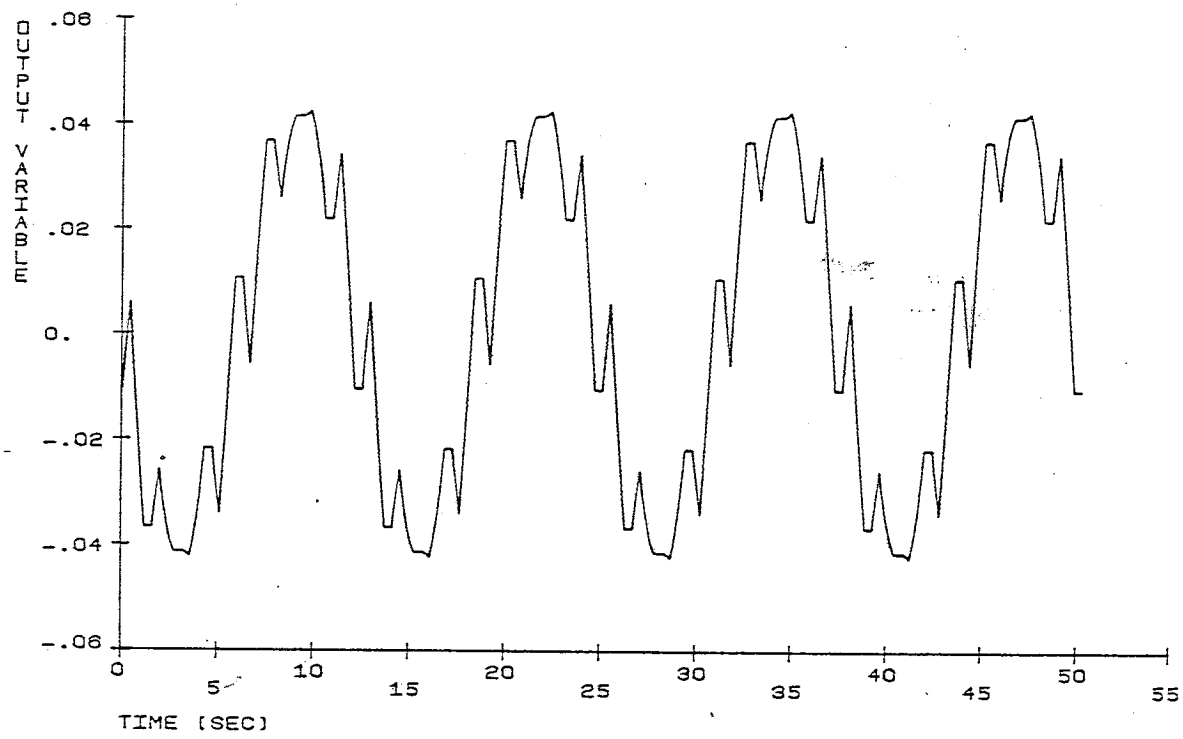

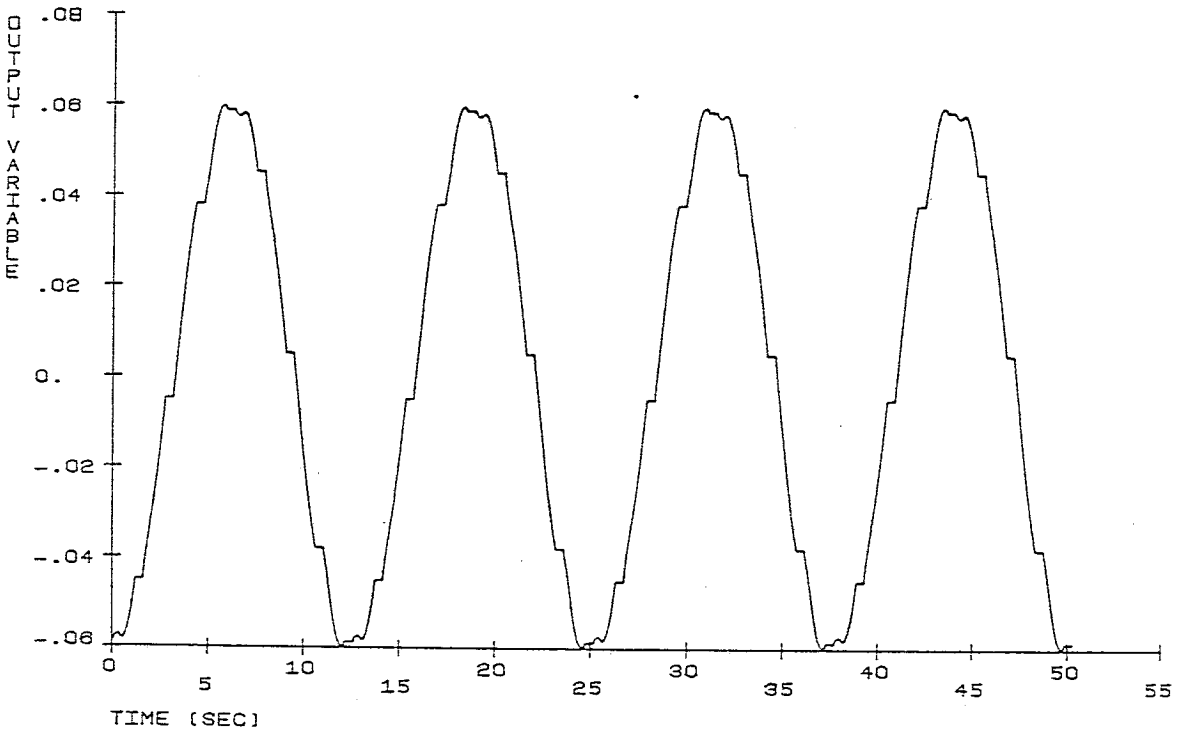

Figure 15 - (a) Bandpass continuous time output for ω_{in} = 0.5 rad/sec, ω_{o} = 0.75 rad/sec bandwidth = 0.025 rad/sec.
(b) Lowpass continuous time output for the same case as (a).

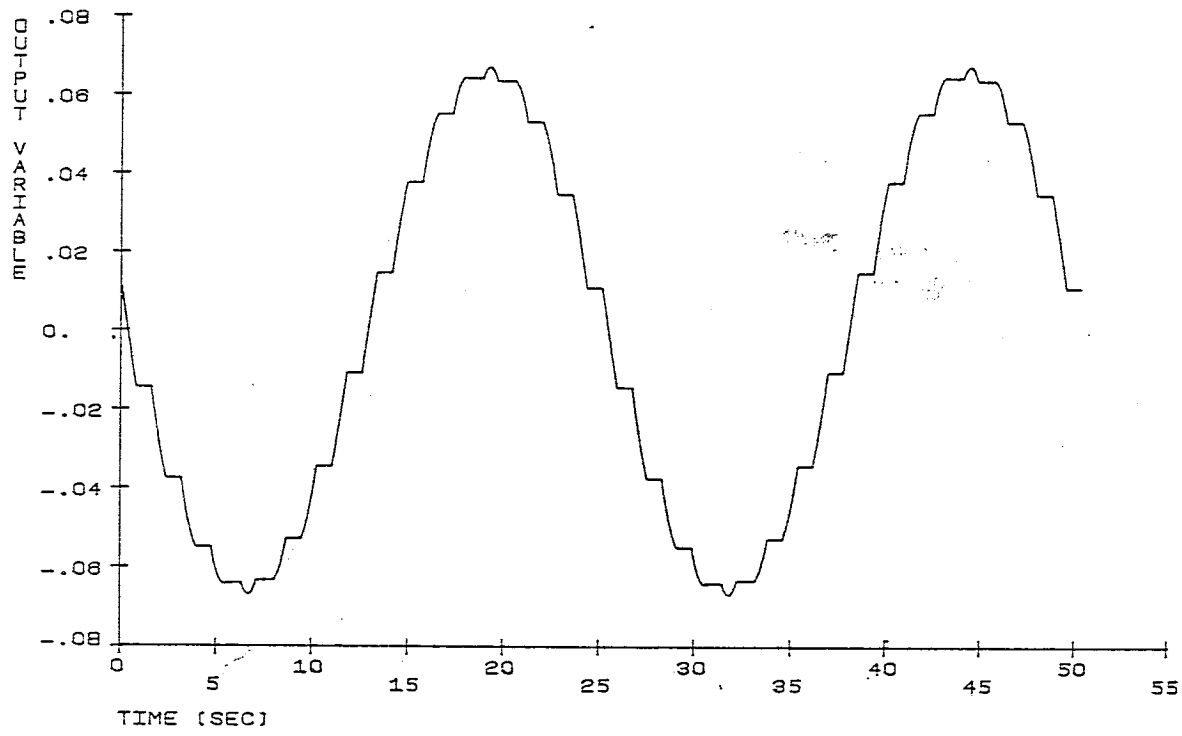

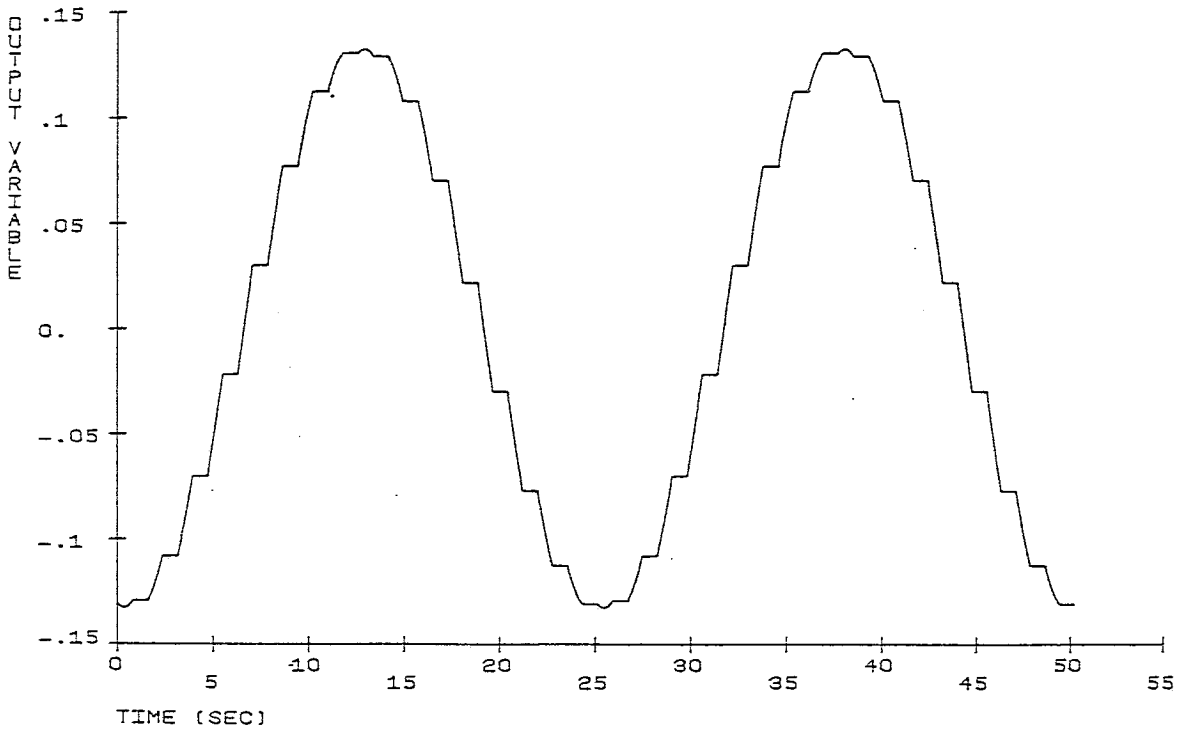

Figure 16 - (a) Bandpass continuous time output for ω_{in} = 0.25 rad/sec, ω_o = 0.5 rad/sec constant Q case.
(b) Lowpass continuous time output for the same case as (a).

4.3 Filter Distortion

The program then takes the 1024 point fast Fourier transform of the output signals to determine the frequency spectrum of the bandpass and lowpass outputs. The frequency spectrums for the cases shown in Figures 15 and 16 are shown in Figures 17 and 18 respectively. Notice that the high frequency distortion components are always at the sum and difference of the input frequency and multiples of the sampling frequency. These frequency components are actually impulse functions since only discrete frequencies exist.

If this program is run at input frequencies of 0, 0.125, 0.25, 0.375, ..., 1.875 it can be shown that in each case the distortion component frequencies as well as the fundamental frequencies are all different and do not overlap. This allows the 16 different frequency responses to be superimposed as the solid curves of Figures 19 and 20 show for the same case that was shown in Figure 17. By knowing where the output distortion components should be, the distortion of the filter to any particular input frequency can be determined. This plot gives the filter designer a great deal of information about the frequency response and output distortion of the switched resistor filter. For comparison, the same type of magnitude response for a sampled and held output is shown with a broken line.

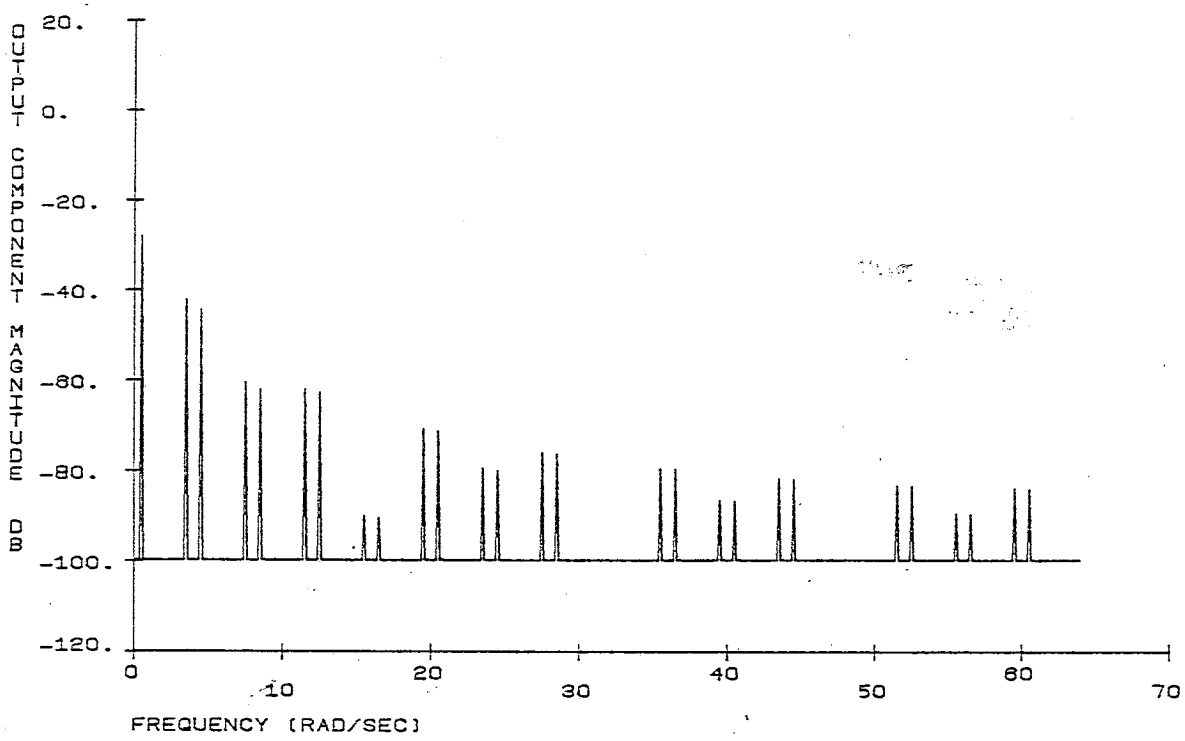

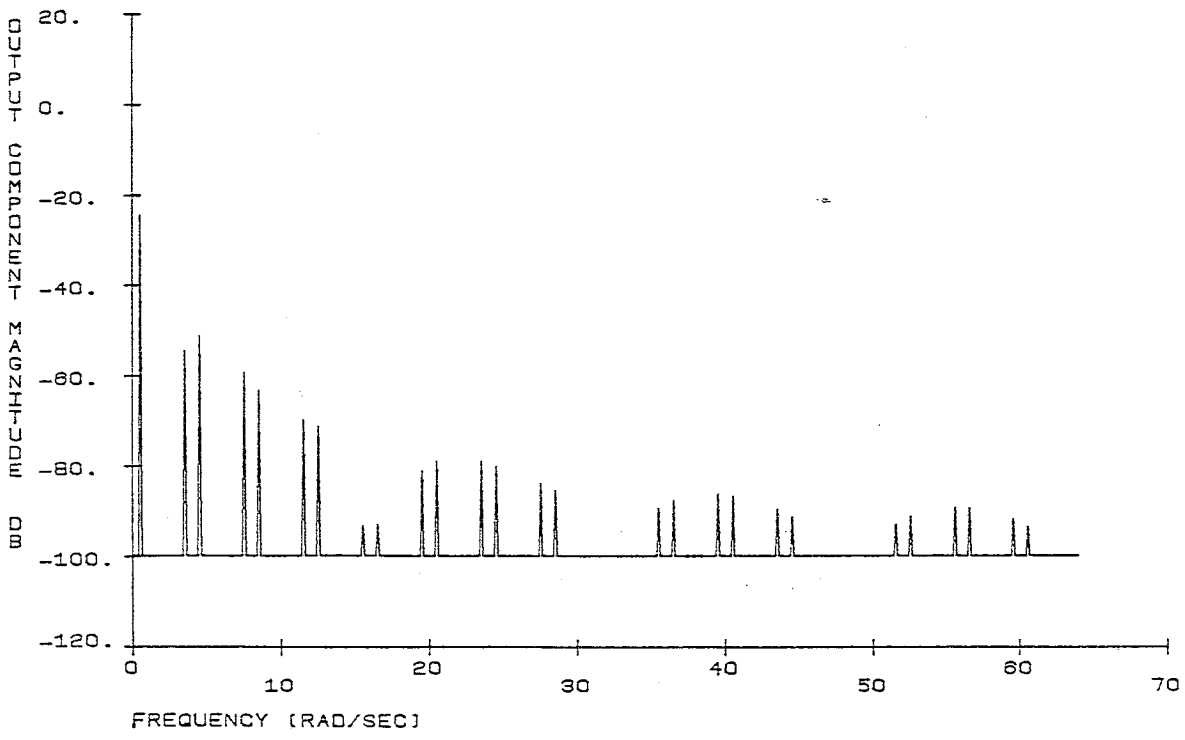

Figure 17 - (a) Bandpass output spectrum.
(same case as Figure 15(a).)
(b) Lowpass output spectrum.
(same case as Figure 15(b).)

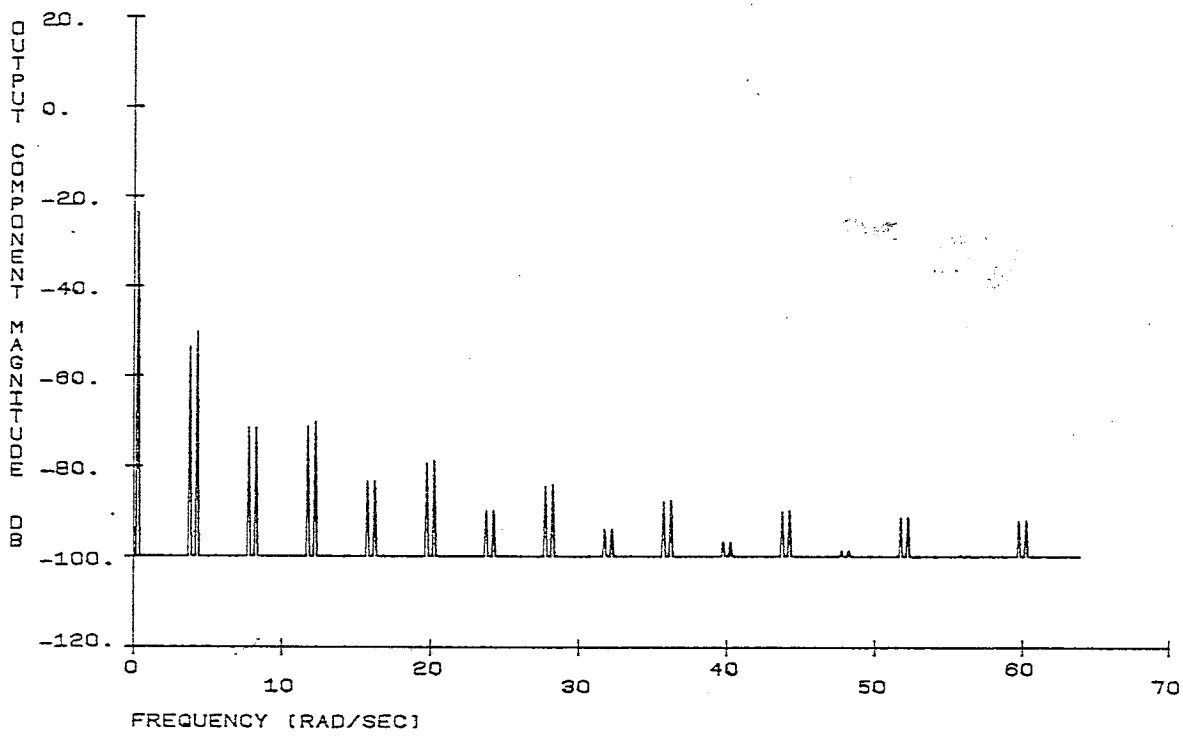

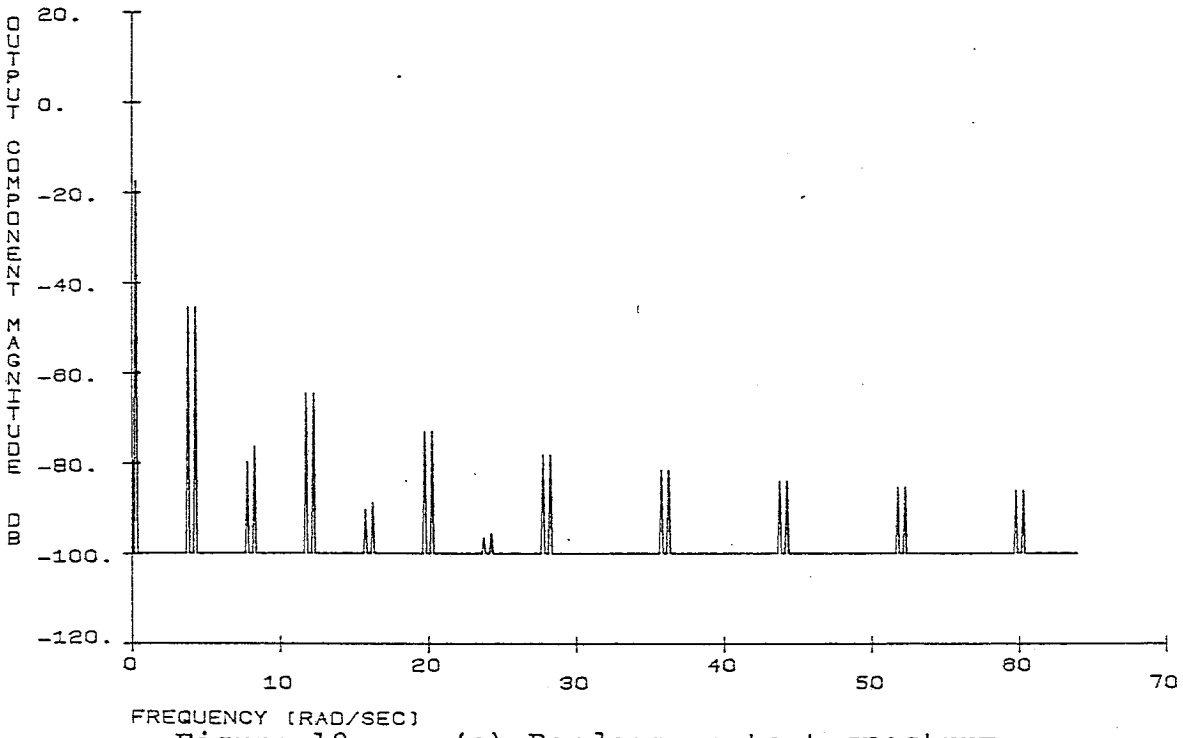

Figure 18 - (a) Bandpass output spectrum. (same case as Figure 16(a).)
(b) Lowpass output spectrum. (same case as Figure 16(b).)

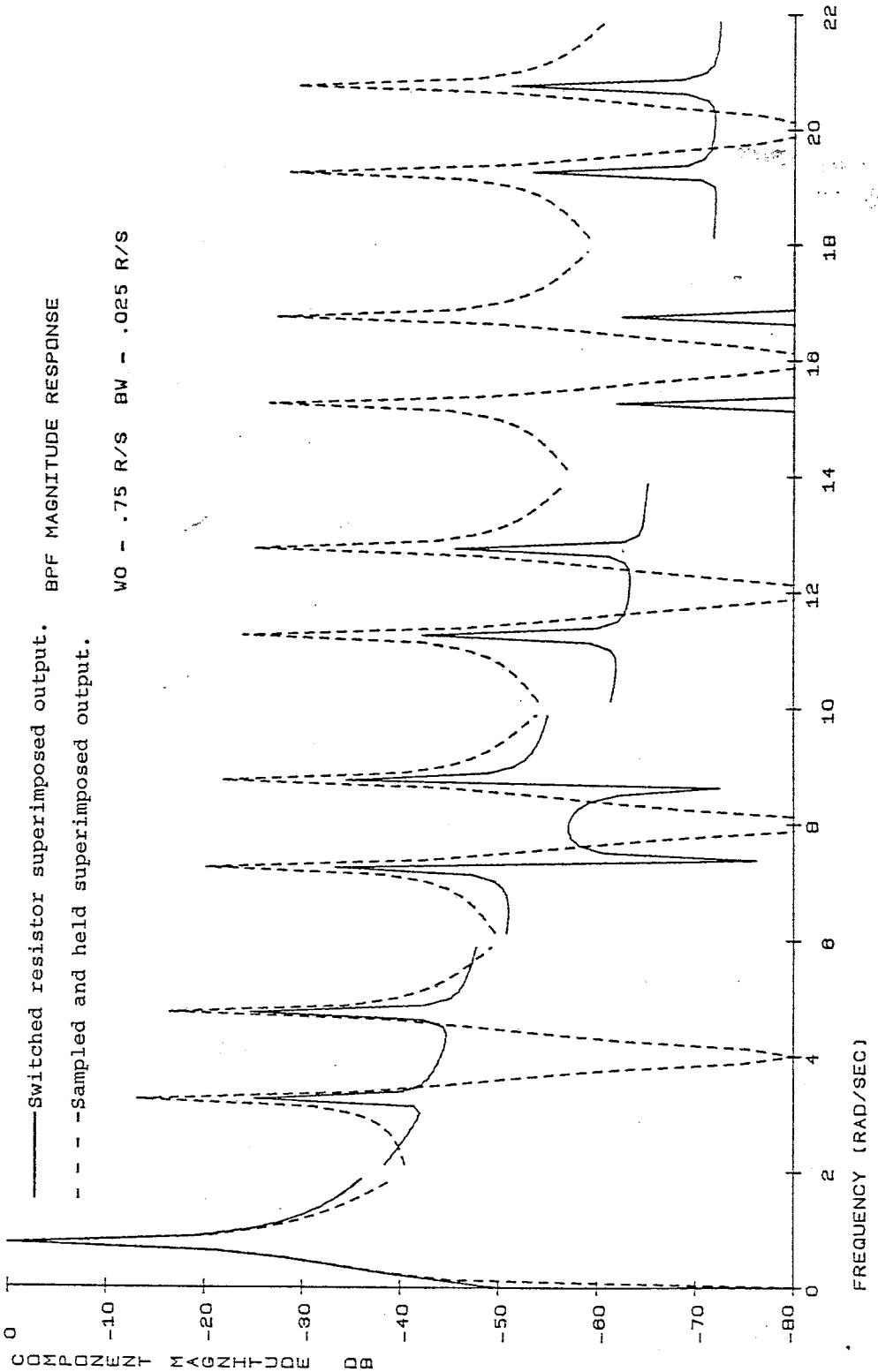

Figure 19 - Bandpass superimposed output spectrum.

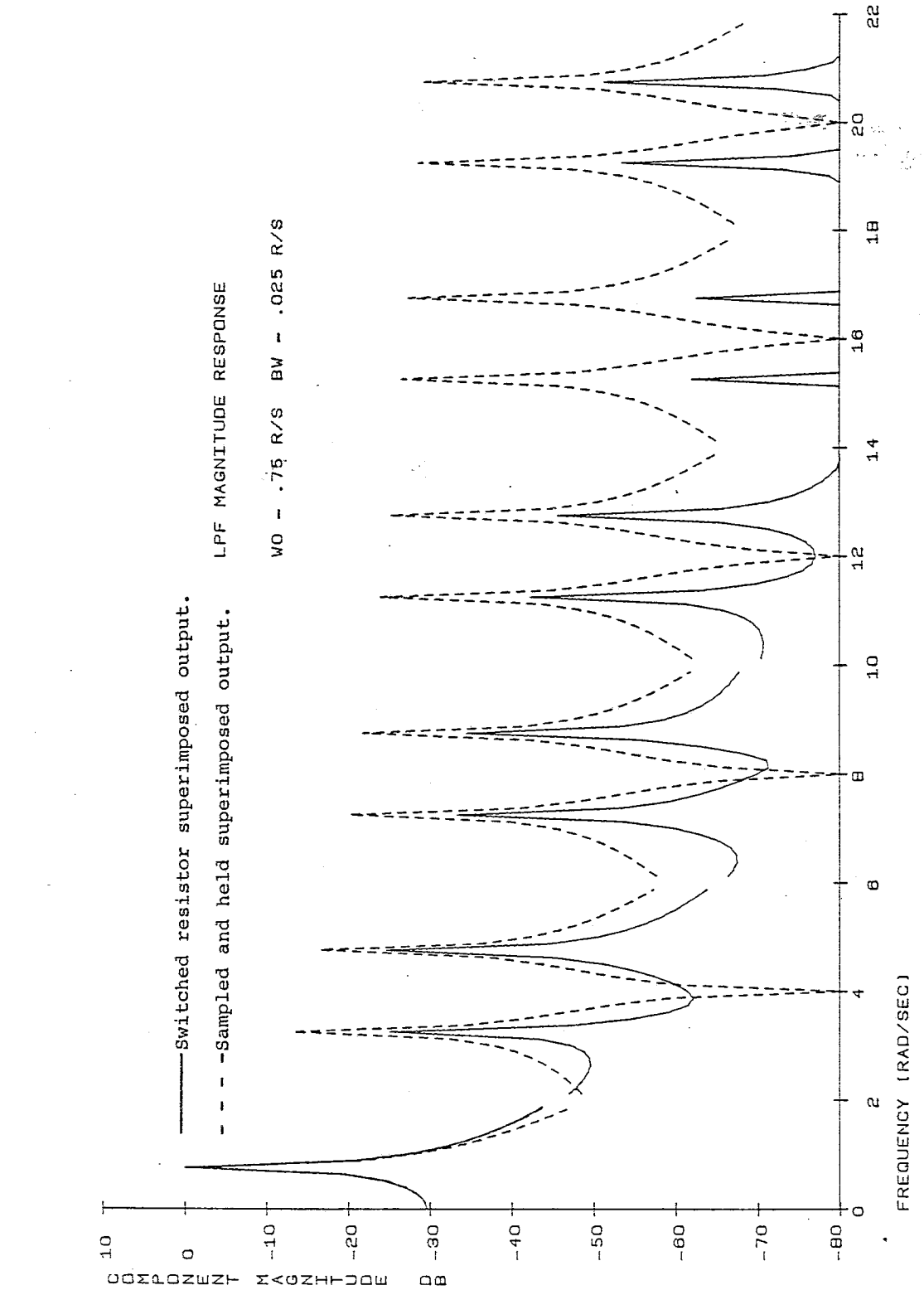

Figure 20 - Lowpass superimposed output spectrum.

Figures 21 and 22 show similar superimposed plots for the constant Q case. It can be seen that the distortion components of the constant Q switched resistor filter are always less than the sample and held values.

Using the same type of data presented in Figures 19 and 20 the total harmonic distortion as defined in equation (4.2) can be computed. Figure 23 shows plots of the THD versus input frequency for four different center frequencies in the constant Q case. The broken curve shows the distortion of the sample and held system. It can be seen that the distortion of a constant Q switched resistor filter is less than an equivalent sample and hold system (such as a switched capacitor system). Also, as the duty cycle approaches unity the distortion approaches zero.

Figures 24 and 25 show the THD of four examples of case A and case B respectively. In these cases, the distortion of the bandpass output increases when the input frequency is somewhat below the center frequency of the filter. This is not a major problem, however, since when the input frequencies are low the first distortion component is far from the fundamental frequencies of interest.

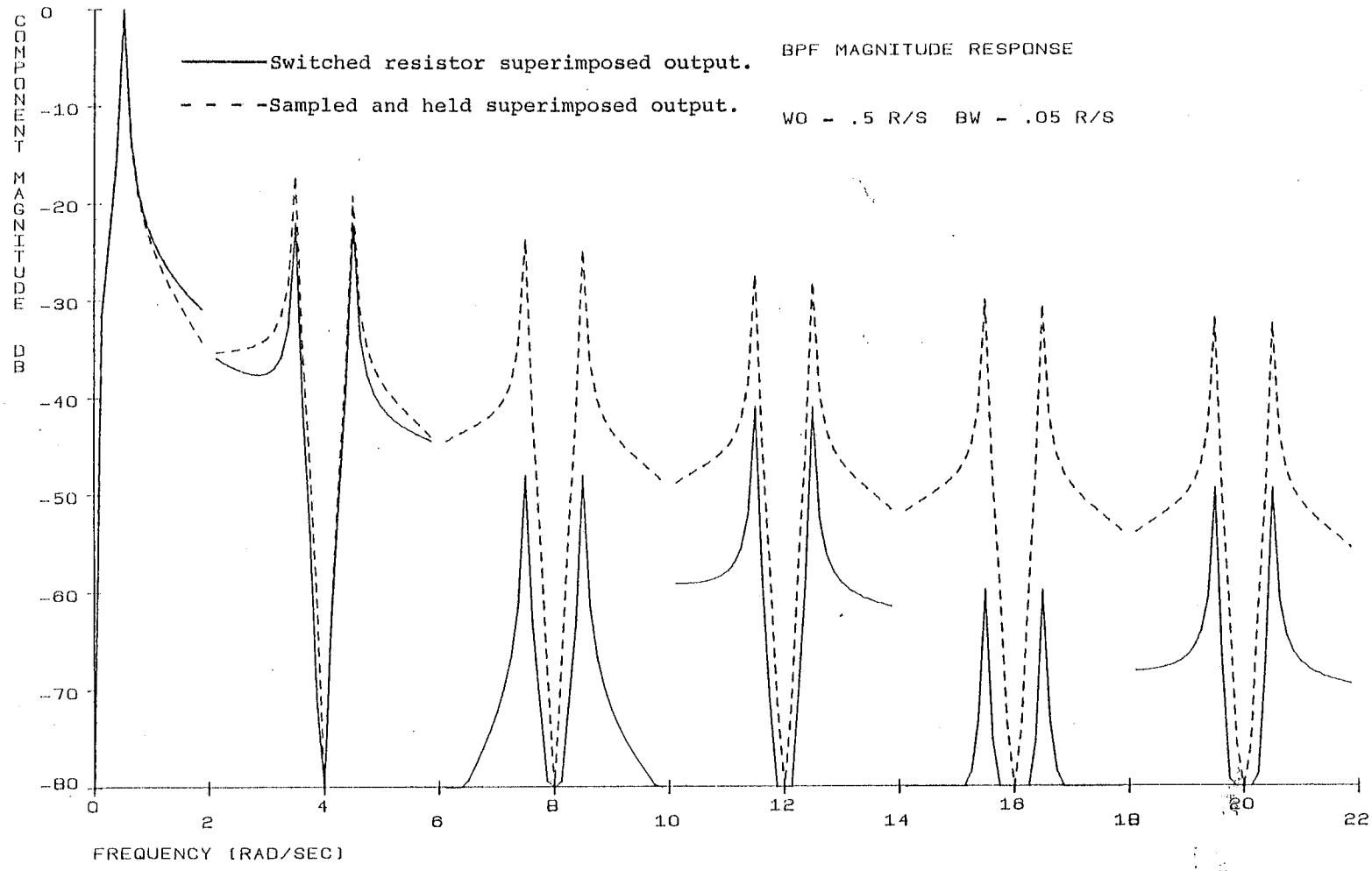

Figure 21 - Bandpass superimposed output spectrum. (constant Q case.)

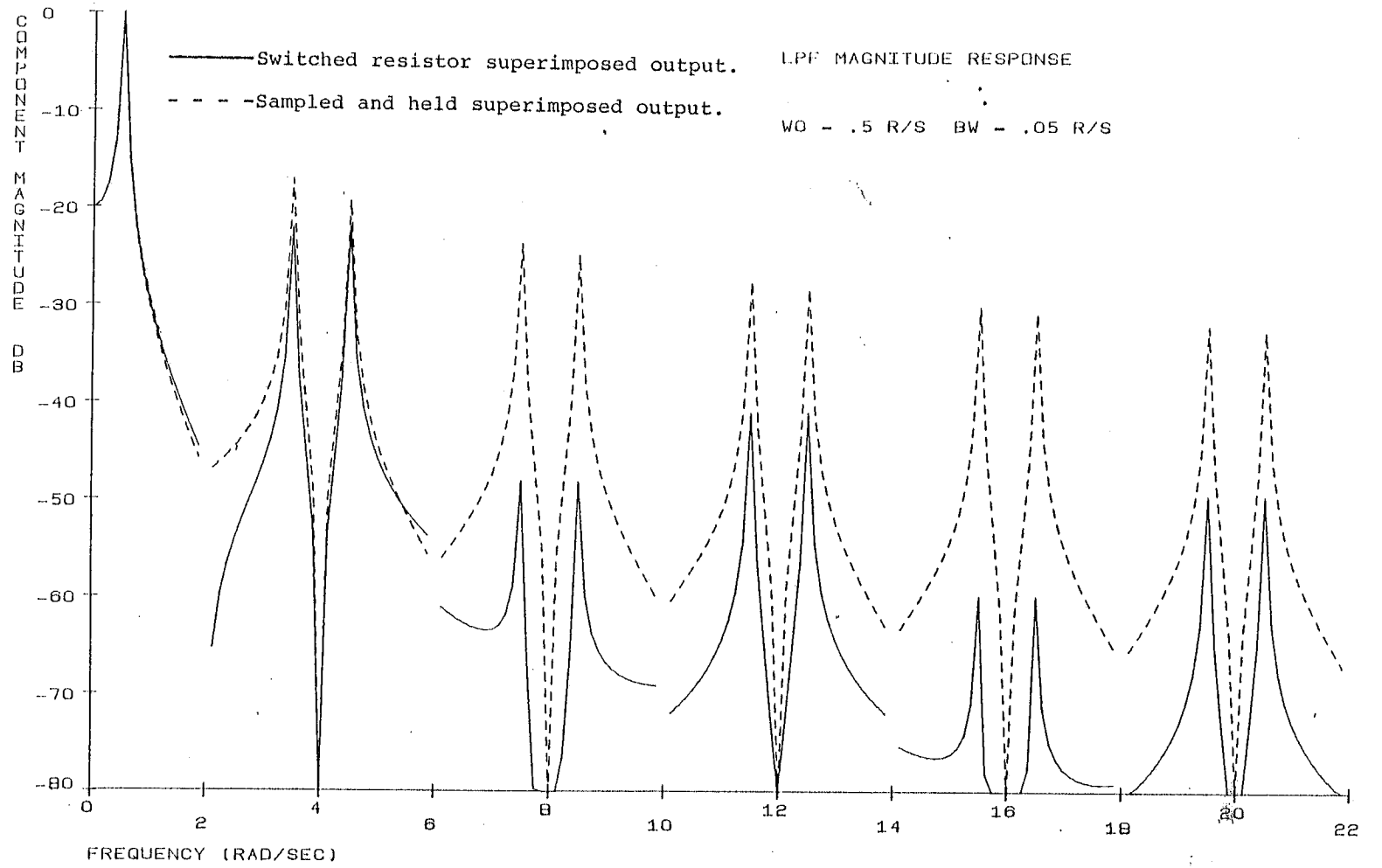

Figure 22 - Lowpass superimposed output spectrum. (constant Q case.)

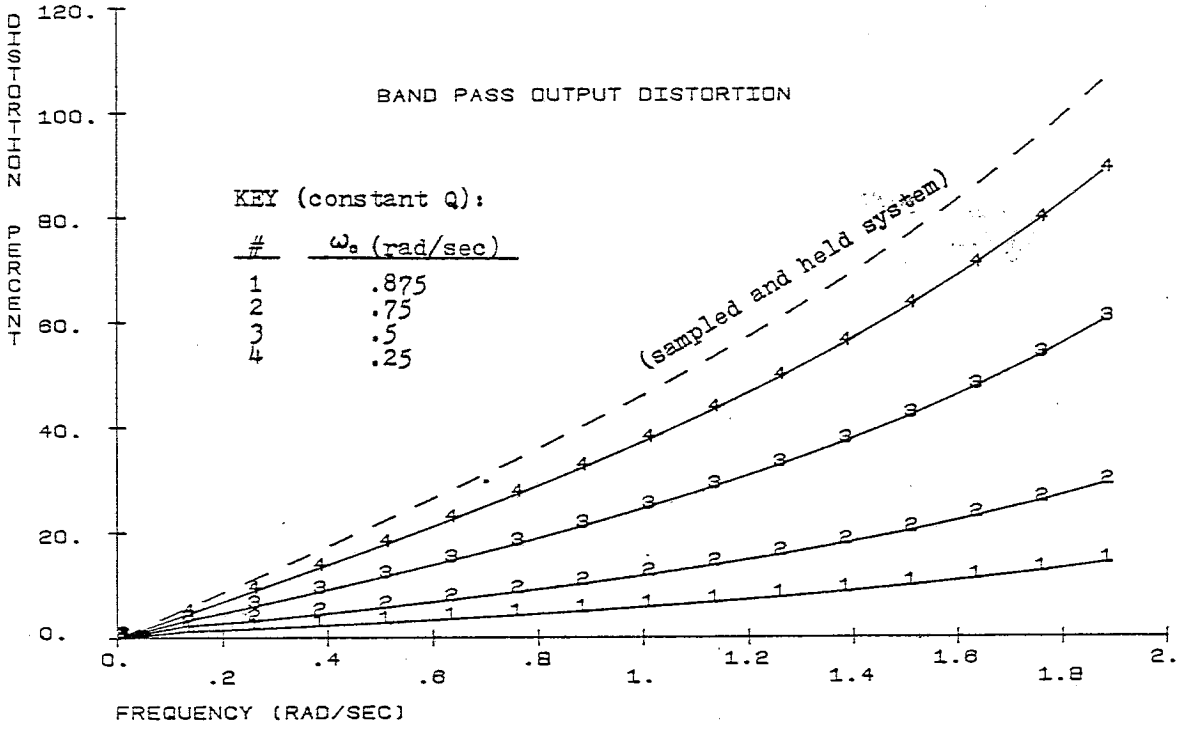

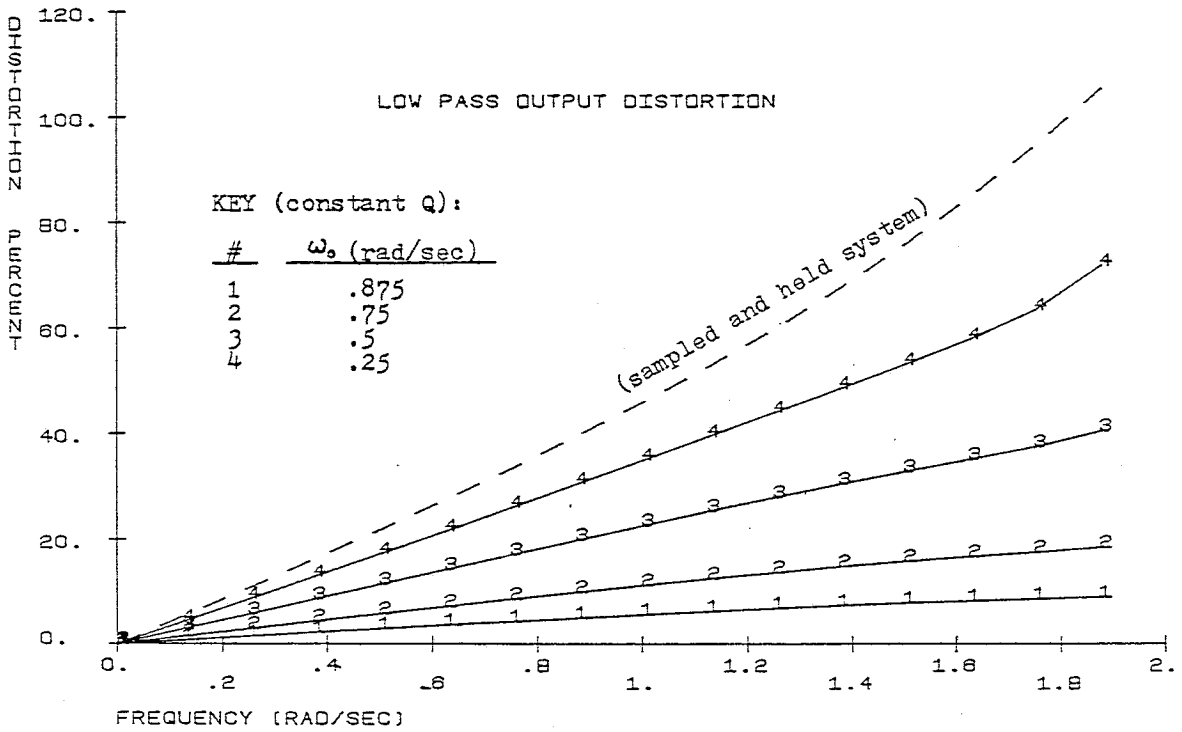

Figure 23 - Total harmonic distortion versus input frequency for constant Q case.
(a) Bandpass
(b) Lowpass

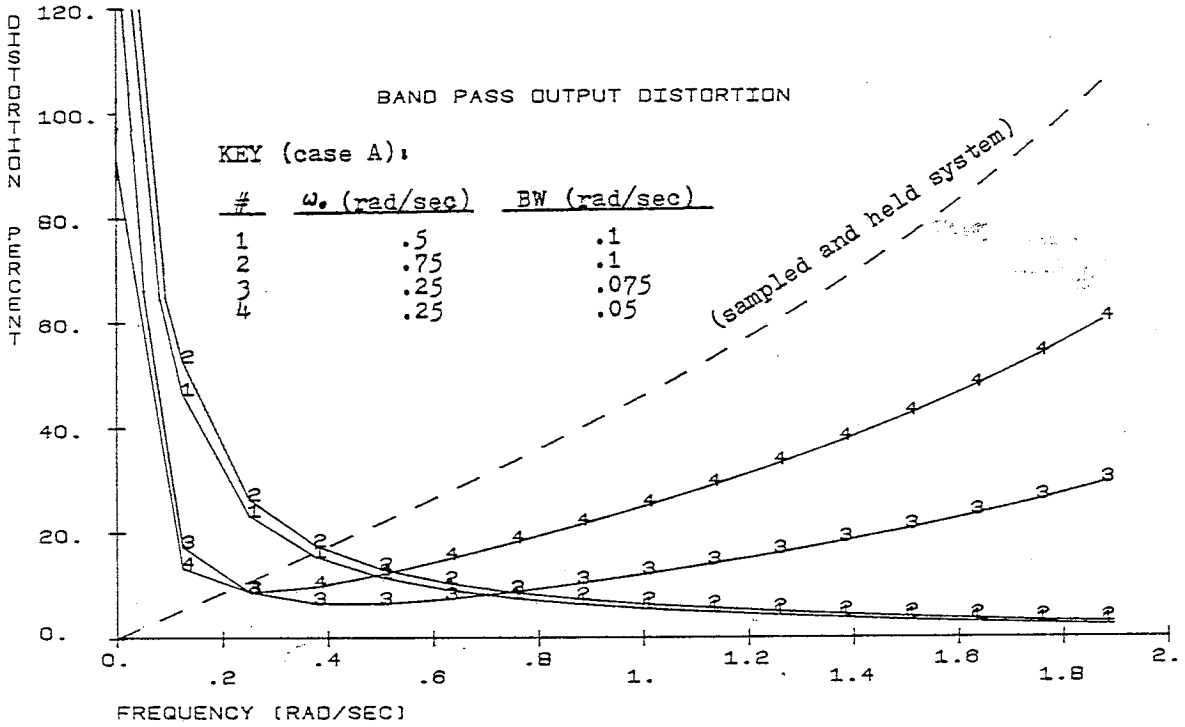

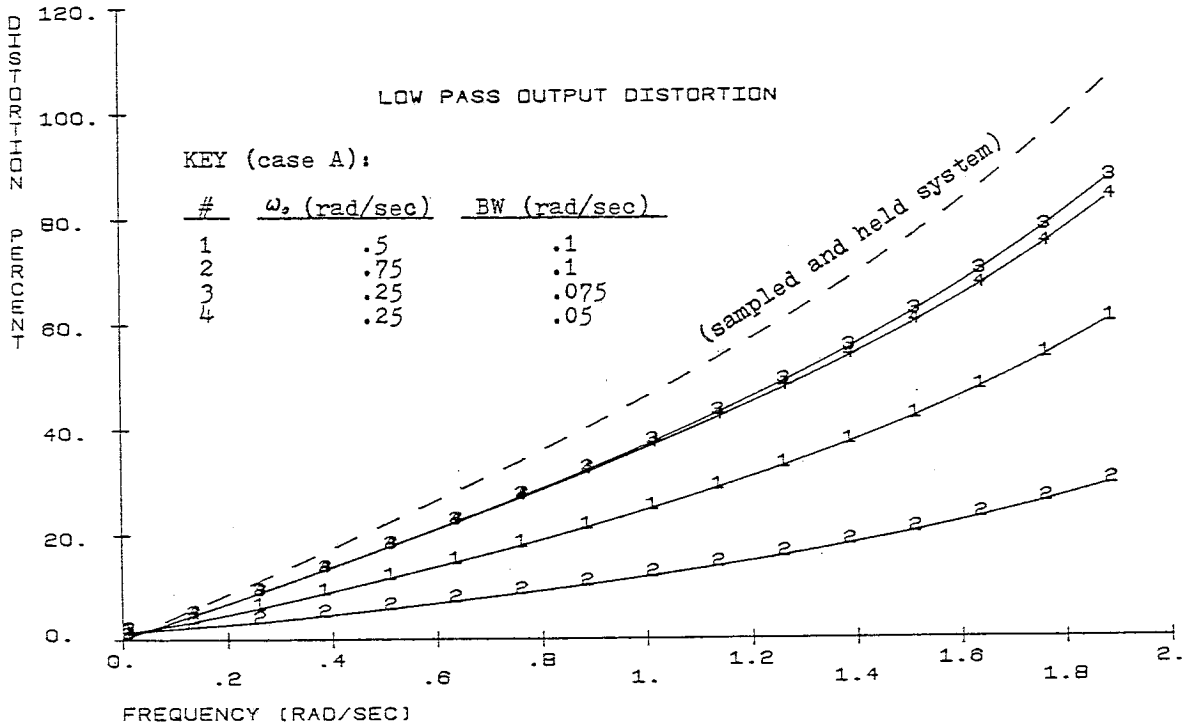

Figure 24 - Total harmonic distortion versus input frequency for case A examples.
(a) Bandpass
(b) Lowpass

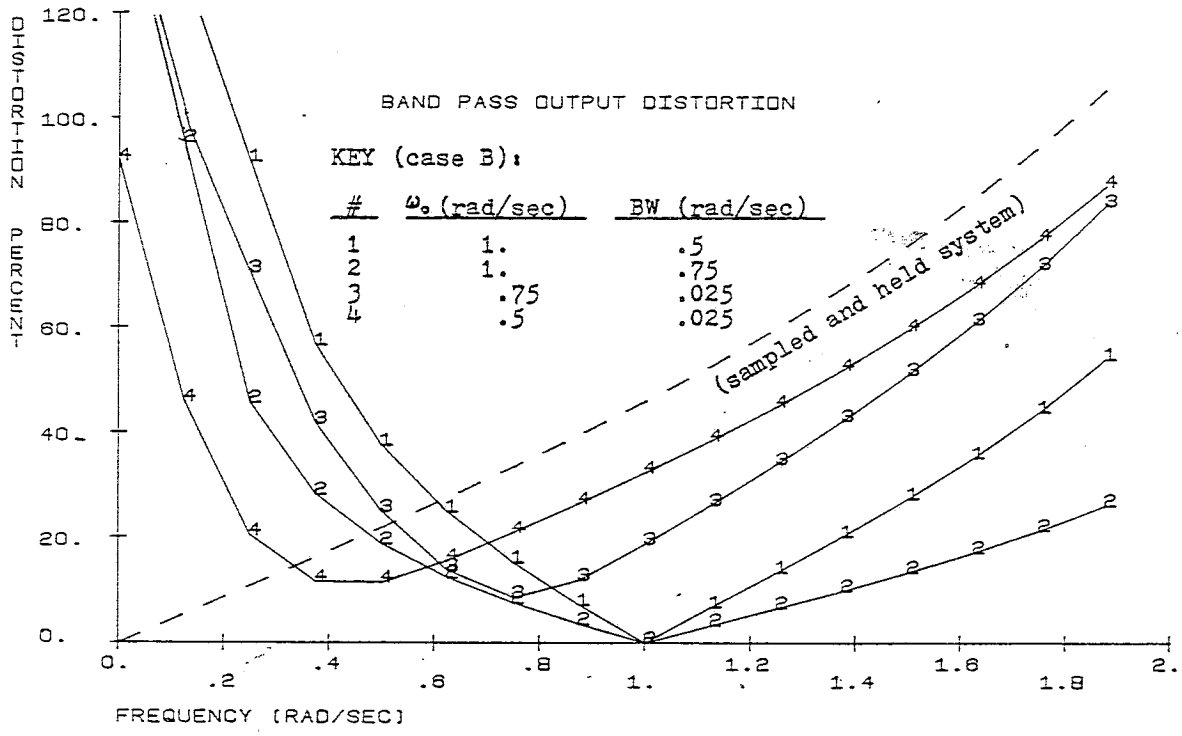

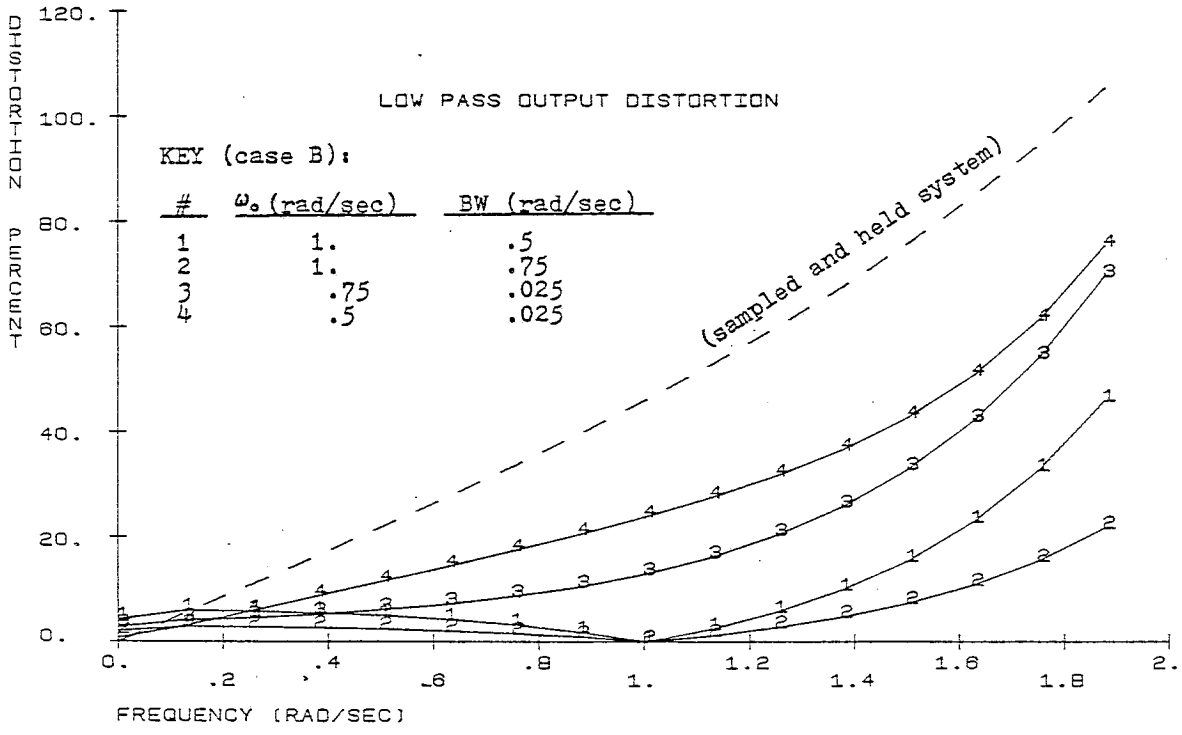

Figure 25 - Total harmonic distortion versus input frequency for case B examples..
(a) Bandpass
(b) Lowpass

4.4 Fundamental Frequency Magnitudes

As shown in previous figures, the fundamental magnitudes are different from the fundamental magnitudes obtained from a sampled data system. Figure 26 shows a detailed comparison of the fundamental magnitudes in the constant Q case obtained from the above described program (solid line) and the ideal continuous time filter transfer function (broken line).

In the constant Q case, the bandpass transfer functions seem to agree almost exactly with the ideal response. The lowpass transfer function, however, is slightly less than the ideal response at high frequencies. This high frequency deviation increases as the duty cycle is decreased. It seems that as the duty cycle decreases, the switched resistor system begins to perform more like a sampled data system.

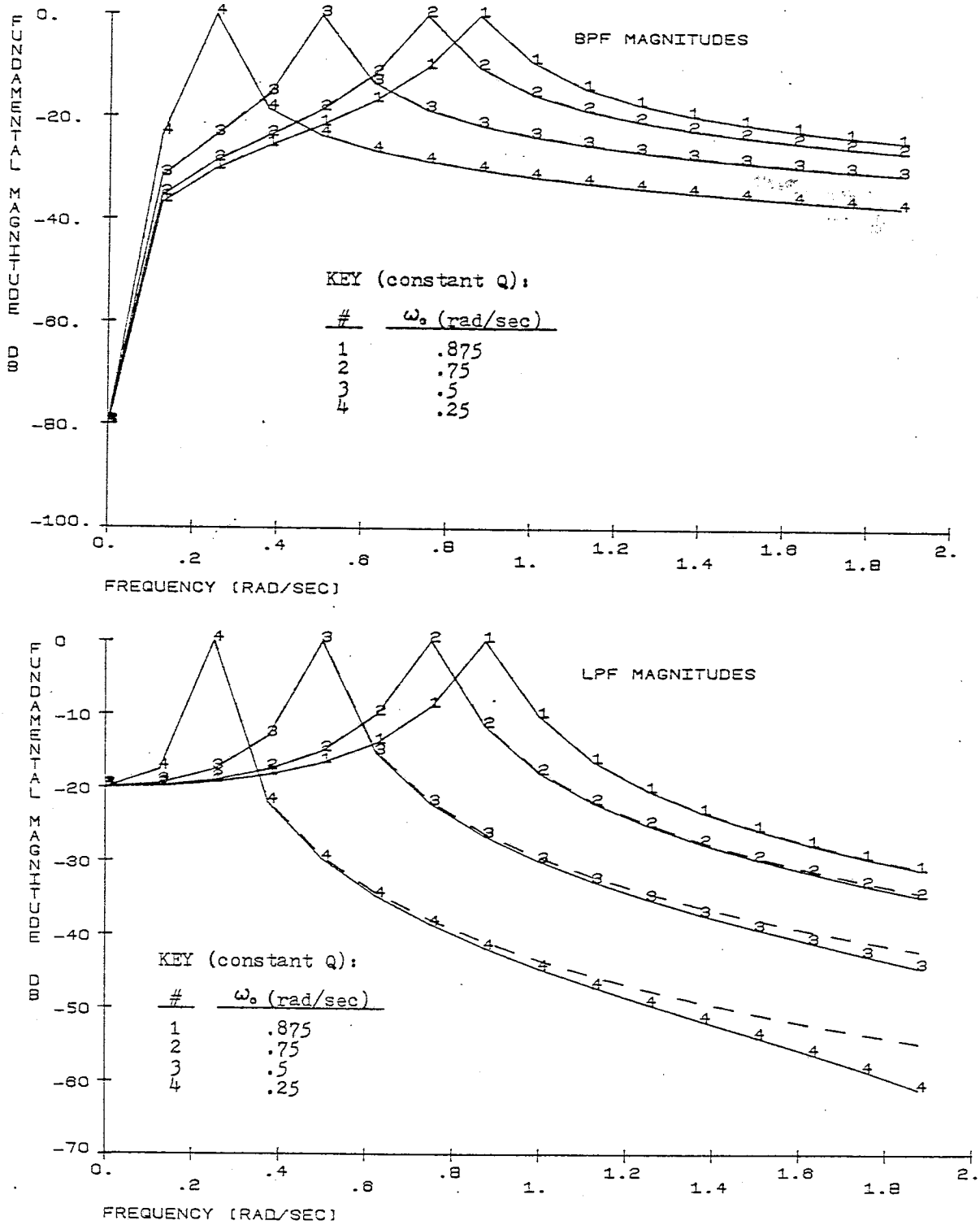

Figure 26 - Fundamental magnitudes for the constant Q cases shown in Figure 23.

Figures 27 and 28 show the fundamental amplitudes for the same non-constant Q cases shown in Figures 24 and 25. It can be seen that at low frequencies, the bandpass transfer functions deviate from ideal. The DC response for some cases is in the order of -40 dB instead of infinite attenuation. This DC response is significantly lower than that shown in the steady state frequency response curves in Chapter 3 (-28 dB in Figure 13 for example). The lowpass transfer function, on the other hand, is quite close to the ideal response.

Overall, the frequency response of the switched resistor system is much closer to the ideal continuous time system than the sampled data system. Furthermore, the output distortion of the switched resistor system may make the output filter requirements less stringent than the required output filter for an equivalent sampled data filter. This would indicate that sample and hold circuits on the filter outputs are neither desirable nor necessary.

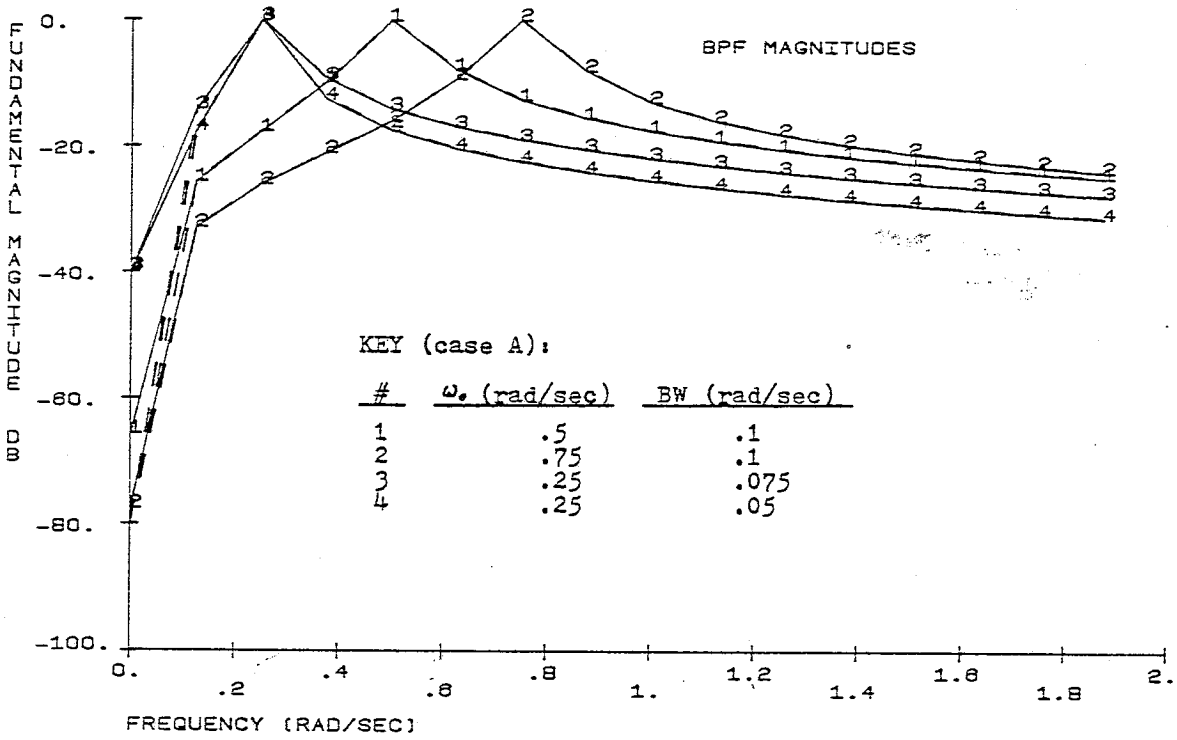

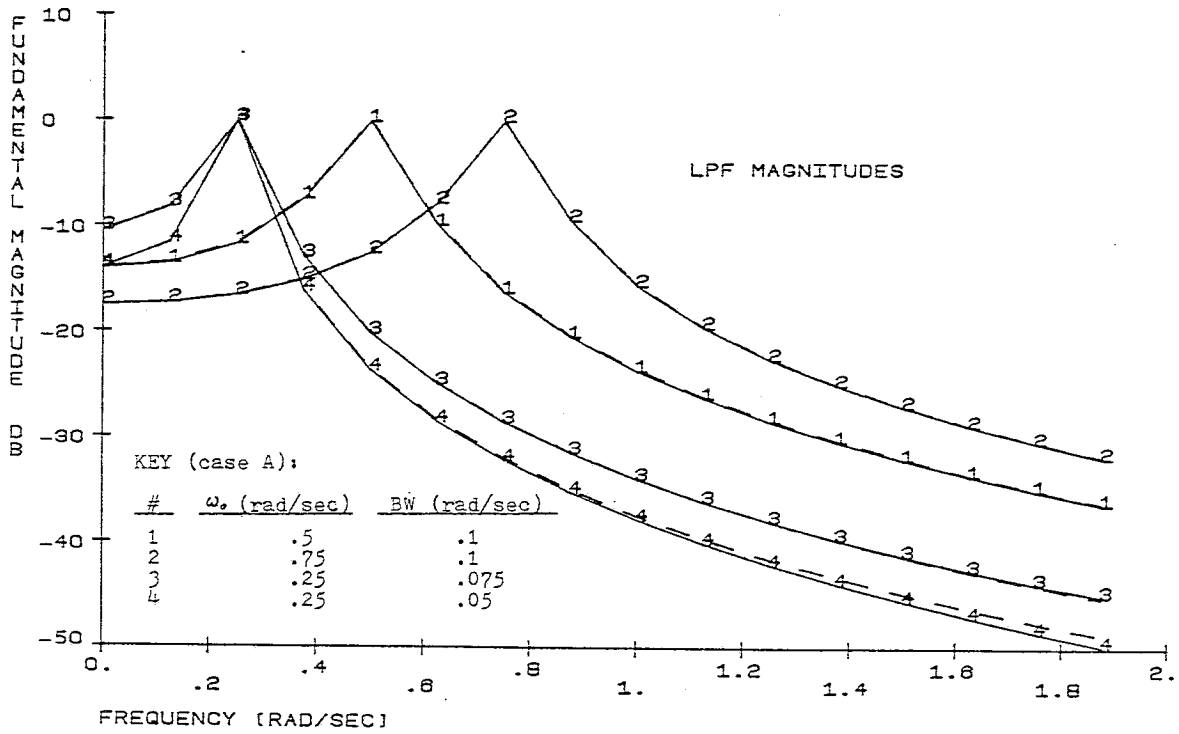

Figure 27 - Fundamental magnitudes for the same case A examples shown in Figure 24.
(a) Bandpass
(b) Lowpass

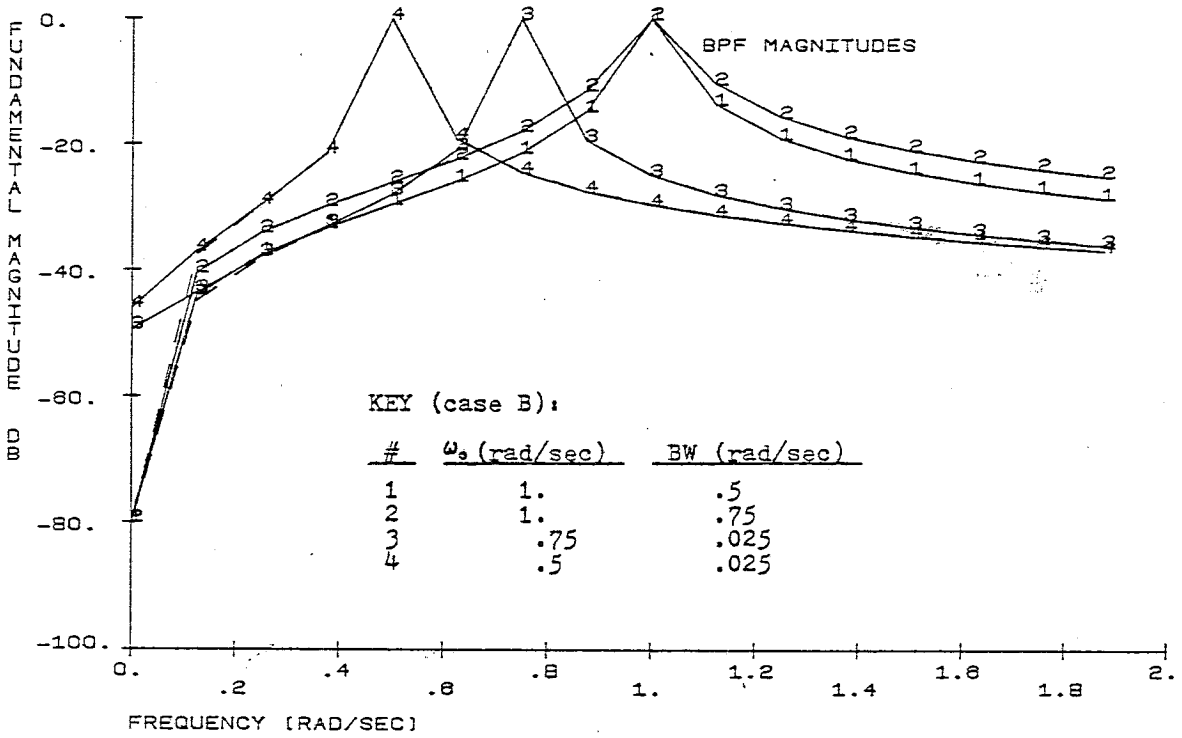

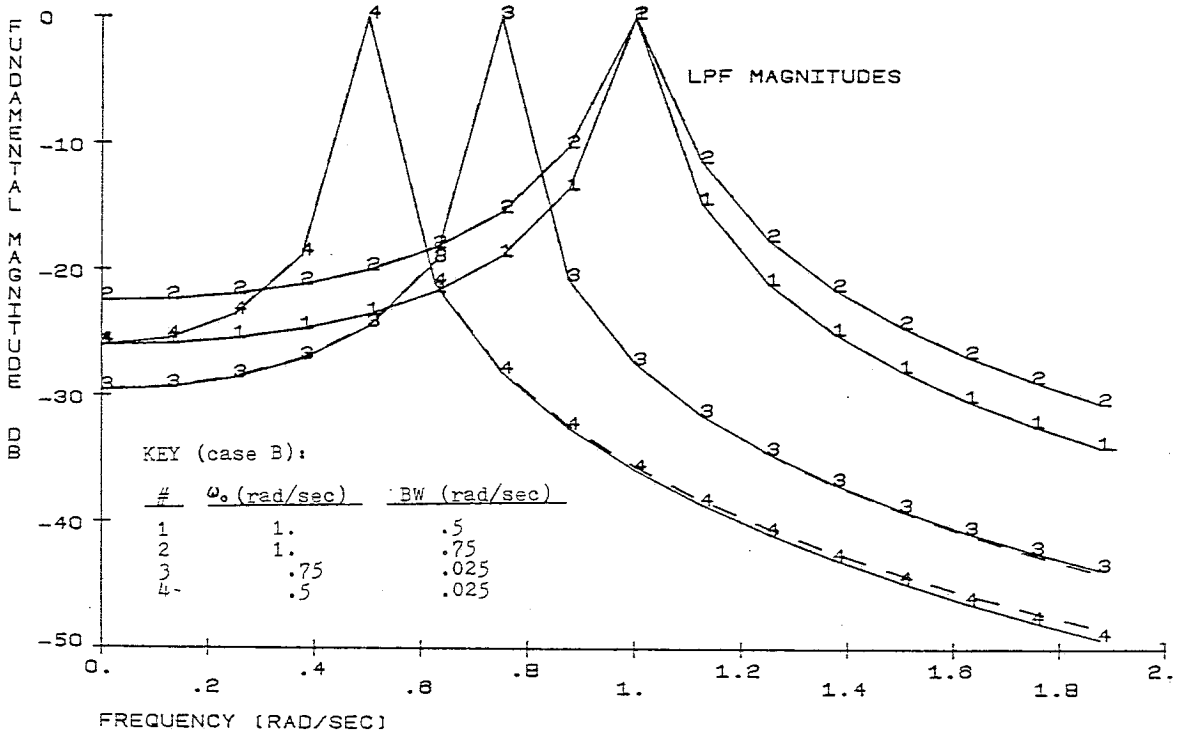

Figure 28 - Fundamental magnitudes for the same case B examples shown in Figure 25.
(a) Bandpass
(b) Lowpass

Chapter 5 - EXPERIMENTAL RESULTS

5.1 Filter Topology

The circuit diagram shown in Figure 29 is the prototype designed and constructed for this investigation. The topology is similar to that of Figure 5. Instead of using an inverting integrator followed by a unity gain inverting stage, a higher quality integrator was made by connecting the positive input of the inverting stage to the inverting input of the operational amplifier used in the integrator. This design improves the quality of the non inverting integrator by a factor of 3 [21], and thereby reduces the Q enhancement effects without additional circuit complexity.

The resistor and capacitor values shown were choosen to give a center frequency of 10 kHz and a bandwidth of 1 kHz when all the switches are closed. Also, resistors in series with the CMOS switches are made large compared to the switch's on resistance of approximately 350 ohms.

Unless otherwise stated, the sampling rate is assumed to be 40 kHz (four times the maximum center frequency of 10 kHz). This sampling rate was choosen to insure that the CMOS switches will turn fully on and off.

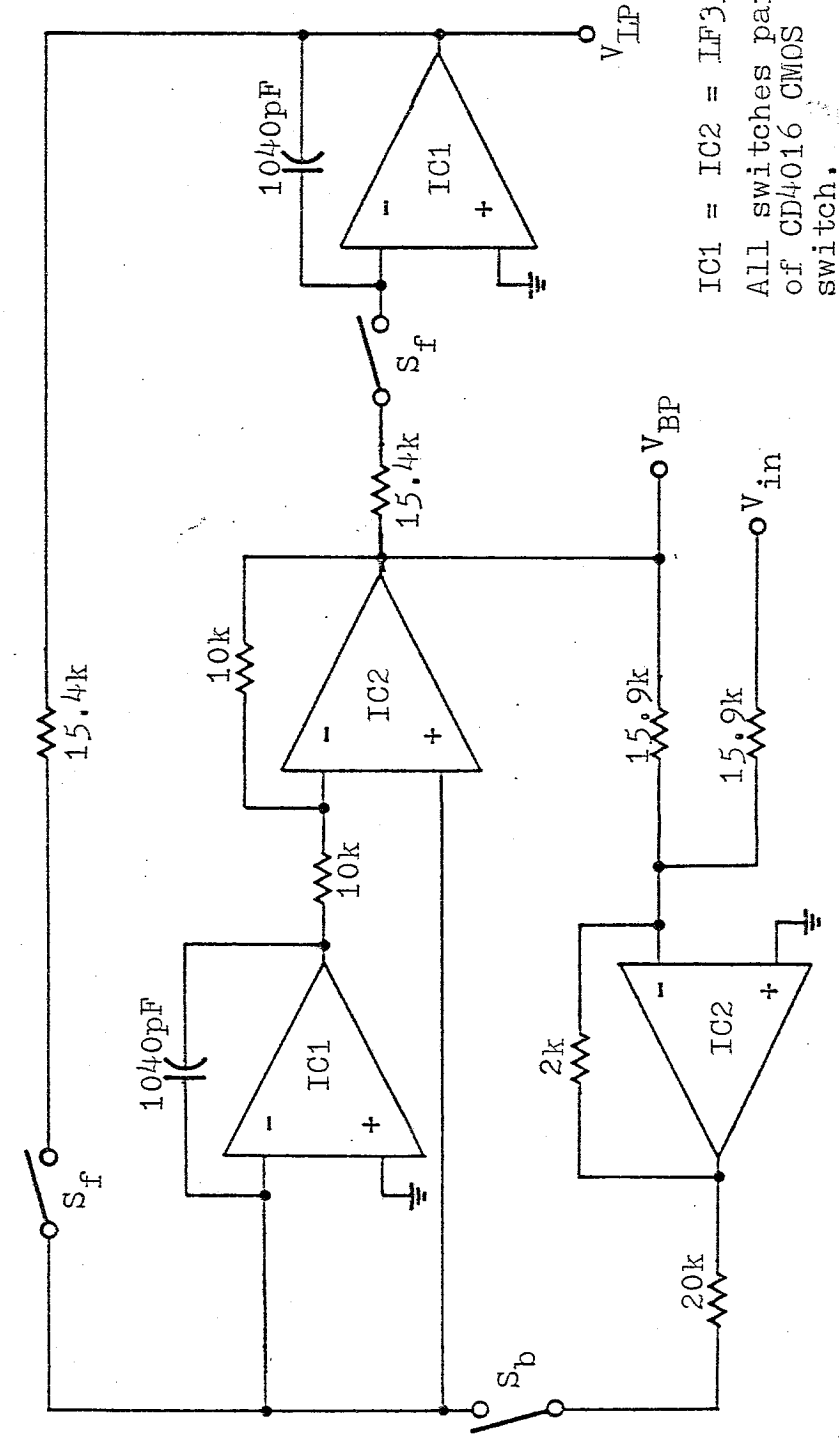

Figure 29 - Experimental prototype switched resistor filter.

5.2 Near Center Frequency Performance

Figure 30 shows the effects of tuning the second order bandpass section. This frequency response data was recorded using a Hewlett-Packard model HP8556 spectrum analyzer and a small microcomputer based data acquisition system. This Figure shows the frequency response near four different center frequencies. In each case, bandwidth switch duty cycles of 15%, 35%, 55%, and 75% are shown. From this data, the following center frequencies, 3 dB bandwidths, and maximum gains can be extracted:

	Center Frequency (kHz)	Bandwidth at -3dB (Hz)	Gain at Center Frequency (dB)
A	2.456	141.	0.48
	2.457	338.	0.14
	2.456	537.	0.05
	2.456	736.	0.00
B	4.929	134.	0.96
	4.926	328.	0.35
	4.928	523.	0.15
	4.928	720.	0.07
C	7.394	123.	1.61
	7.393	312.	0.62
	7.392	503.	0.34
	7.389	694.	0.20
D	9.881	116.	2.16
	9.879	303.	0.88
	9.877	496.	0.53
	9.876	689.	0.35

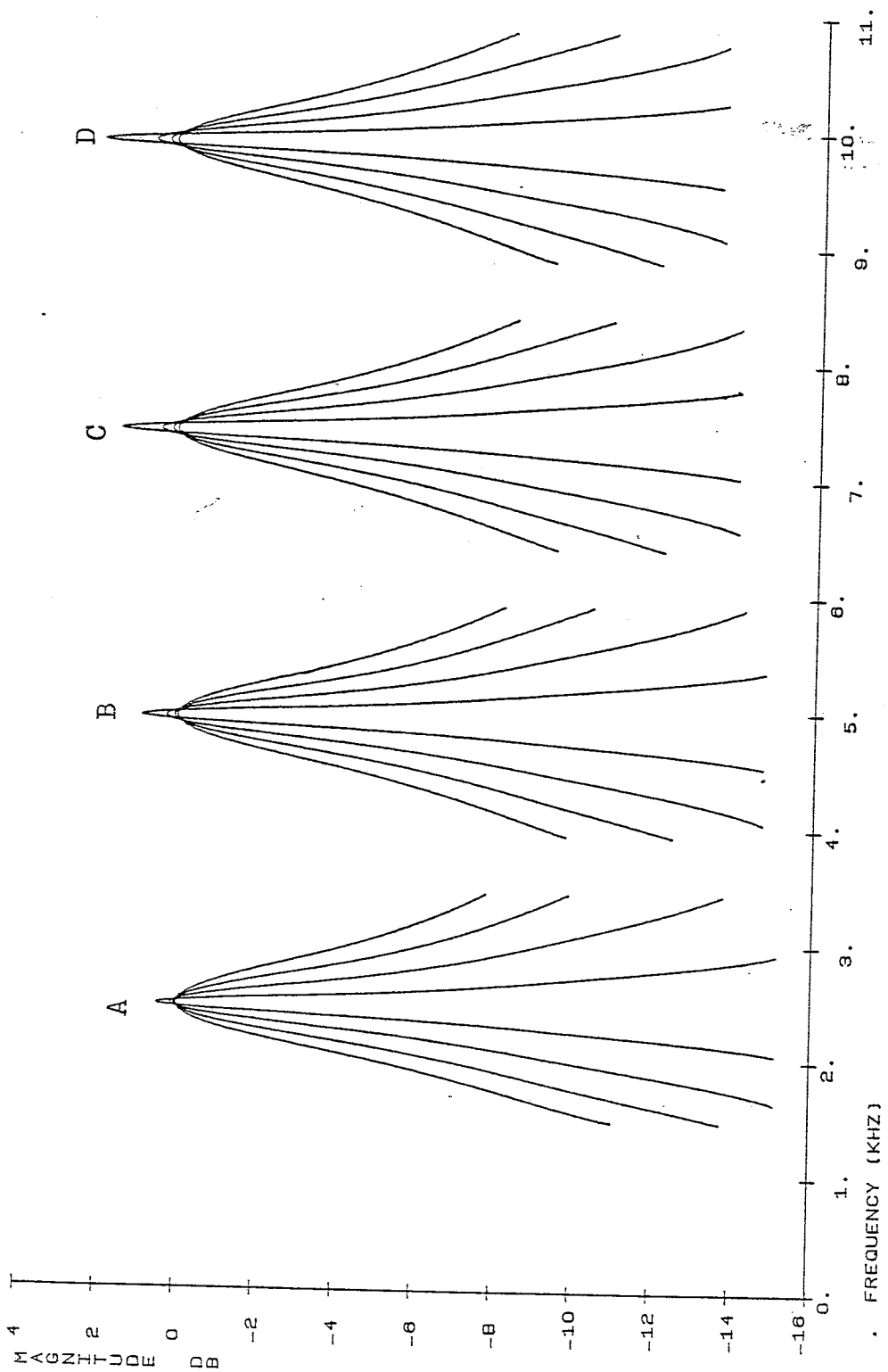

Figure 30 - Near center frequency bandpass frequency response.

As expected, the bandwidth does not remain constant as the center frequency is changed. Figure 31 shows this graphically. The broken curve shows the bandwidth calculated from component and duty cycle values assuming the amplifiers are ideal. Because the LF353 operational amplifiers have a gain-bandwidth product of about 4 MHz, the bandwidth decreases as the center frequency is increased. Also, as can be seen in the table on the previous page, the magnitude at the center frequency increases by several dB over the range of bandwidth-center frequency cases considered. Note that this data represents a quality factor change from 3.33 to 84.8. The 2 dB rise in the gain over this large change in Q is quite good for a filter of this type.

In order to investigate the change in the center frequency with duty cycle, additional data was recorded. This data for the constant Q case is displayed graphically in Figure 32. The center frequency remains proportional to the duty cycle of the switching signal over a wide range. This graph shows that the center frequency of a filter can be reduced by a factor of 100 with very little loss of accuracy.

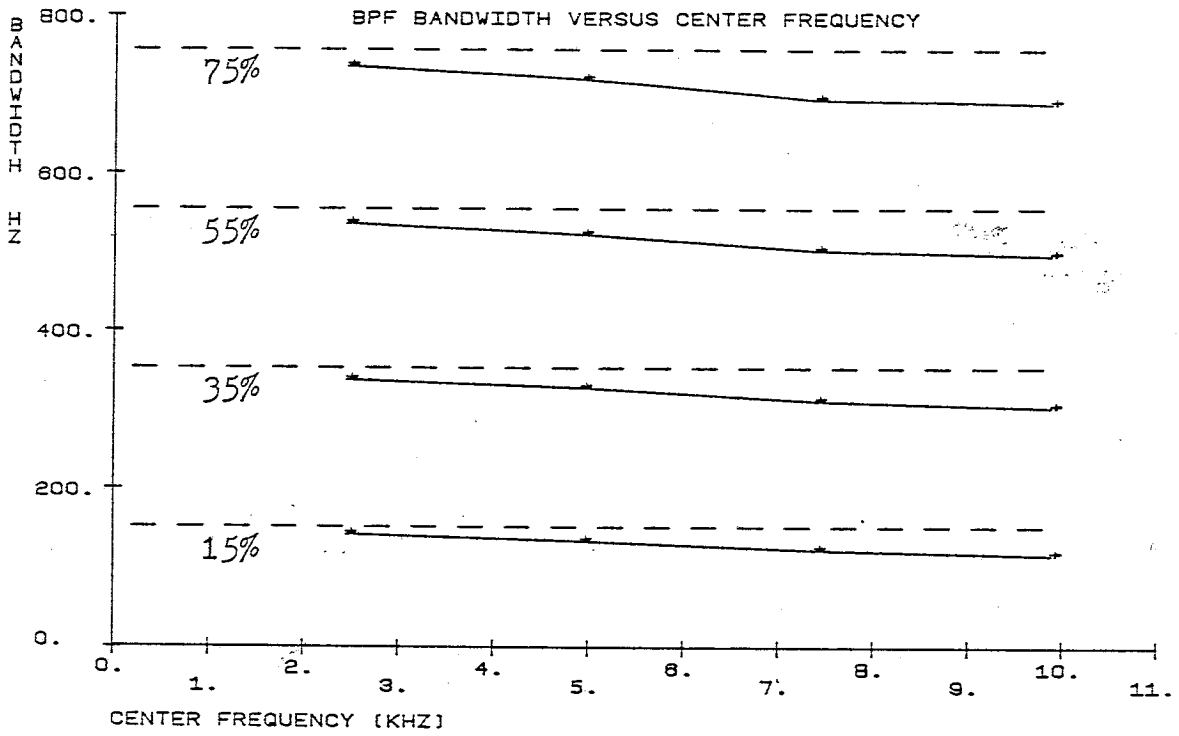

Figure 31 - Experimental bandwidth of bandpass switched resistor filter versus center frequency.

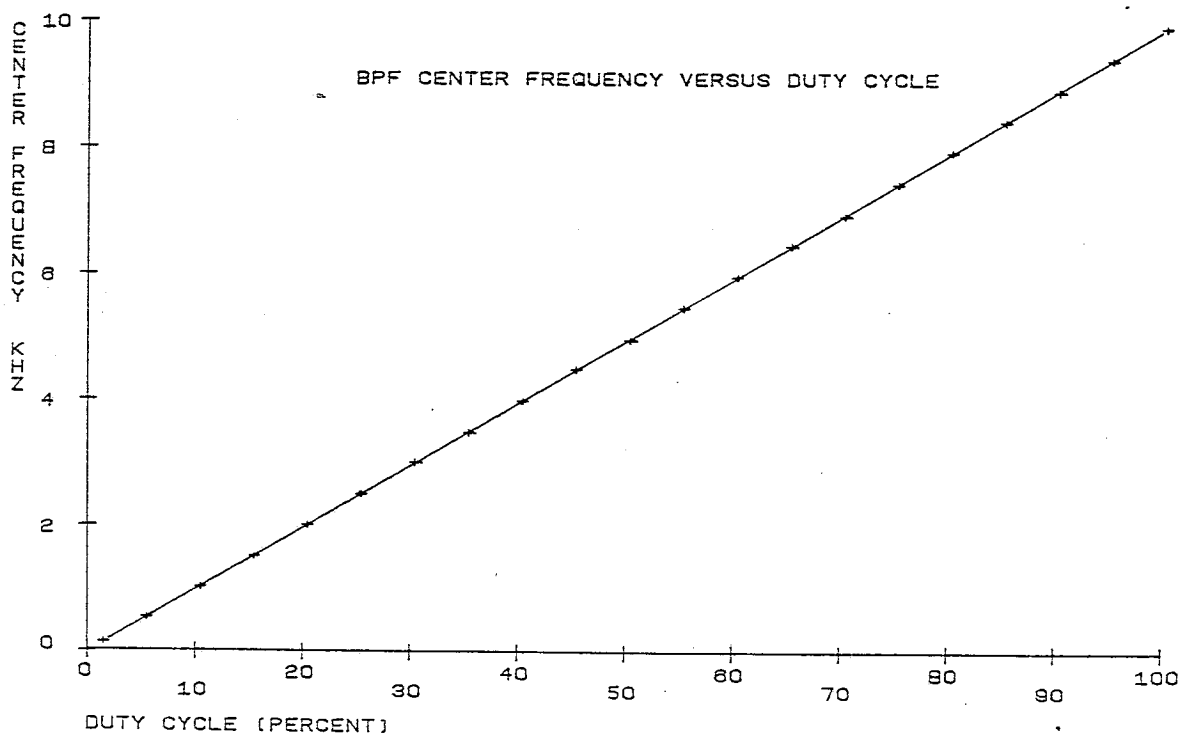

Figure 32 - Experimental center frequency versus center frequency duty cycle.

5.3 Constant Q Frequency Response

Figure 33 shows the lowpass frequency response for four different constant Q center frequencies (duty cycles of 25%, 50%, 75% and 100% are shown). Spectrum analyzer data is shown from about 0.2 kHz to 32 kHz. In all but the 100% duty cycle case, aliasing occurs above 20 kHz and the spectrum analyzer output no longer is a true frequency response. This data above 20 kHz would not be expected to agree with any previous analysis data and is of very little practical value.

It can be seen from this figure that at high frequencies the lowpass transfer function is actually lower than the equivalent continuous time transfer function. This deviation increases as the duty cycle is reduced. The measured performance shown in Figure 33 agrees with the computer analysis shown in Figure 25.

Similar data for the bandpass frequency response for the constant Q case is shown in Figure 34. Here almost no deviation from the ideal bandpass transfer function can be detected. This again agrees with the computer analysis.

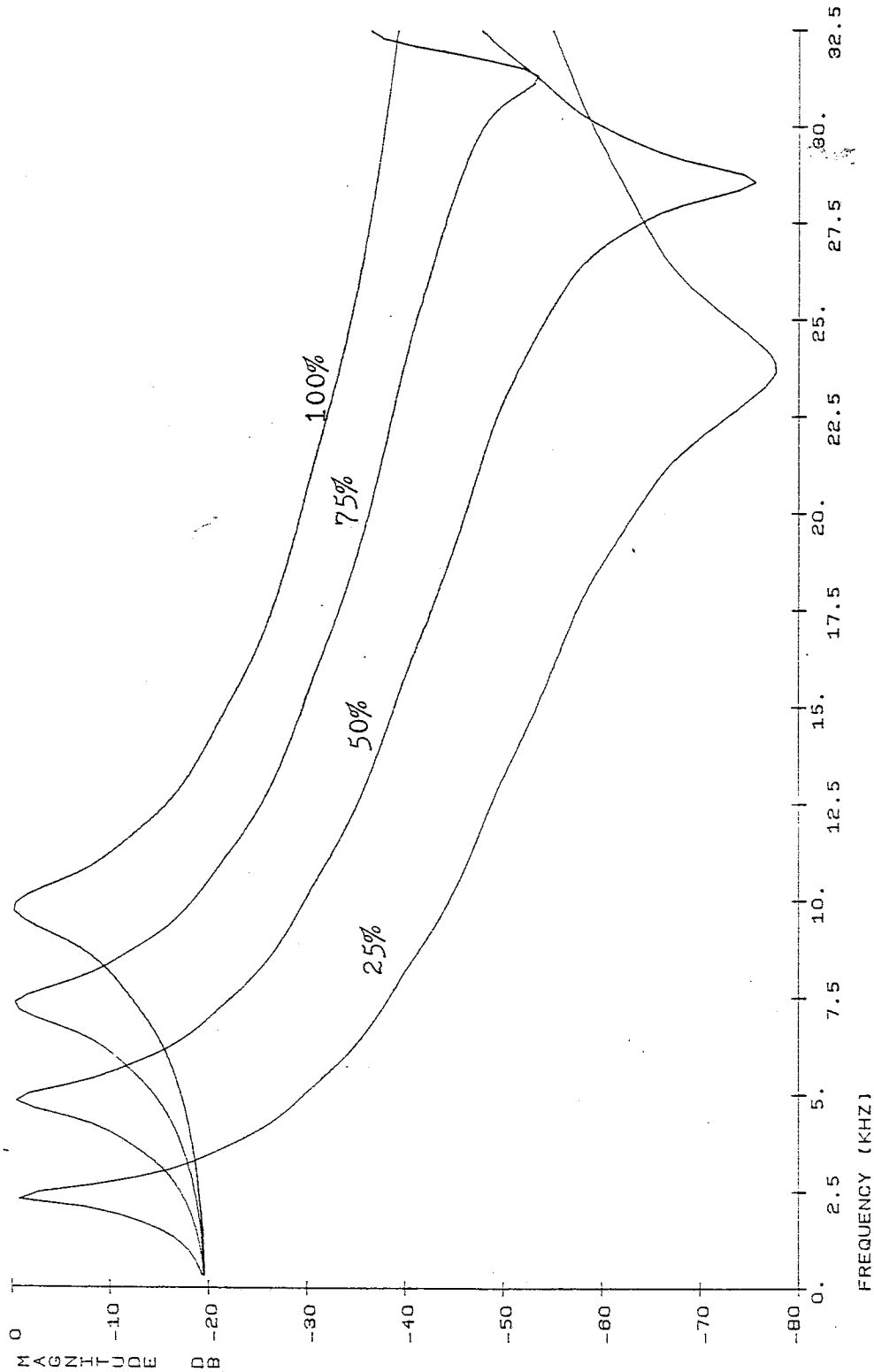

Figure 33 - Experimental constant Q lowpass frequency response.

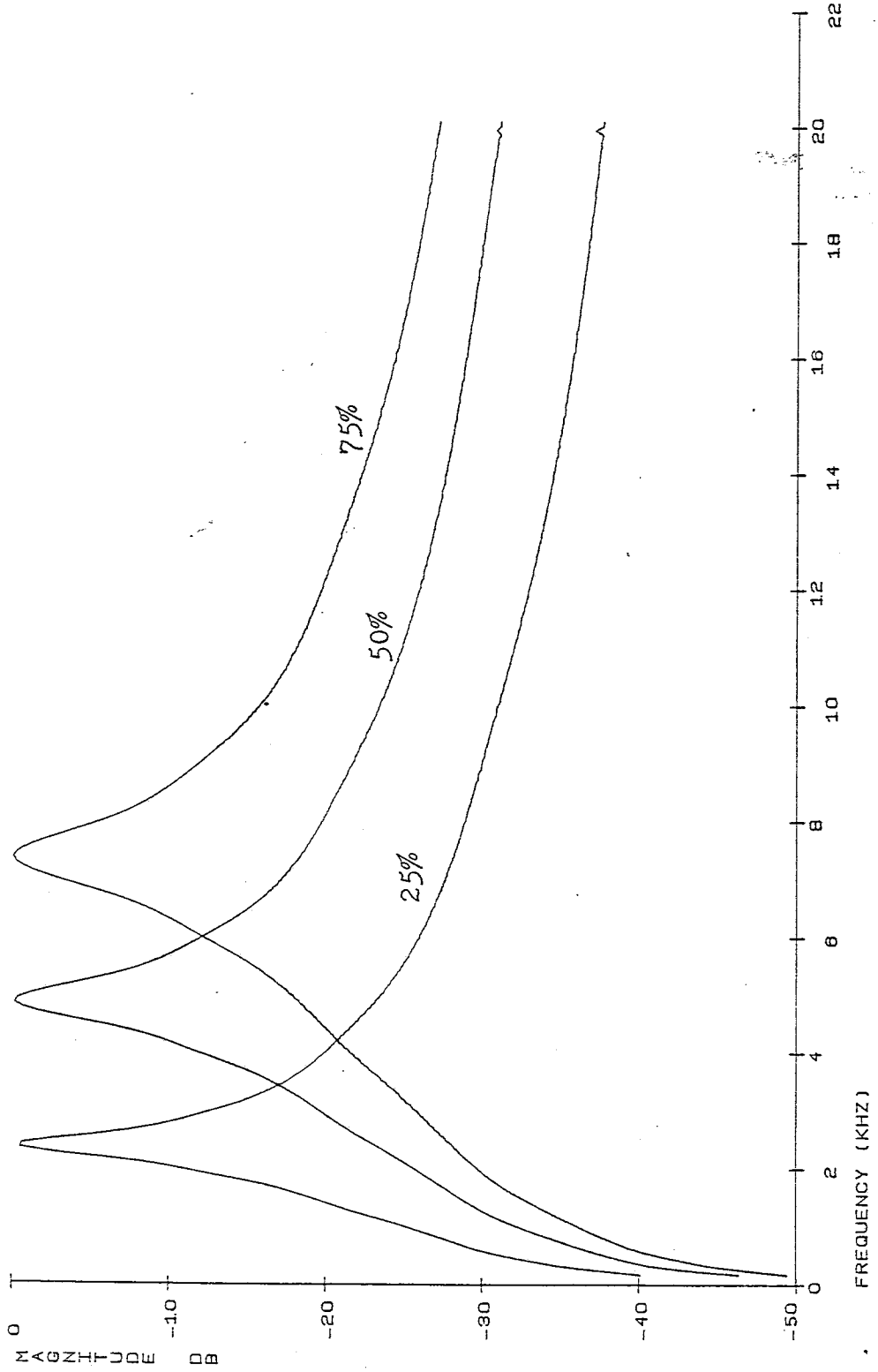

Figure 34 - Experimental constant Q bandpass frequency response.

5.4 Bandwidth Tuning

Figure 35 shows a typical case where the bandwidth is changed with a constant 5 kHz center frequency. It can be seen that when the bandwidth duty cycle is small (say 25%) the low frequency attenuation is not as large as it should be. This aliased spectrum at low frequencies is the same effect the analysis shows in Figures 13 and 28.

To investigate this low frequency deviation, the data shown in Figure 36 was taken. The center frequency and bandwidth duty cycles were set to 75% and 25% respectively. The sampling rate was changed from 20 kHz to 80 kHz. The three curves shown indicate that as the sampling rate is reduced the aliasing of the filter transfer function at low frequencies increases. At high frequencies, however, no similar effect is indicated. Once again, this agrees with results predicted by the state variable computer analysis. The low frequency distortion of the bandpass transfer function may not be a major drawback since a simple highpass filter could be added to remove the non-zero DC and low frequency response.

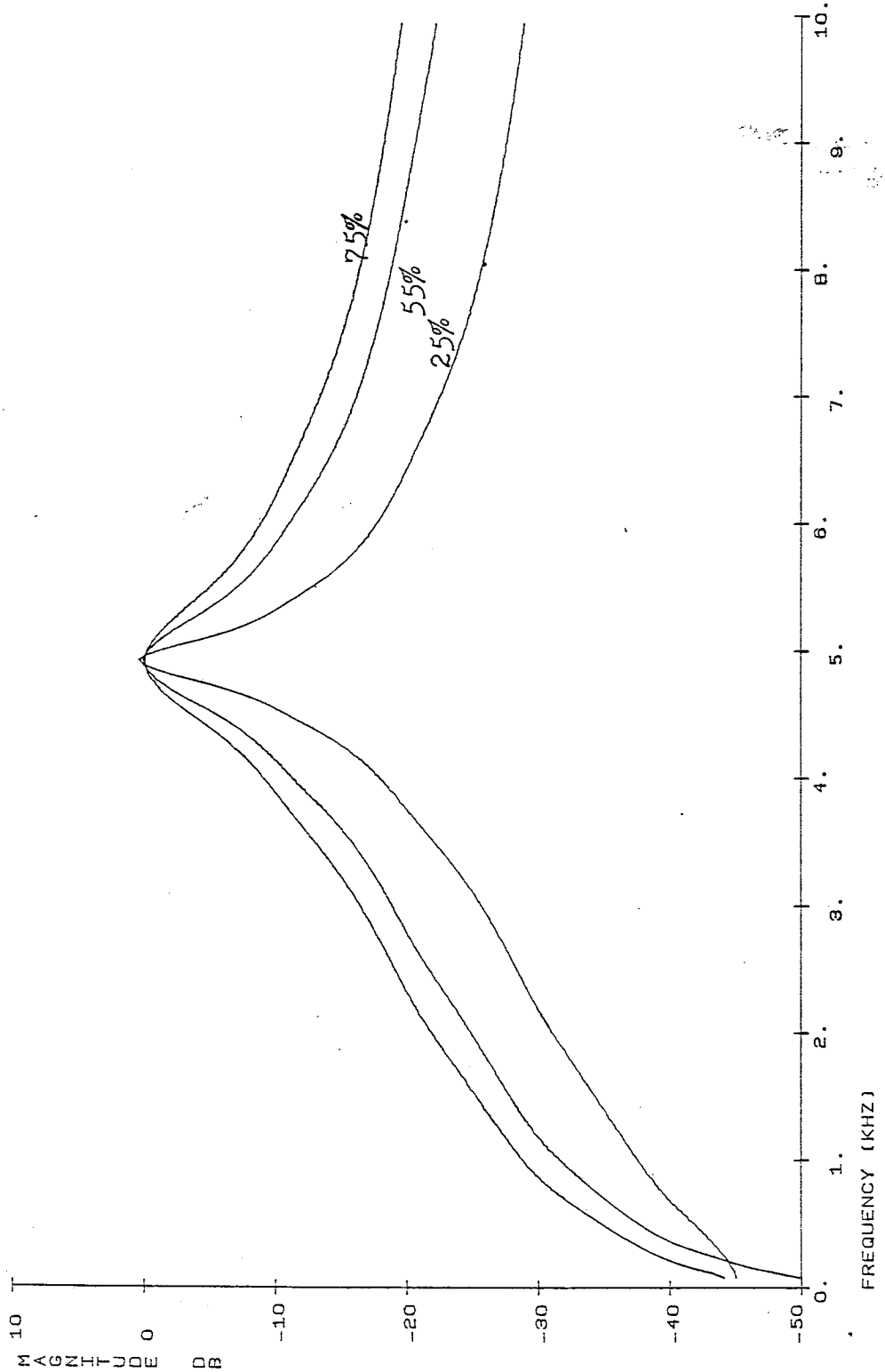

Figure 35 - Experimental bandwidth tunning of bandpass frequency response. (bandwidth duty cycle is indicated for each curve.)

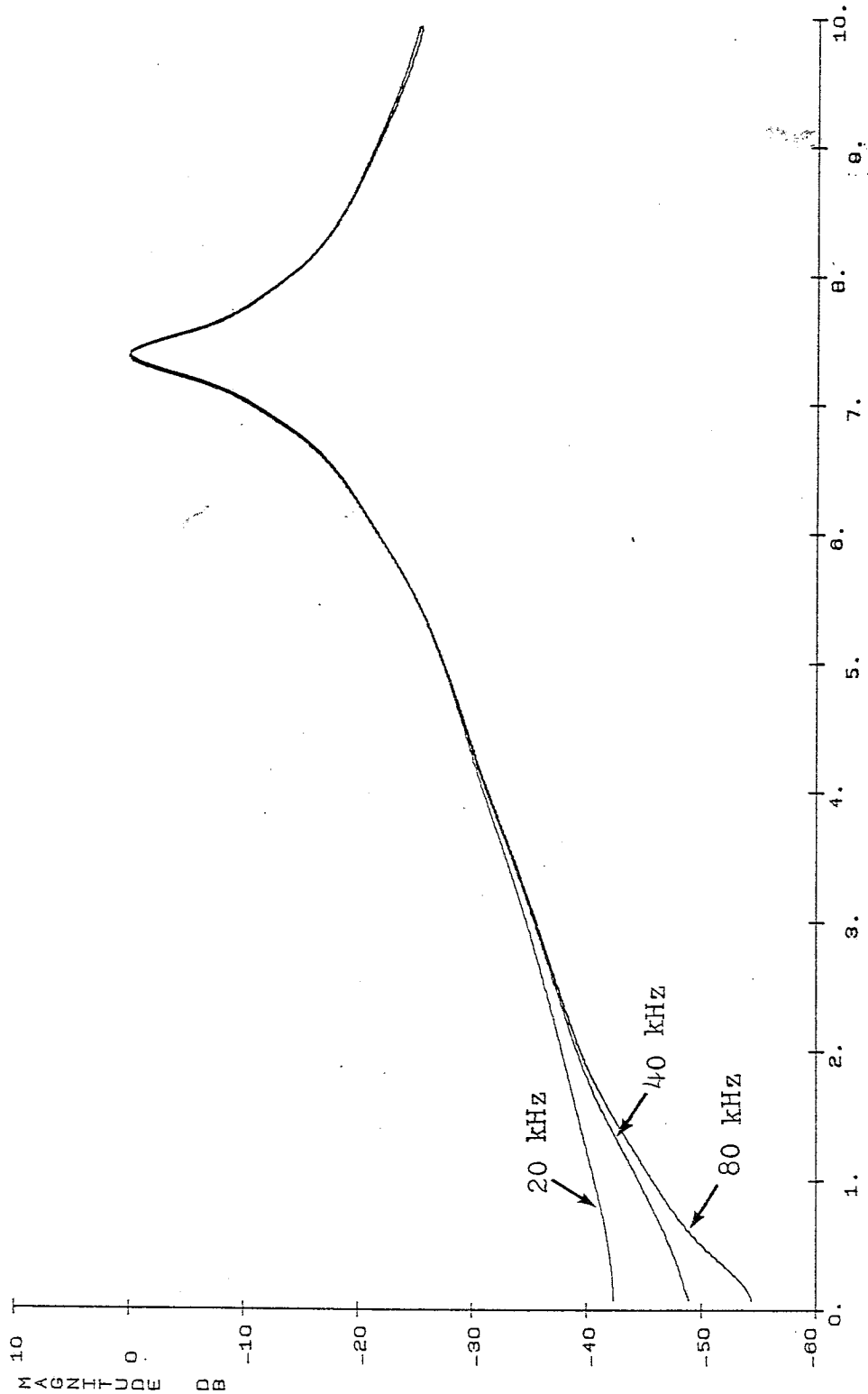

Figure 36 - Experimental low frequency bandpass deviation for center frequency = 7.5 kHz and bandwidth = 250 Hz. (sampling rate indicated for each curve.)

5.5 Filter Output Distortion

By connecting the input of the filter to a separate sine wave generator and connecting the output of the bandpass filter to the spectrum analyzer input, a crude measurement of the output frequency spectrum can be made. Figure 37 shows the superposition of three such measurements. The center frequency duty cycle of the filter is set to 75% and the bandwidth duty cycle is 25%. Three input frequencies are shown (2.5 kHz, 7.5 kHz, and 12.5 kHz).

Several non-ideal effects can be observed in Figure 37. First, the sine wave generator has a significant 2nd and 3rd harmonic content. Note that -60 dB harmonics represent .1% distortion which is quite difficult to achieve in a standard sine wave generator. In each case the output spectrum is above -60 dB at 40 kHz - f_{in}, 40 kHz + f_{in}, 80 kHz - f_{in}, and 80 kHz + f_{in} as expected. This data also shows that the random noise components present in the system are well below -70 dB which is quite good for a breadboard prototype.

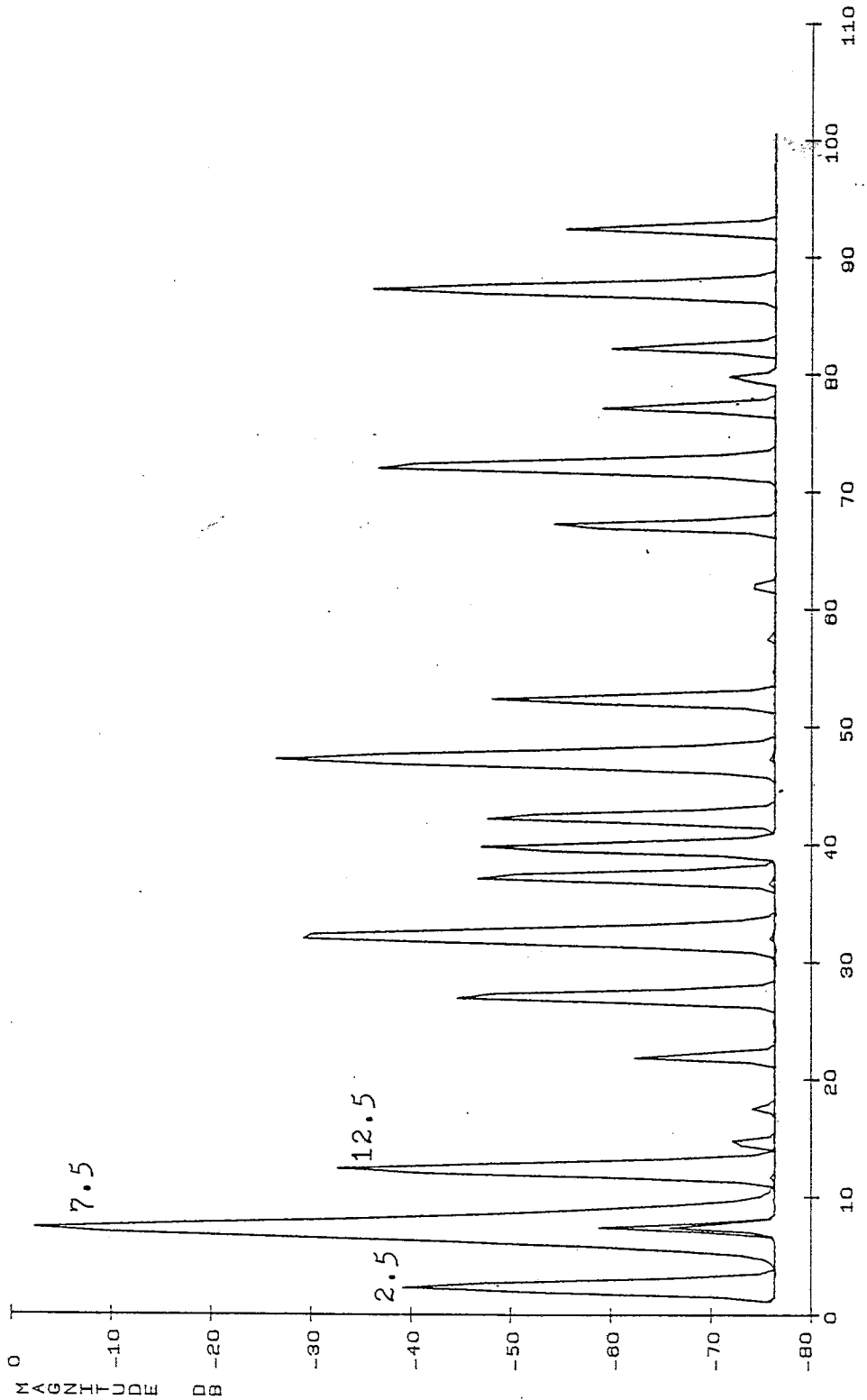

Figure 37 - Experimental output distortion of bandpass switched resistor filter for center frequency = 7.5 kHz and bandwidth = 250 Hz. (input frequency indicated for each curve.)

Also, all three cases shown have equal components at 40 kHz (-47 dB) and 80 kHz (-72 dB). These frequency components were not predicted in the computer analysis presented in Chapter 4. They are probably caused by capacitive feedthrough of the sampling frequency into the amplifier inverting inputs. This is a well known phenomenon in sample and hold circuits and causes the so called "hold step". The fact that equal amplitudes are observed for three different input frequencies seems to indicate a non-ideal effect (not dependent on the filter transfer function). Also, the remaining frequency components agree favorably with the computer analysis shown in Figure 19.

Chapter 6 - SUMMARY

Equivalent resistor-switch analysis techniques, which assume an equivalent resistance inversely proportional to duty cycle, are accurate only near the center frequency of the filter. These techniques can be used to determine the bandwidth and center frequency of the filter. Above and below the center frequency the transfer functions of switched resistor filters deviate from the equivalent ideal bandpass or lowpass transfer functions.

The frequency response of an ideal sampled data switched resistor filter, determined by extensive algebraic manipulation of state equations, gives important information about the performance of switched resistor biquadratic sections. This analysis of the sampled and held filter indicates significant differences between bandpass and lowpass outputs and their respective ideal responses.

A switched resistor filter without a sample and hold circuit on its output has a transfer function which is closer to the ideal continuous time system than the equivalent sampled and held switched resistor system. This frequency response can be determined by evaluating the spectrum of the steady state continuous time outputs of the

switched resistor filter. Thus, the frequency response of a biquadratic switched resistor filter is very close to the ideal two-pole response.

The output distortion of the constant Q switched resistor system is less than the distortion of an equivalent sampled data system. The totally tunable lowpass filter also has less output distortion than a sampled data lowpass filter. However, output distortion of a totally tunable switched resistor bandpass section can be greater than the sampled data distortion at frequencies significantly less than the center frequency of the filter.

Experimental measurements of a second order switched resistor prototype indicate that the computer aided analysis of the ideal switched resistor filter is accurate in predicting filter performance. These measurements also indicate that the bandwidth and center frequency of a switched resistor filter can be tuned accurately by digital means. Hence, filter designers requiring tunable second order sections may find switched resistor filters rather attractive.

APPENDIX

Using the same notation for REDUCE output introduced in Chapter 3, the steady state frequency response vectors for case A (H_A) and case B (H_B) are shown below. In each case, the first element (1) is the low pass response and the second element (2) is the band pass response.

```
                                                                2*t2*L + t1*L
H_A(1)=((((SIN(t1*B)*L-COS(t1*B)*B)+E                                      *Z*B)
                ((w*j + L)*t1 + t1*j*B)
      *((E                              - 1)*(w*j + L - j*B)
   t1*j*B      (w*j + L)*t1       t1*j*B
- E         *(E                - E         )*(w*j+L+j*B))*
                                (w*j+L)*t1 + t1*j*B           2*t1*j*B
(w*j + 2*L)-((-2*E                                  *w*B + E           *
                          2*t1*j*B           2*t1*j*B · 2
        w*L*j + E                   *w*B + E           *L  +
       2*t1*j*B   2                          2    2
     E          *B  - w*L*j + w*B - L  - B )*(w*j + 2*L)
          t1*w*j + t1*L + t1*j*B      t2*w*j + 2*t2*L
  + 2*E                          *(E                  - 1)*
                      2   2                                 t1*j*B
       ((w*j + L)  + B )*j*B)*SIN(t1*B))*L)/(E                    *
    2*t2*L + t1*L                          t1*L
(- E               *SIN(t1*B)*Z*L+E             *SIN(t1*B)*Z*L+B-
    2*t2*L + t1*L                          t1*L
  E              *COS(t1*B)*Z*B - E           *COS(t1*B)*Z*B
     2*t2*L + 2*t1*L   2                                2  2
 + E                 *Z *B)*(w*j+2*L)*((w*j+L)  +B )*j*B)
```

$$H_A(2) = (- (((-2*E^{(w*j + L)*tl + tl*j*B)} *wB + E^{2*tl*j*B} *w*L*j + E^{2*tl*j*B} *w*B + E^{2*tl*j*B} *L + E^{2*tl*j*B} *B^2 - w*L*j + w*B - L^2 + B^2)*$$

$$(w*j + 2*L) + 2*E^{tl*w*j + tl*L + tl*j*B} *$$

$$(E^{t2*w*j + 2*t2*L} - 1)*((w*j + L)^2 + B^2)*j*B)*$$

$$(SIN(tl*B)*L + COS(tl*B)*B - E^{tl*L} *Z*B) -$$

$$((E^{(w*j + L)*tl + tl*j*B} - 1)*(w*j + L$$

$$- j*B) - E^{tl*j*B} *(E^{(w*j + L)*tl} -$$

$$E^{tl*j*B})*(w*j + L + j*B))*(w*j + 2*L)*$$

$$(L^2 + B^2)*SIN(tl*B))*L)/(E^{tl*j*B} *$$

$$(-E^{2*t2*L+tl*L} *SIN(tl*B)*Z*L + E^{tl*L} *SIN(tl*B)*Z*L+B-$$

$$E^{2*t2*L+tl*L} *COS(tl*B)*Z*B - E^{tl*L} *COS(tl*B)*Z*B$$

$$+E^{2*t2*L+2*tl*L} *Z^2 *B)*(w*j+2*L)*((w*j+L)^2 +B^2)*j*B)$$

$$H_B(1)=(((((E^{(w*j + L)*tl + tl*j*B} -1)*(w*j+L-j*B) - E^{tl*j*B}*(E^{(w*j + L)*tl} - E^{tl*j*B})$$

$$*(w*j + L + j*B))*SIN(t2)$$

$$+ (-2*E^{(w*j + L)*tl + tl*j*B}*w*B + E^{2*tl*j*B}*w*L*j + E^{2*tl*j*B}*w*B + E^{2*tl*j*B}*L^2 +$$

$$E^{2*tl*j*B}*B^2 - w*L*j + w*B - L^2 + B^2)$$

$$*COS(t2))*((SIN(t2)*L - COS(t2))*SIN(tl*B)$$

$$- SIN(t2)*COS(tl*B)*B)$$

$$+ (((E^{(w*j + L)*tl + tl*j*B} - 1)*(w*j + L - j*B) - E^{tl*j*B}*(E^{(w*j + L)*tl} -$$

$$E^{tl*j*B})*(w*j + L + j*B))*COS(t2) -$$

$$(2*-E^{(w*j + L)*tl + tl*j*B}*w*B + E^{2*tl*j*B}* w*L*j + E^{2*tl*j*B}*w*B + E^{2*tl*j*B}*L^2 +$$

$$E^{2*tl*j*B}*B^2 - w*L*j - w*B - L^2 + B^2)$$

$$*SIN(t2))*((SIN(tl*B)*SIN(t2) + SIN(tl*B)*$$

$$COS(t2)*L - COS(tl*B)*COS(t2)*B) + E^{tl*L}*Z*B))*L)$$

```
          tl*j*B                2         2
     /(E         *(SIN(tl*B) *SIN(t2) *B +

          2         2        tl*L
SIN(tl*B) *COS(t2) *B + E       *SIN(tl*B)*SIN(t2)*

     2     tl*L                              2
  Z*L  + E       *SIN(tl*B)*SIN(t2)*Z*B  +

          tl*L                                    2
       E       *SIN(tl*B)*SIN(t2)*Z + SIN(t2) *

                2                 2         2
     COS(tl*B) *B + COS(tl*B) *COS(t2) *B - 2*

  tl*L                                  2*tl*L   2
E       *COS(tl*B)*COS(t2)*Z*B + E          *Z *B)*

     (w*j + L + j*B)*(w*j + L - j*B)*j*B)
```

$$H_B(2) = (((((E^{(w*j + L)*tl + tl*j*B} - 1)*(w*j+L-j*B) - E^{tl*j*B})*(E^{(w*j+L)*tl} - E^{tl*j*B})*(w*j+L+j*B))*SIN(t2) + (-2*E^{(w*j + L)*tl + tl*j*B}*w*B + E^{2*tl*j*B}*w*L*j + E^{2*tl*j*B} * (w*B + L^2 - B^2) - w*L*j + w*B - L^2 + B^2)*COS(t2))*((SIN(tl*B)*SIN(t2)*L^2 + SIN(tl*B)*SIN(t2)*B^2 - SIN(tl*B)*COS(t2)*L - COS(tl*B)*COS(t2)*B)*(E^{tl*L}*Z*B) + (((E^{(w*j + L)*tl + tl*j*B} - 1)*(w*j+L-j*B) - E^{tl*j*B})*(E^{(w*j+L)*tl} - E^{tl*j*B})*(w*j+L+j*B))*COS(t2) - (-2*E^{(w*j + L)*tl + tl*j*B}*w*B + E^{2*tl*j*B}*w*L*j - E^{2*tl*j*B}*w*B + E^{2*tl*j*B}*L^2 + E^{2*tl*j*B}*B^2 - w*L*j + w*B - L^2 - B^2)*SIN(t2))*(((L^2 + B^2)*COS(t2) + SIN(t2)*L)*SIN(tl*B) + SIN(t2)*COS(tl*B)*B))*L)/(E^{tl*j*B}*(SIN(tl*B)^2*SIN(t2)^2*B^2 + SIN(tl*B)^2*COS(t2)^2*B + E^{tl*L}*SIN(tl*B)*SIN(t2)*Z*L^2 + E^{tl*L}*SIN(tl*B)*SIN(t2)*Z*B^2 + E^{tl*L}*SIN(tl*B)*SIN(t2)*Z + SIN(t2)^2*COS(tl*B)^2*B + COS(tl*B)^2*COS(t2)^2*B - 2*E^{tl*L}*COS(tl*B)*COS(t2)*Z*B + E^{2*tl*L}*Z^2*B)*(w*j + L + j*B)*(w*j + L - j*B)*j*B)$$

REFERENCES

[1] J. J. Hill, "Digital Control of Active Filter Characteristics," International Journal of Electronics, vol. 41, pp. 405-410, October 1976.

[2] O. G. Boyle, "Control an LP-filter's cutoff frequency," Electronic Design, vol. 21, pp. 62-65, October 11, 1978.

[3] L. T. Bruton and R. T. Pederson, "Tunable RC- Active Filters Using Periodically Switched Conductances," IEEE Transactions on Circuit Theory, vol. CT-20, pp. 294-301, May 1973.

[4] J A. Kaehler, "Periodic-Switched Filter Networks- A Means of Amplifying and Varying Transfer Functions," IEEE Journal of Solid-State Circuits, vol. SC-4, pp. 225-230, August 1969.

[5] Y. Sun and I. T. Frisch, "Resistance Multiplication in Integrated Circuits by Means of Switching," IEEE Transactions on Circuit Theory, vol. CT-15, pp. 184-192, September 1968.

[6] D. J. Fried, "Analog Sampled-Data Filters," IEEE Journal of Solid-State Circuits (Corresp.), vol. SC-7, pp. 302-304, August 1972.

[7] R. W. Brodersen, P. R. Gray and D. A. Hodges, "MOS Switched Capacitor Filters," Proceedings of the IEEE, vol. 67, pp. 61-75, January 1979.

[8] D. J. Allstot, R. W. Brodersen and P. R. Gray, "MOS

Switched Capacitor Ladder Filters," IEEE Journal of Solid-State Circuits, vol. SC-13, pp. 806-814, December 1978.

[9] P. E. Fleischer and K. R. Laker, "A Family of Active Switched Capacitor Biquad Building Blocks," The Bell System Technical Journal, vol. 58, pp. 2235-2269, December 1979.

[10] J. T Caves, M. A. Copeland, C. F. Rahim, and S. D. Rosenbaum, "Sampled Analog Filtering using Switched Capacitors as Resistor Equivalents," IEEE Journal of Solid-State Circuits, vol. SC-12, pp. 592-599, December 1977.

[11] G. C. Temes, H. J. Orchard and M. Jahanbegloo, "Switched-Capacitor Filter Design Using the Bilinear Z-Transform," IEEE Transactions on Circuits and Systems, vol. CAS-25, pp. 1039-1044, December 1978.

[12] M. L. Liou and Y. L. Kuo, "Exact Analysis of Switched Capacitor Circuits with Arbitray Inputs," IEEE Transactions on Circuits and Systems, vol. CAS-26, pp. 213-223, April 1979.

[13] C. F. Lee, "An Investigation of Computer-Aided Analysis for Switched Capacitor Sampled-Data Filters," Doctor of Philosophy Thesis, Department of Electrical Engineering, University of Illinois, Urbana, May 1981.

[14] L. Garza, "An In-Depth View of Designing Switched Capacitor Sampled-Data Filters", Master of Science

Thesis, Department of Electrical Engineering, University of Illinois, Urbana, May 1981.

[15] D. J. Allstot, R. W. Brodersen and P. R. Gray, "An Electrically- Programmable Switched Capacitor Filter," IEEE Journal of Solid-State Circuits, vol. SC-14, pp. 1034-1041, December 1979.

[16] U. Kleine, D. Herbst, B. Hoefflinger, B. J. Hosticka and R. Schweer, "Real-Time Programmable Unit-Element SC Filter for LPC Synthesis," Electronics Letters, vol. 17, pp. 600-602, August 1981.

[17] R. L. Geiger, P. E. Allen and D. T. Ngo, "Switched-Resistor Filters- A Continuous Time Approach to Monolithic MOS Filter Design," IEEE Transactions on Circuits and Systems, vol. CAS-29, pp. 306-315, May 1982.

[18] W. J. Kerwin, L. P. Huelsman and R. W. Newcomb, "State Variable Synthesis for Insensitive Integrated Circuit Transfer Functions," IEEE Journal of Solid-State Circuits, vol. SC-2, pp. 87-92, September 1967.

[19] L. C. Thomas, "The Biquad: Part 1 -- Some Practical Design Considerations," IEEE Transactions on Circuit Theory, vol. CT-18, pp. 350-357, May 1971.

[20] T. A. Hamilton and A. S. Sedra, "A Novel Application of a Gyrator-type Circuit," 5th Record of the Asilomar Confrence on Circuits and Systems, pp. 343-348, 1971.

[21] A. S. Sedra and P. O. Brackett, Filter Theory and

Design: Active and Passive. Champaign, Il.: Matrix Publishers, Inc., 1978, Chapter 9.

[22] A. Budak, Passive and Active Network Analysis and Synthesis. Boston: Houghton Mifflin Company, 1974, Chapter 10.

[23] D. Akerberg and K. Mossberg, "A Versatile Active RC Building Block with Inherent Compensation for the Finite Bandwidth of the Amplifier," IEEE Transactions on Circuits and Systems, vol. CAS-21, pp. 75-78, January 1974.

[24] P. O. Brachett and A. S. Sedra, "Active Compensation for High-Frequency Effects in Op. Amp Circuits with Applications to Active-RC filters," IEEE Transactions on Circuits and Systems, vol. CAS-23, pp. 68-73, Febuary 1976.

[25] D. R. Frey, "Low-Cost Alternatives in High- Quality State-Variable Filters," Journal of the Audio Engineering Society, vol. 27, pp. 750-756, October 1979.

[26] R. B. Pavin and G. H. Hostetter, "Design and Performance of Digitally Tuned Switched-Element Active Filter," 13th Record of the Asilomar Confrence on Circuits and Systems, pp 429-432, 1979.

[27] A. C. Hearn, REDUCE User's Manual. Salt Lake City: University of Utah, reprinted by University of Illinois Computing Services Office, 1974.